

FATIGUE CHARACTERISTICS OF URANIUM

by

Jack Richard Bohn

**A Thesis Submitted to the
Graduate Faculty in Partial Fulfillment of
The Requirements for the Degree of
MASTER OF SCIENCE**

Major Subject: Nuclear Engineering

Signatures have been redacted for privacy

**Iowa State University
Of Science and Technology
Ames, Iowa**

1959

TABLE OF CONTENTS

I.	INTRODUCTION	1
II.	REVIEW OF THE LITERATURE	4
	A. Fatigue Process	4
	1. Microstructural damage	4
	2. Theories of fatigue	6
	3. Interpretation of fatigue results	9
	B. Deformation of Uranium	10
	1. Crystallography	10
	2. Mechanical properties	12
III.	OBJECTIVES OF THE INVESTIGATION	15
	A. Analytical Objective	15
	B. Experimental Objectives	15
IV.	MATERIALS	17
V.	EXPERIMENTAL PROCEDURES AND APPARATUS	19
	A. Specimen Preparation	19
	1. Machining	19
	2. Polishing	19
	3. Encapsulating	20
	B. Testing	29
	1. Fatigue	29
	2. Tensile	32
	C. Microanalysis	32
	1. Etching	32
	2. Microscopy	36
VI.	DISCUSSION OF VARIABLES INTRODUCED BY TECHNIQUES	39
VII.	RESULTS	41
	A. Presentation of S-N Data	41

1. Normal uranium	42
2. Chromium-uranium alloy	50
B. Statistical	58
C. Micro-analytical	62
VIII. DISCUSSION	72
A. S-N Determination	72
1. Normal uranium	73
2. Chromium-uranium alloy	89
B. Damage	96
IX. SUMMARY AND CONCLUSIONS	113
X. SUGGESTIONS FOR FURTHER INVESTIGATION	116
XI. LITERATURE CITED	118
XII. ACKNOWLEDGMENTS	121
XIII. APPENDIX	122
A. Tabulated Data	123
B. Stress-strain Records	132

I. INTRODUCTION

The so-called "elastic properties of materials" together with an appropriate safety factor usually form the basis for most design considerations. The elastic properties, though well defined, are not always representative of the deformation taking place in a given structural component. It is a well known fact that plastic action can take place in some materials well below the elastic limits by the mechanism of creep. It is also observed that most nonferrous materials do not exhibit, strictly speaking, elastic properties. Estimates of approximate values of the properties for design calculations must be made on the basis of such standardized techniques as the yield strength and the secant modulus. When the structural component in service is subjected to conditions and environments other than those typical of a laboratory specimen the burden of survival rests on the choice of an appropriate safety factor. Economics and human safety impose serious limitations on the safety factor, so often regarded as the "catch-all".

Aircraft weight and safety considerations brought to bear the need of more sophisticated thinking toward the problem of repeated loading. Numerous investigations relative to the effects of cyclic loading on light-weight high-strength materials resulted. Literature published from the investigations presented useful design data and some information which

contributed to a better understanding of the problem of cyclic stresses.

The recent advent of the nuclear reactor has provided the need for renewal of interests in cyclic stresses where the basic problems remain unsolved and further aggravated by new materials and environments. A power reactor in normal operation undergoes continuous thermal cycling, imposing on its varied components a wide spectrum of cyclic stress situations. Uranium and its environment in a reactor is a prime example. In an effort to obtain an overall solution of the stress problems arising it is necessary to isolate and examine the influence of each of the contributing factors. Recently, great numbers of investigators have dealt with the effects of high temperature cyclic stress on uranium. Investigations for the most part have dealt only with high stress levels for short durations, disregarding the implications suggested by fatigue considerations, involving moderate to low stresses for extended periods.

This investigation dealt with the experimental findings relative to the fatigue characteristics of uranium. Tests were conducted on normal and alloyed uranium from 25 to 600° C in a controlled atmosphere. The results of such tests are presented in the form of the familiar S-N diagram and empirical relationships. Particular consideration was given the microstructural effects of damage and the statistical

aspects of scatter with application to the theoretical models
of fatigue.

II. REVIEW OF THE LITERATURE

A. Fatigue Process

1. Microstructural damage

In 1902 Ewing and Humphrey (1) outlined the process of fatigue based on microscopic observations. Since that time the overall picture of the process has remained basically unchanged. For a ductile material the process is considered as taking place in three stages, perhaps somewhat analogous to the three stages of creep. The three stages are:

Stage 1. The material suffers bulk deformation upon loading; slip and the resulting disorientation of crystals takes place.

Stage 2. Slip lines become more numerous and broaden into what are termed as slip bands oriented in the same general direction as maximum shear. A limit is reached for this process in a localized area and submicroscopic cracking ensues.

Stage 3. Cracks join, decreasing the effective load carrying cross-section to a point where failure takes place.

From the literature it appeared difficult to ascertain quantitatively the extent of damage a particular stage played in the overall role of deformation and failure. This stemmed from the fact that each investigator used as a criterion for

the occurrence of a particular stage observations which were convenient or consistent with the detection equipment employed. The detection of a crack several microns in length appears possible with an electron microscope whereas the optical microscope is capable of observing cracks only if they have a minimum length of several thousandths of an inch. Failure may be designated by the detection of a crack of a predetermined length, an amount of extension or deflection, or by complete separation with fracture. The various methods of crack detection have been discussed by Dener (2) who has also summarized the effect of certain variables on the length of the various stages of the fatigue process as follows:

a. Material. The number of slip systems, purity, number of phases present, grain size, homogeneity of the structure and heat treatment of a material would be expected to affect the operativeness of a particular stage.

b. Specimen size and shape. The stress gradients determined by size and shape are important in crack growth. It is known that the characteristics of cracking for smooth and notched specimens are quite different. Specimen surface conditions are considered important using arguments based on the same reasoning.

c. Loading. The method of load application is important due to the variations in the state of stress on the surface and in the body of the specimen. Specimens tested under

constant maximum stress or strain amplitude would obviously not assume the same rate of crack propagation as one tested under constant moment or load.

d. Frequency of loading. Deformation marks on the surfaces of fatigue specimens display a pronouncedly different appearance for test frequencies above a certain critical value. One might suspect that insufficient heat dissipation at higher frequencies could produce a temperature rise in the specimen.

e. Temperature. Temperature effects act to vary the physical properties of material as well as accelerating corrosive action of test environments.

2. Theories of fatigue

Many theories of fatigue have been proposed in an attempt to explain the basic processes observed, mentioned in the preceding section. The majority of theorists have concentrated their efforts on the first and second stages of the fatigue process. No one theory has come close to providing even a partial answer to the voluminous experimental findings on record.

The importance of plastic inhomogeneities in hysteresis, elastic after-working, and fatigue was pointed out by Gough and Hanson (3). X-ray photographs supported a conclusion stating that alternating stresses could produce localized

plastic deformation (strain hardening) without causing visible macroscopic strain.

A quantitative theory of failure was developed by Orowan (4). The theory was based on work hardening of localized structural inhomogeneities situated in an elastic surrounding, as illustrated through the use of mechanical model. The model consisted of a plastic member in series with an elastic member coupled in parallel with two larger elastic members. The plastic member represented a favorably oriented crystal in a polycrystalline material, so that the applied stress, σ , was greater than the yield stress, σ_y , for the particular crystal but not greater than the yield stress for the surrounding material. Through the use of several simplifying assumptions, the theory was extended to account for many experimental findings. The resulting analytical expression for the S-N relationship was

$$A n = \ln \frac{\sigma_m - \sigma_y}{\sigma_m - \sigma_f} \quad (1)$$

where

- A = constant, effect of strain hardening
- n = cycles to failure, based on cracking
- σ_m = maximum stress of the inhomogeneity due to applied stress
- σ_f = fracture stress (constant for a given material)
- σ_y = yield stress (constant for a given material).

The equation brought about the existence of two ranges of stress for consideration; a safe range and an unsafe range. If σ_f was greater than σ_m , fracture was not possible, corresponding to the safe range. If σ_f was less than σ_m , fracture took place when sufficient work hardening had occurred to raise the applied stress σ to σ_f , corresponding to the unsafe range. The effects of thermal softening were considered in an analysis which resulted in a negative work hardening phenomenon. Conclusions drawn showed that the effects of thermal softening tended to increase the safe range if the other influencing quantities remained constant. This meant that the effect of temperature was to shift the S-N diagram up or down, depending on the influencing quantities involved.

A theory of fatigue based on the dislocation theory was proposed by Machlin (5). An equation was developed relating the dependence of the number of cycles to failure to stress, temperature, material parameters and frequency of loading. The equation, in terms of the author's nomenclature, was

$$\log N = \log \frac{2\pi\omega h M}{kT} + \frac{\Delta F_g}{2.3kT} - \frac{0.422c\eta V_x F \sigma_m}{2.3kT} \quad (2)$$

where

- N = cycles to failure
- ω = frequency of cyclic stress
- h = Planck's constant

M = crack growth per crack source necessary for failure

k = Boltzmann's constant

T = temperature, °K

ΔF_g = activation energy to produce a dislocation

x = ratio of distance between atoms in slip direction
to interplanar spacing of slip planes

V = volume

f = fraction, Norwick and Machlin (6)

σ_m = maximum tensile stress

c = proportionality constant, relating τ_a to $\sigma_m/2$

τ_a = average resolved shear stress for polycrystalline
specimen

q = stress concentration factor.

A quantitative correlation between fatigue and creep was suggested to exist.

3. Interpretation of fatigue results

Several alternatives have been offered in planning a fatigue testing program, depending on the degree of scatter observed initially in a particular testing situation. If the first few test points show good continuity through a more or less uniform distribution on the S-N diagram, the procedure as given in the A.S.T.M. manual on fatigue testing is suggested (7). If continuity is not evidenced, testing should be planned to be most compatible with a forthcoming

statistical analysis. Usually a number of specimens are tested at a given stress level providing several groups throughout the cyclic range desired.

Scatter in test data appears to be an inherent feature of fatigue, the degree depending on the nature of the material tested and the conditions of testing. In most situations the latter imposes the greater restrictions, especially where elevated temperature environments are present.

Statistical considerations can seriously affect the validity of conclusions drawn from fatigue results, as is the case with most experimental findings. The majority of literature available on fatigue deals with its statistical nature. It is fairly well agreed that the statistics of fatigue are most accurately governed by a logarithmic normal frequency distribution relationship.

Using a theoretical argument and the statistical approach of Cramer (8), Fruedenthal (9) has shown the frequency distribution to be log normal,

$$p(N) = \frac{1}{N\sqrt{2\pi}} \exp \left[-\frac{1}{2} (\log N)^2 \right] \quad (3)$$

B. Deformation of Uranium

1. Crystallography

Uranium exists in three phases. The alpha phase, which displays an unusual orthorhombic crystal structure, transforms

to the beta phase at 663° C. The beta phase is reportedly tetragonal and transforms to the body centered cubic gamma at 770° C. Uranium melts at 1130° C and boils at 3700 to 4200° C. The alpha phase is particularly unique since two of four atoms in a unit cell form covalent bonds with atoms in neighboring cells.

The deformation of uranium takes place more predominantly by the process of twinning up to approximately 350° C, after which slip predominates. The slip systems of uranium as summarized by Holden (10) are listed in order of decreasing importance and certainty.

plane	direction
010	100
001	100
110	110
001	100

The 010 plane is noted as the plane of easiest glide since the strong covalent bonds would not be broken by slip on this plane. The low value of yield stress for uranium (450 psi) may be accounted to this. Slip on the other slip systems listed do require severance of the covalent bonds, which could account for the 110 plane being favored at the elevated temperatures where the bonds are more easily broken.

2. Mechanical properties

A rather complete discussion of the mechanical properties of uranium was given by Holden (10) in "The Physical Metallurgy of Uranium". Mechanical properties are sensitive to purity, grain size and orientation, and state of cold work (fabrication). For reason of brevity, only the properties of beta heat treated alpha uranium, when stated, will be of interest.

Uranium behaves semiplastically, displaying a poorly defined proportional limit, if at all, in that the stress-strain curve of the first loading shows curvature at extremely low stresses (~ 500 psi) (11). For this reason difficulty is encountered in obtaining consistent values of Young's modulus. An average for values obtained from both tension and compression is 17.0×10^{11} dynes/cm² (10). Elastic constants obtained by ultrasonic techniques and reported by Laquer (12) are

Shear Modulus	8.34×10^{11} dynes/cm ²
Young's Modulus	20.5×10^{11} dynes/cm ²
Bulk Modulus	12.6×10^{11} dynes/cm ²
Poisson's Ratio	0.23 .

The effect of increasing temperature is to decrease rapidly the shear modulus and Young's modulus with a discontinuity near 300° C.

The damping capacity plotted versus temperature as

observed by Maringer (13) increases gradually to approximately 200° C, falls off slightly to 350° C, then increases rapidly up to the transformation temperature. Grain boundary relaxation was suggested for the rapid increase above 350° C.

Hardness versus temperature also displays the distinct break in continuity at approximately 350° C. Vicker's hardness number (10 kg load) reported from data by Chubb (14) decreases from 230 to 70 going from 0 to 350° C, and from 70 to 10 from 350 to 663° C.

Some typical values for the tensile properties are given as follows (10):

<u>Material</u>	<u>Yield strength</u>	<u>Tensile strength</u>	<u>Elongation</u>
Alpha rolled	(2 per cent offset), psi	psi	per cent
Beta-quenched	30-35 x 10 ⁸	70-95 x 10 ⁸	10-15
Beta annealed	25-35 x 10 ⁸	55-65 x 10 ⁸	6-10

Properties of the particular uranium used in this investigation are given in the section on materials.

The effect of temperature on the tensile properties is to lower the yield strength from 35 x 10⁸ to 4 x 10⁸ psi, and the ultimate strength from 90 x 10⁸ to 1 x 10⁸ psi in the temperature range of 0 to 600° C. Uranium displays a brittle-ductile transition slightly above room temperature, depending on purity, fabrication and the like. The large variation in the reported data of the various properties is attributed to

this phenomenon. Work on impact strength is also confirming of this fact.

The creep behavior of uranium has been studied extensively resulting in a large amount of inconsistent data. It is believed that the inconsistencies are due in part from effects of thermal-cycling growth which occur in elevated temperature tests from slight variations ($\pm 2^\circ \text{C}$) in temperature control. From creep results performed at Battelle (15) it is observed that an abrupt change in stress to produce a given creep rate exists in 300-400° C temperature range, the same apparent anomaly as was observed for other properties.

The only reported consideration given to the fatigue strength of uranium was by Coffin (16) who studied the effects of large strain cycles causing failure at several thousand cycles.

It will be noted throughout the literature that abrupt changes in mechanical properties near 300° were also observed for many other physical properties. Thermal conductivity, temperature-induced changes in volume, and growth rate for thermal cycling are such examples.

III. OBJECTIVES OF THE INVESTIGATION

A. Analytical Objective

The objective of the analytical investigation was to describe the deformation of polycrystalline uranium under fatigue loading (completely reversed rotating bending) in the form of an empirical equation relating the variables stress, cycles, and temperature. By this means it was proposed to form a basis of comparison of uranium in its natural state with that of an alloy, by attaching physical significance to the mathematical terms of the equation obtained. It was hoped that correlation might be found between the classical theoretical models and empirical results, in order to provide additional justification for proposed mechanisms of fatigue.

B. Experimental Objectives

Experimental results of S-N phenomena were sought to provide design criteria in primary applications of uranium as a nuclear fuel. Specific information was desired concerning the behavior of uranium under completely reversed cyclic loading throughout the useful design range of temperature (0-600° C). Particular emphasis was directed toward observing the effects of fatigue damage on the microstructure, in order to gain insight into the fundamental processes which

govern the deformation of uranium, and to quantitatively estimate the relative life remaining after a given percentage of the life expectancy had been reached.

IV. MATERIALS

The materials used in this investigation were natural uranium (commonly referred to as normal uranium) and a low percentage chromium alloy of uranium. As received, the material was in the form of 1.4 inch diameter slugs. The chemical specifications of the natural uranium as given by the fabricator were, based on impurity content, less than one per cent C, Cl, Cr, Si, B, Mg, Mn, Ni and N. The composition of the chromium-uranium alloy was not available.

The tensile properties of normal uranium as reported by Lewis (17) were

Modulus of elasticity:	21,800,000 psi ¹
Yield strength: (0.1 per cent offset)	33,500 psi
Ultimate strength:	91,200 psi
Reduction in area:	9 per cent
Elongation in one inch:	8 per cent

Mechanical properties for the chromium-uranium alloy were not available.

The variation of modulus of elasticity with temperature for the same material as reported by Hunter (18) is given in Fig. 1.

¹Average value for six consecutive cycles in tension.

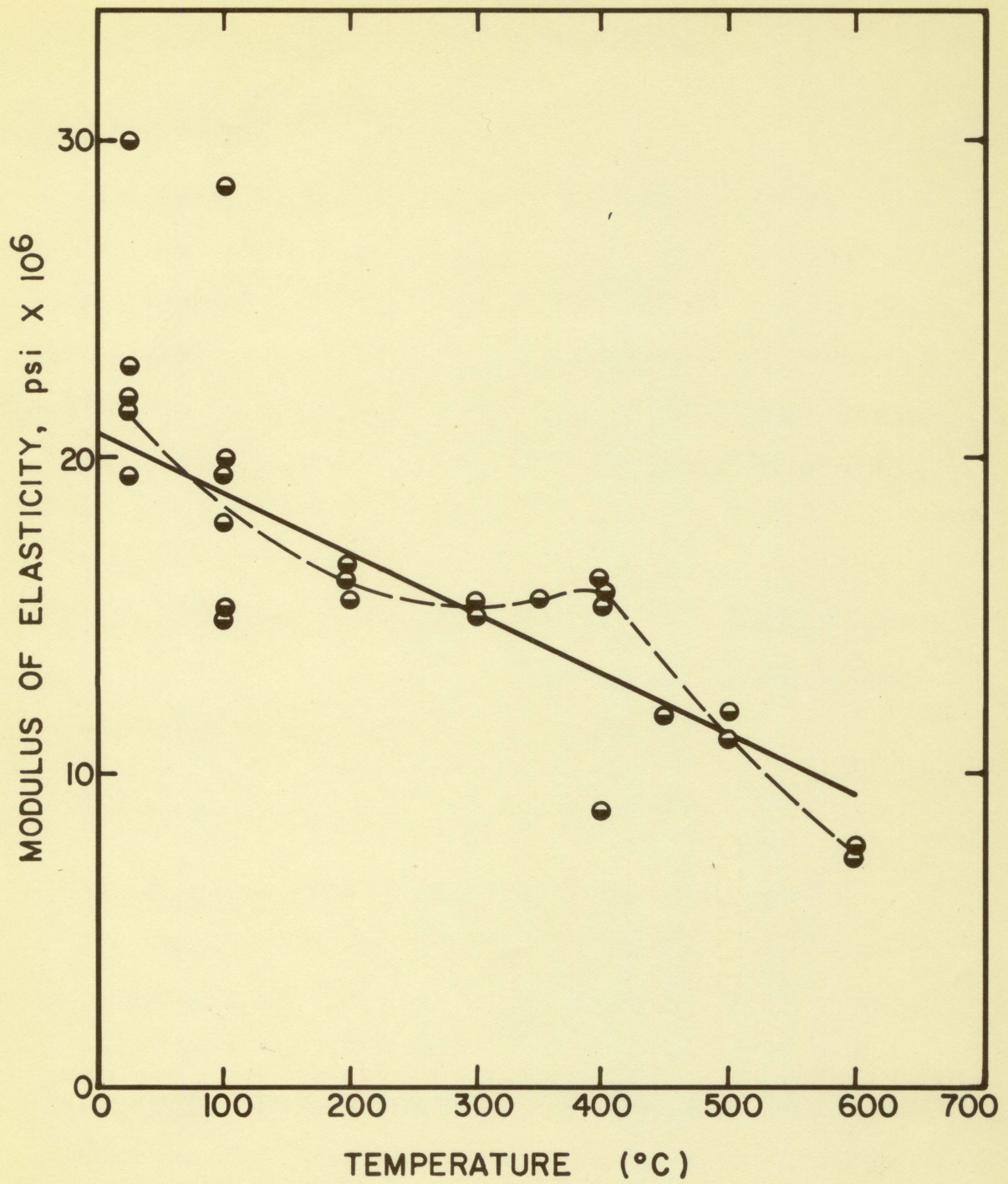


Fig. 1. Variation of modulus of elasticity with temperature

V. EXPERIMENTAL PROCEDURES AND APPARATUS

A. Specimen Preparation

1. Machining

The fatigue specimens were fabricated by sawing the uranium slugs longitudinally into four quarters. Each quarter was machined into a rod 4 inches long and $0.467 (+ 0.0005 - 0.0000)$ inches in diameter. The midsection of the rod was turned to $0.252 (\pm 0.001)$ inches in diameter, which corresponds to the minimum diameter of a fillet with a 2.5 inch radius. Machining techniques were employed which utilized special jigs and fixtures necessary to produce satisfactory finishes on fatigue sample test sections. Replaceable carbide tool tips aided in machining and were used in final turning operations, keeping undesirable tool marks to a minimum.

2. Polishing

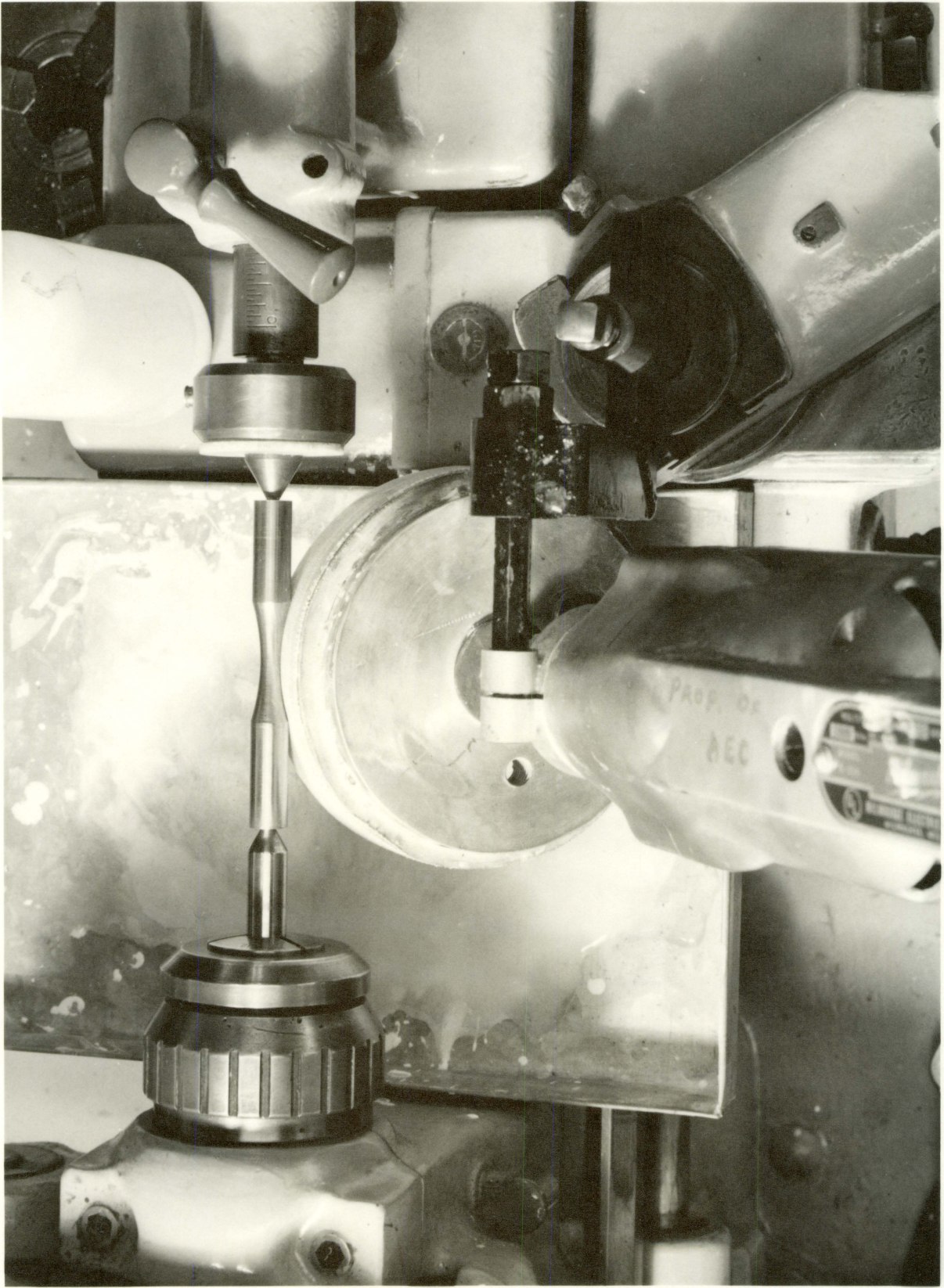
The procedure used in polishing the test section of a fatigue specimen was similar to that employed in preparing metallurgical samples for microscopic observation. Rough polishing was accomplished using silicon carbide paper, starting with 320 grit and finishing with 600. Final polishing was done with 600 grit levigated alumina followed by 0.3 micron synthetic sapphire (Linde A).

Commercial polishing equipment was not adaptable to the geometry of the fatigue specimen surface to be polished, thus it was necessary to construct suitable polishing apparatus. The apparatus consisted of a 5-inch diameter wheel 1 inch wide covered with a soft rubber pad (tire). The wheel served to hold 1-inch wide strips of the silicon carbide paper or velvet microcloth in a manner consistent with the geometry of the fatigue specimen fillet. With the fatigue specimen mounted between centers in a lathe and rotating, the rotating polishing wheel was held against the specimen fillet to produce the desired action. The direction of polishing as indicated by microscopic abrasion was adjusted by varying the relative angular velocities of the specimen and the polishing wheel. A cross-hatched pattern of abrasion desirable in polishing was accomplished by reversing the direction of rotation of the specimen. The polishing wheel was driven by an electric drill mounted on the tool post of the lathe. Power to the drill was supplied by a powerstat, providing speed variation of the polishing wheel. A working setup of the apparatus is shown in Fig. 2. Results using the method outlined were comparable to those obtained using conventional metallurgical equipment and techniques.

3. Encapsulating

Elevated temperature fatigue testing poses difficulties

Fig. 2. Arrangement for micro-polishing the test section of a fatigue specimen

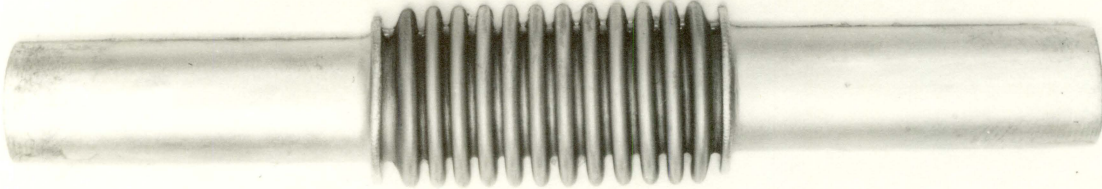
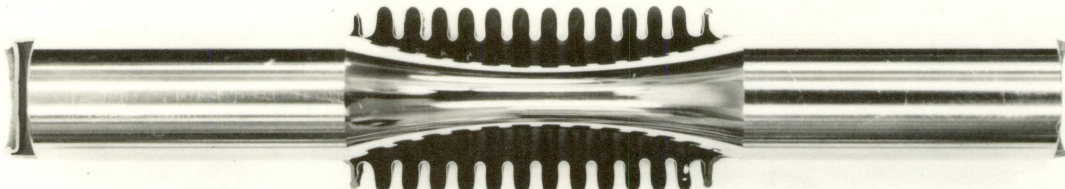
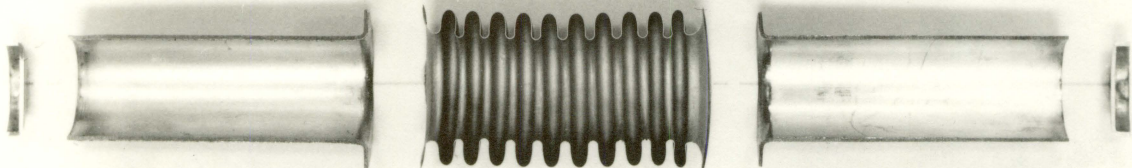
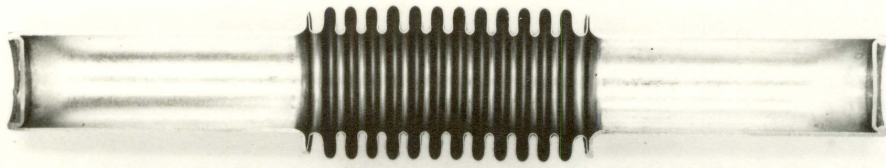


when the material is subject to oxidation. Uranium is such a material, suffering extensive oxidation even at room temperature. It follows then that protection from the atmosphere must be provided without interruption during fatigue testing for periods lasting as long as 4 months in endurance limit determinations. A procedure for protection was developed in the course of this investigation which involved encasement of the specimen in a flexible capsule capable of withstanding cyclic stresses and exposure to the atmosphere at temperatures in excess of 600° C (19).

The flexible capsule consisted of a section of bellows and closed lengths of tubing welded to each end. Fig. 3 shows a section assembly of the capsule components before and after fabrication and a view with the specimen included. The capsule was assembled and fabricated around the specimen using shielded arc welding techniques. Inert argon which serves to support the arc was ultimately sealed in the capsule with the specimen.

Type 310 stainless steel thin walled tubing (0.500 in outside diameter by 0.018 in wall) was cut into 1 9/16 in sections. One end of the tube was flared to 3/4 inch diameter in a spinning operation to match a corresponding flare on each end of the bellows. A slight taper was formed in the flared end of the tube. The caps which close off the end of the tube were punched and formed from 0.020 in

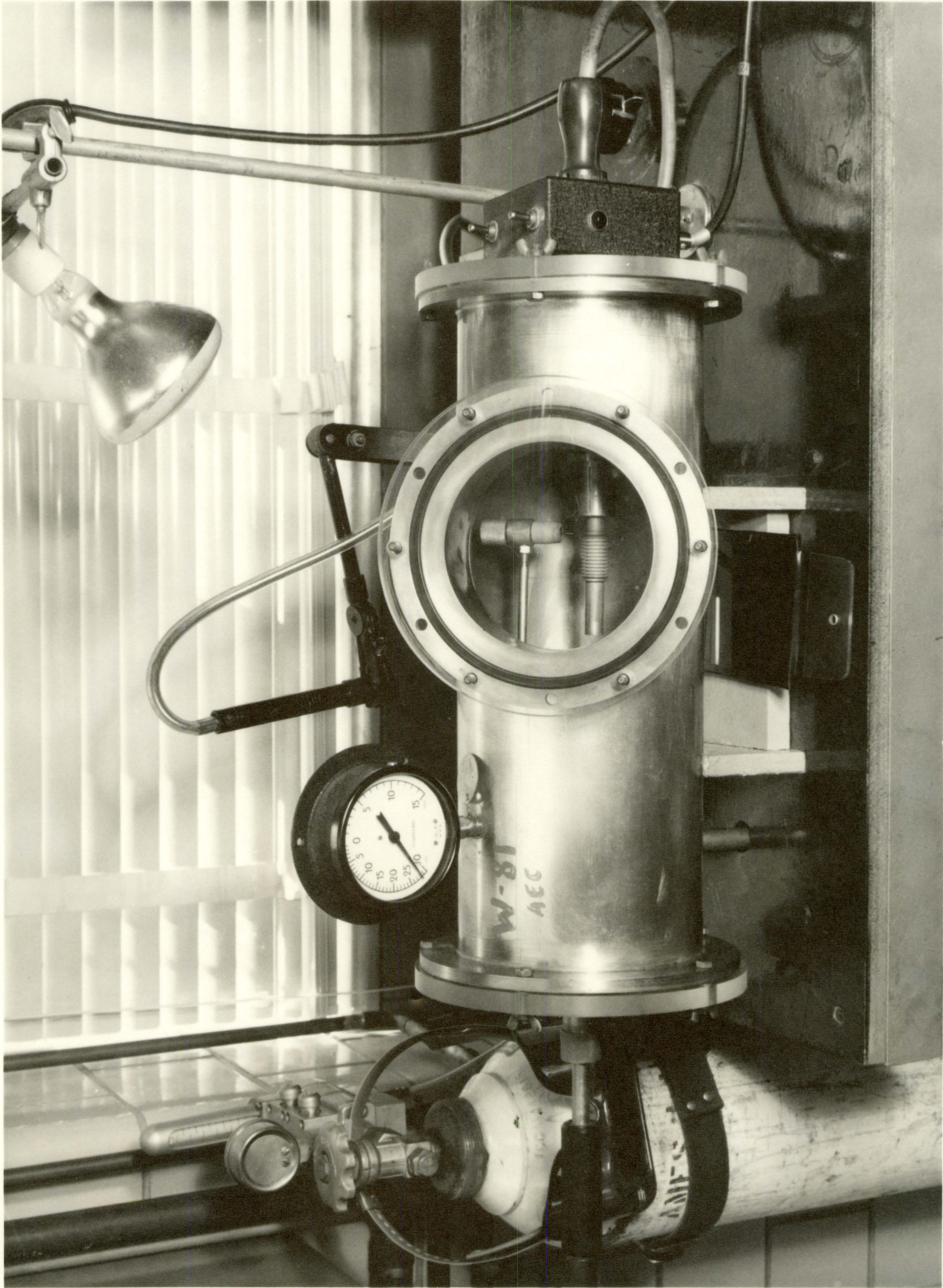
Fig. 3. Sectioned flexible capsule components before and after welding - the exterior of a flexible capsule and a sectioned assembly with specimen included



stainless steel sheet in a hand operated die. They were pre-welded to the flared tube before final assembly of the capsule. The flexible portion of the capsule was a stainless steel thin-walled seamless bellows, having a $1/2$ inch inside and a $3/4$ inch outside diameter. A section $1/4$ inch long, with 16 active convolutions was used. The end convolutions were formed to match the flare on the tube. Components of the flexible capsule were assembled by placing the bellows over the mid-section of the specimen and then pressing the flared tube onto the specimen's shoulders. The press fit of the flared tube on the specimen shoulders was necessary to insure good mechanical coupling with the fatigue machine collets. In this state the capsule assembly was sealed in a welding chamber specially designed for this purpose.

The welding chamber was a 6-inch diameter tube mounted parallel to its longitudinal axis with a combination sight glass and access port on one side. Power connections were made through plexiglass disks which provided insulation and constituted the ends of the chamber. The work was held and rotated by a drive mechanism providing constant angular rotation at speeds from $1/3$ to 3 rpm, as shown in Fig. 4. The electrode remained stationary during welding operations. Its position was adjustable from outside the chamber. A "Y" fitting provided facilities for evacuation, purging and

Fig. 4. Welding apparatus



venting the system. A mechanical forepump was used to evacuate the chamber, providing pressures consistent with the impurity content of the purging gas (several microns of mercury). The power supply used consisted of a Miller electric welder rated at 1.5 to 15 amperes dc, connected in parallel with a Miller high frequency arc starter. In this remote application the high frequency arc facilitated starting the dc arc without touching the electrode to the delicate work. A block diagram of the apparatus is given in Fig. 5.

B. Testing

1. Fatigue

The fatigue testing machines used were constructed at the Ames Laboratory and were of the simply supported rotating beam type, equipped with furnaces and controllers for elevated temperature testing. Eight machines were available for the investigation.

Before a particular test series was started the fatigue machine to be used was balanced and calibrated for the proper temperature setting.

The method of balancing involved inserting a rigid shaft (1/2 inch diameter drill stock) into the fatigue machine collets and recording the elevation of the rotating beam by means of a low power telescope and a reference target. The

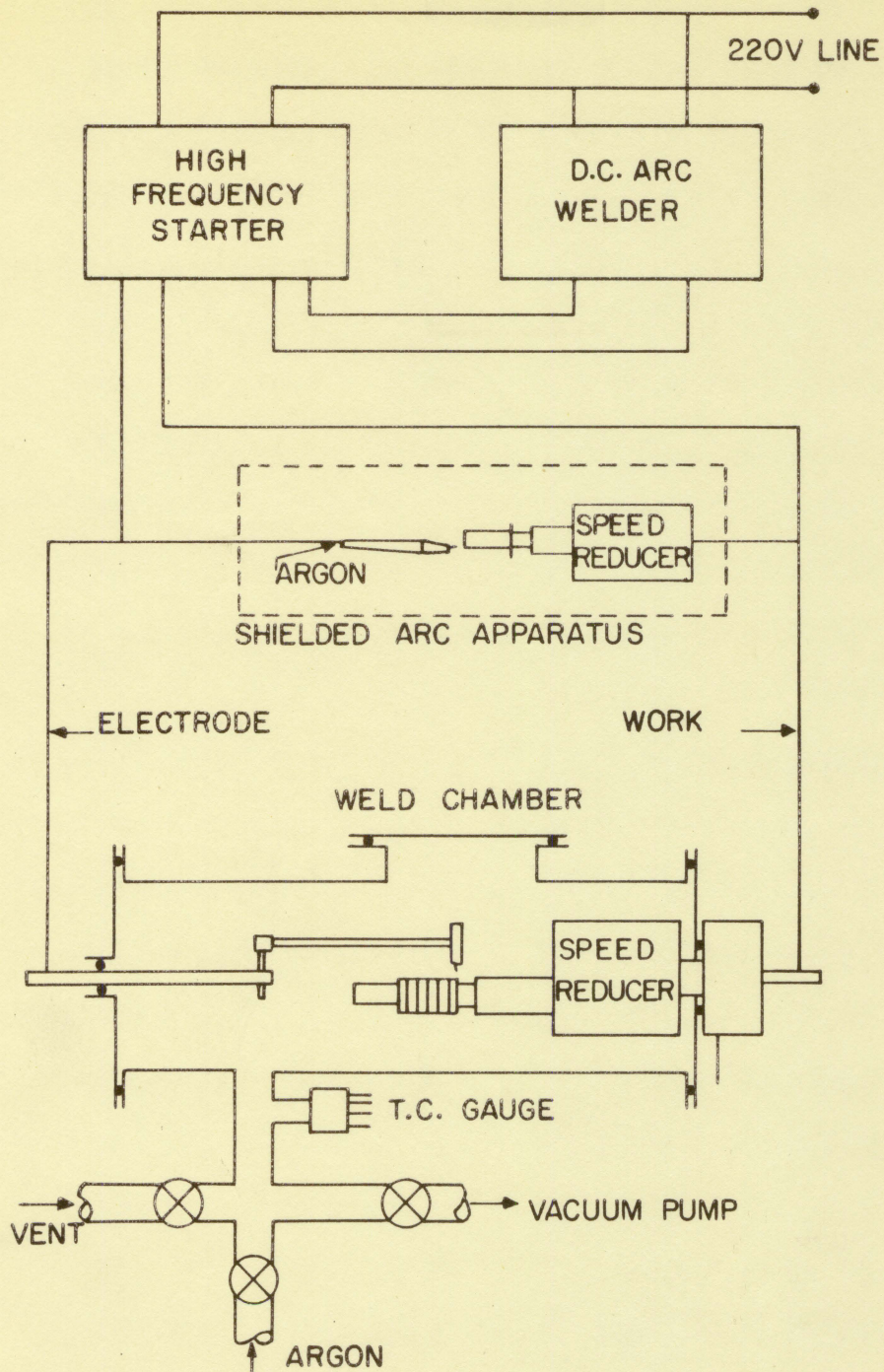


Fig. 5. Diagram of the welding equipment

rigid specimen was then replaced by two halves of the uranium specimen and the beam was adjusted to the observed target reference by an appropriate addition of pan weights (± 0.02 lb.). Both references were taken with the beam rotating, having attained an equilibrium flow of support bearing lubricant.

The test temperature was established using a thermocouple placed approximately $1/16$ inch from the minimum test section diameter of the specimen. The furnace controller was set at a corresponding temperature by adjustment of a potentiometer and powerstat. Temperature calibration was made with the specimen in motion, allowing approximately 48 hours for temperature equilibrium to be reached. The observed variation in temperature at conditions of equilibrium was $\pm 2^\circ \text{C}$.

The procedure for starting a test was as follows. The specimen was mounted in the machine and brought up to temperature. The specimen was then set to rotating with an initial 20 per cent greater drive motor control setting than would be necessary to maintain a normal test speed. This was done to pass as rapidly as possible through the resonant frequencies (3500 to 4500 rpm) of the fatigue machines; after which the speed was carefully reduced to 5000 rpm. Load weights were applied after temperature equilibrium had been reached with the specimen in motion. A count down procedure was used in

synchronizing the application of weights and the zeroing of the revolution counter.

The machines were automatically shut off upon fracture or a given pre-set amount of beam deflection.

2. Tensile

Axial cyclic tensile tests were performed on a 60,000 lb Baldwin-Southwark hydraulic universal testing machine with a Tate-Emery Load Indicator. A Baldwin-Southwark microformer extensometer with a 1-in gage length and a multiplication ratio of 1000 to 1 was used in conjunction with a stress-strain recorder. The tensile tests were conducted at room temperature.

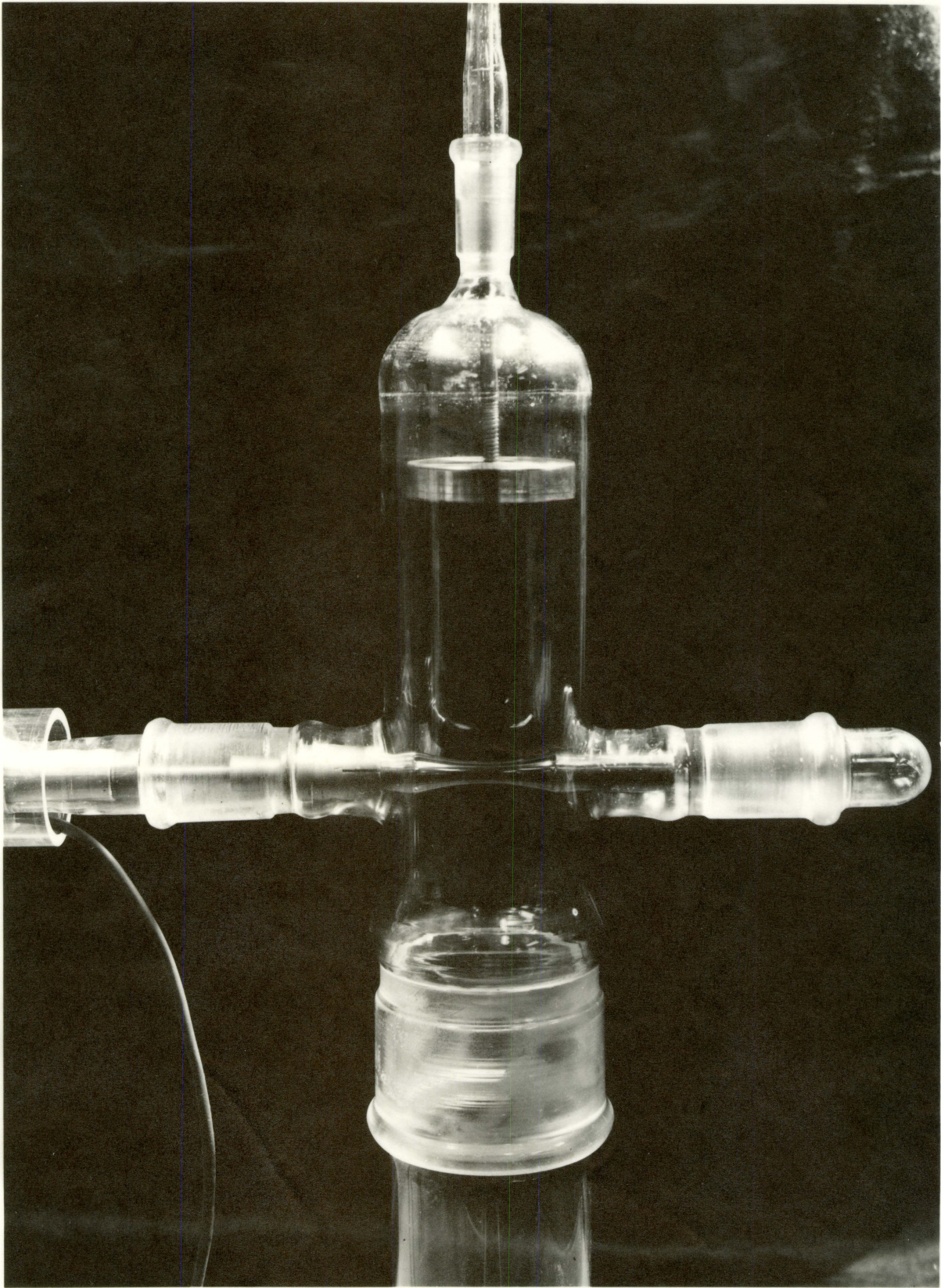
C. Microanalysis

1. Etching

Ionic bombardment was used to produce an etched surface on the test section of the fatigue specimen to enable study of fatigue damage of microstructure. Ionic bombardment had particular advantages over the more common chemical and electrolytic etches, and produced well delineated grain boundaries. Chemical and electrolytical etchants which were tried caused severe preferential attack on impurities, produced excessive staining and gave rise to a questionable corrosive chemical environmental history.

The techniques and basic equipment employed were described by Carlson (20). Briefly, the process involved the removal of surface material by the bombardment with argon ions which were accelerated through a voltage potential in a glow discharge tube. Direct application of available equipment could not be made because of the geometry of the fatigue specimen. Apparatus was designed and constructed to permit placement of the fatigue specimen in the path of the ionized beam. By means of a rotating seal the fatigue specimen was rotated in the beam, having its longitudinal axis normal to the path of the accelerated ions. The specimen served as the cathode with the appropriate electrical connections being made through the rotating seal. A voltage potential of 6 kv was required to produce the desired results, drawing a current of 5-10 milliamperes. A photograph of the apparatus is shown in Fig. 6. The procedure followed was to evacuate the discharge tube to a minimum forepump pressure, purge with argon, then adjust a controlled argon leak to maintain approximately 15 microns of mercury pressure. Voltage was then gradually applied in a manner to maintain the 15 microns of mercury pressure. This process lasted for an incubation period of about 15-30 minutes. Initiation of etching was indicated by an abrupt drop in current and sudden darkening of the glass discharge tube. Etching was completed in approximately 15 minutes from the time of initiation, after

Fig. 6. Ionic bombardment etching chamber

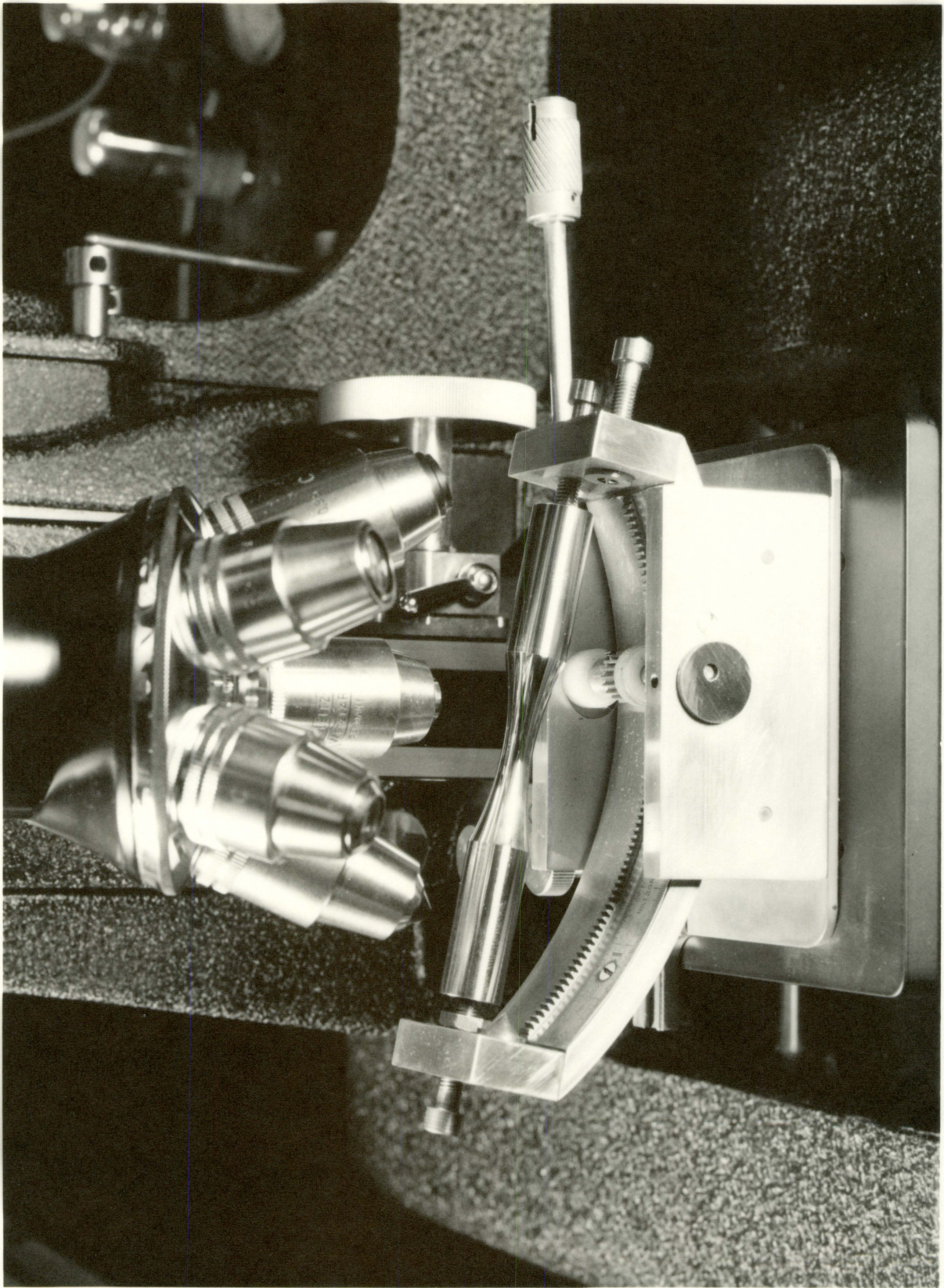


which a cooling period of at least an hour was allowed before removing the specimen.

2. Microscopy

Microscopic observations were made using a metallurgical microscope with photographic attachments and carbon arc illumination. In the study of fatigue damage on microstructure it was desired to record the location of a particular observation relative to a given reference on the fatigue specimen. The conventional microscope stage was found entirely unsuitable due to the geometry of the area to be viewed. A stage was constructed which provided referenced access to any area on the test section of a specimen. It was designed so that the plane of the area being viewed always remained normal to the line of sight of the objective and at a fixed distance from it. The stage is shown in Fig. 7.

Fig. 7. Microscope stage



VI. DISCUSSION OF VARIABLES INTRODUCED BY TECHNIQUES

The resisting moment developed by the flexible capsule relative to the specimen was evaluated, since it was considered significant in determining the actual stress to which the specimen was subjected. A direct analytical method of correlating the relative moments was not apparent due to the variation of cross-section for both the capsule and the specimen as a function of distance along the longitudinal axis. A graphical method was applied which showed that the moment developed by the capsule was about 0.1 per cent of the total resisting moment. The effect was neglected in calculating the stress in the specimen.

It was observed that a change in temperature of the argon gas sealed in the capsule would be accompanied by a change in pressure, resulting in an axial stress which would be transferred through the specimen. The tensile stress was calculated to be 380 psi in an extreme case, for a temperature change from 25 to 600° C. The elimination of the effect by several methods was considered, resulting in serious limitations on the welding techniques. No corrective action was taken, since the effect was significant only at high temperatures, where the flexural stresses were low.

Press fitting the capsule ends onto the shoulders of a specimen introduced a short time compressive stress. The

magnitude of the stress was calculated in an experiment using SR-4 strain measuring equipment. The stress due to the press fit of the capsule on the specimen shoulders was adjusted on the basis of machining tolerances so that it did not exceed 1500 psi. This magnitude of stress did not seem to warrant special consideration relative to the history of the material.

VII. RESULTS

A. Presentation of S-N Data

The test conditions and environments were maintained constant, as closely as possible, for all of the S-N determinations of the investigation. Since eight elevated temperature fatigue testing machines were available for the investigation, tests at a given temperature were conducted on one particular machine. Each machine was checked for proper temperature calibration periodically using the same standard thermocouple.

Stress calculations were made using the flexure formula-Eq. 4, which is subject to the limitations as discussed by Murphy (21).

$$S_f = \frac{M c}{I} \quad (4)$$

where

S_f = flexural stress (psi, ksi = 1000 psi)

M = moment

= $L P$ (in-lb)

L = moment arm (in)*

P = load (lb)

c = $d_o/2$

d_o = minimum test section diameter (in)

*The moment arm for all simply supported testing machines was fixed at eight inches.

I = moment of inertia of the cross-sectional area

$$= \frac{\pi d_o^4}{64} \text{ (in}^4\text{) from which}$$

$$S_f = \frac{256}{\pi} \frac{P}{d_o^3} \quad .$$

Failure is designated in this investigation by a given amount of specimen deflection determined by the automatic fatigue machine shut-off. In general it was observed that for low stresses failure by complete separation (fracture) occurred before critical deflection. At high stresses, particularly at elevated temperatures, critical deflection predominated as the mode of failure.

1. Normal uranium

The data of S-N results are listed in Tables 6 and 7. As was noted previously by other authors the properties of uranium vary considerably depending on prior history, fabrication, impurities, and the like. Here too, obvious discrepancies in the data occur which may be attributed to structural differences in the uranium slugs. For this reason a material designation number is included to identify a particular specimen relative to the slug from which it was machined. All of the normal uranium specimens were machined from 4-inch slugs, yielding four specimens each. S-N diagrams plotted from the data at the various temperatures are given in Figs. 8 through 12.

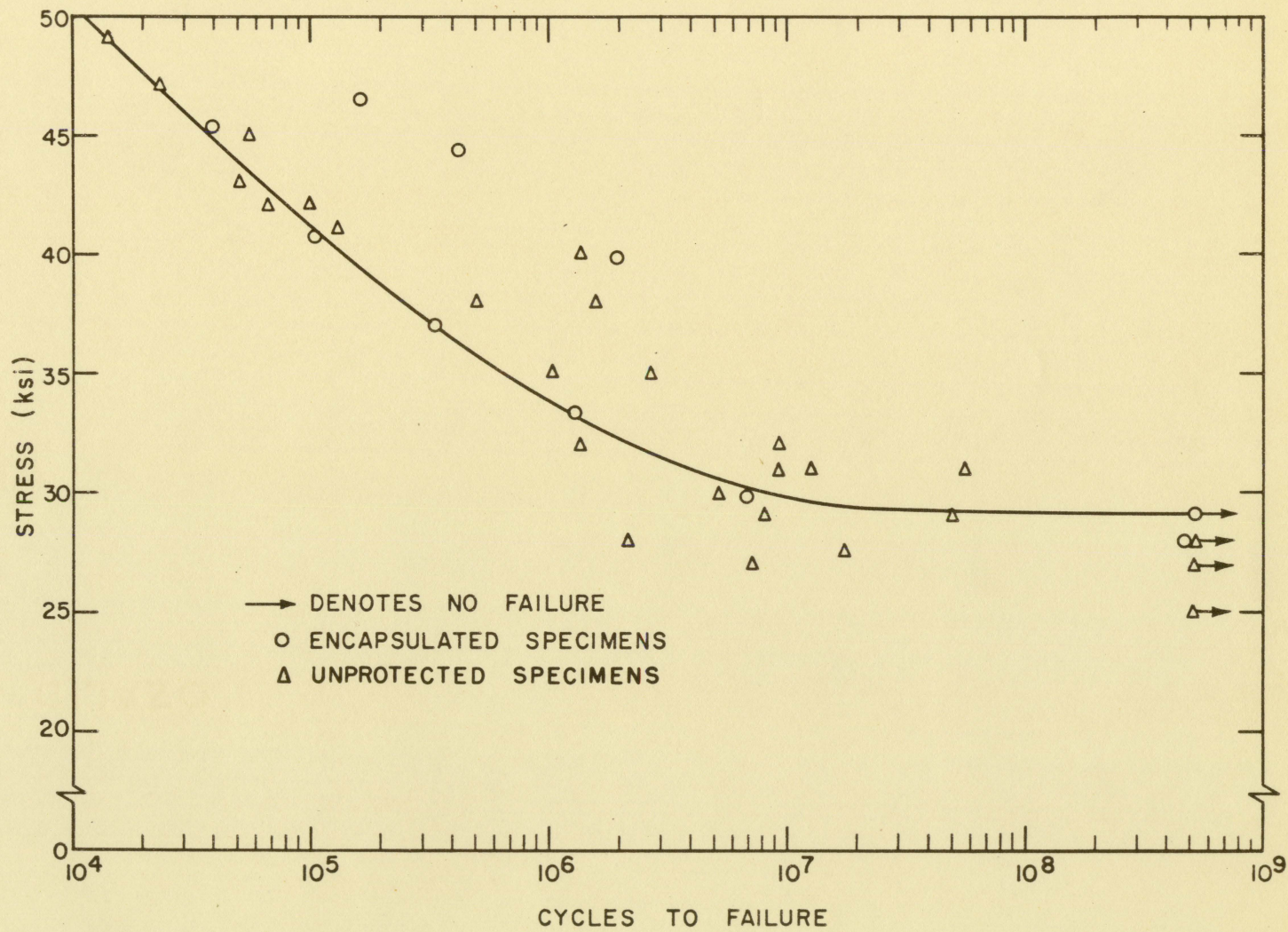


Fig. 8. S-N diagram for normal uranium at 25° C (room temperature)

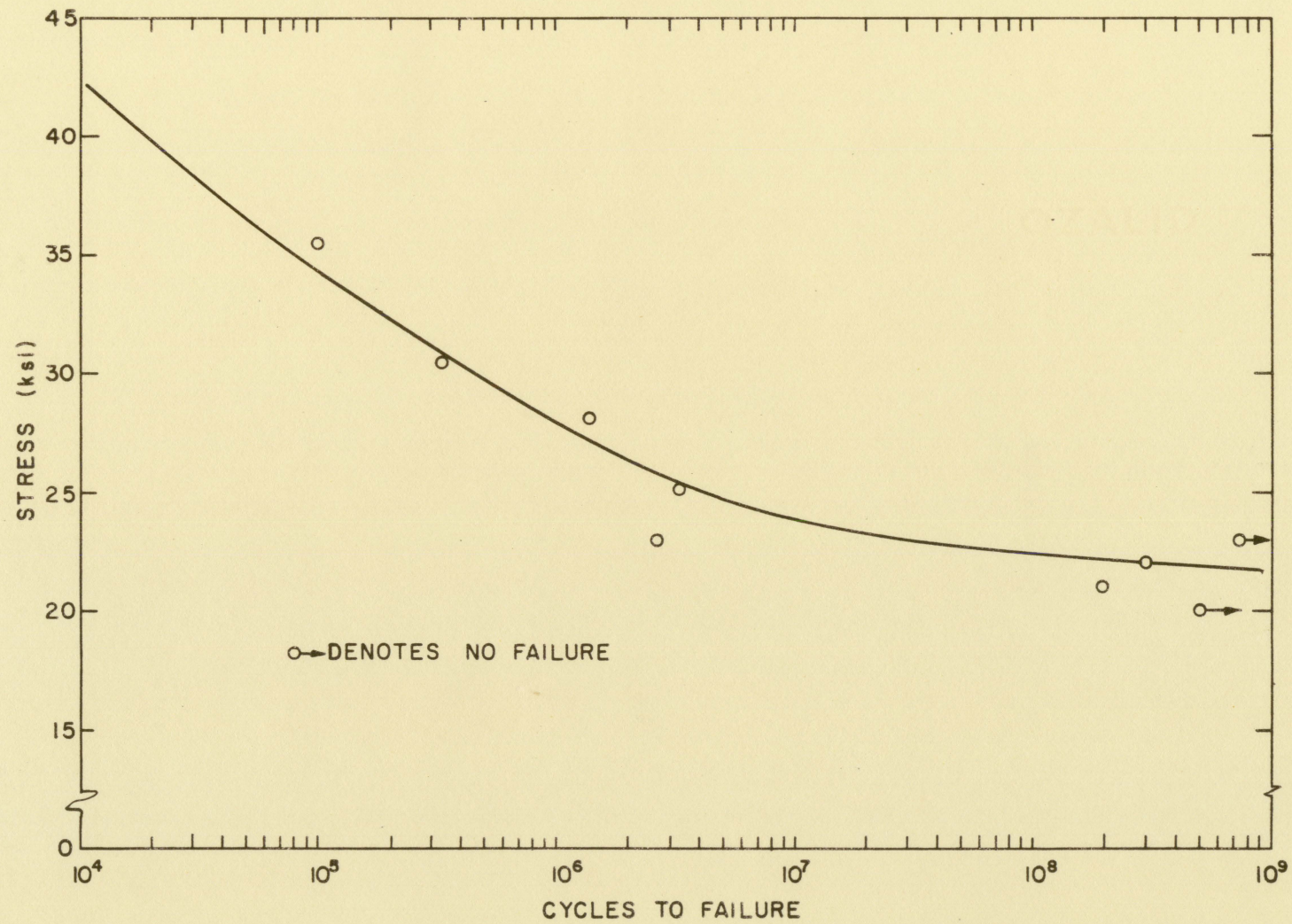


Fig. 9. S-N diagram for normal uranium at 150° C

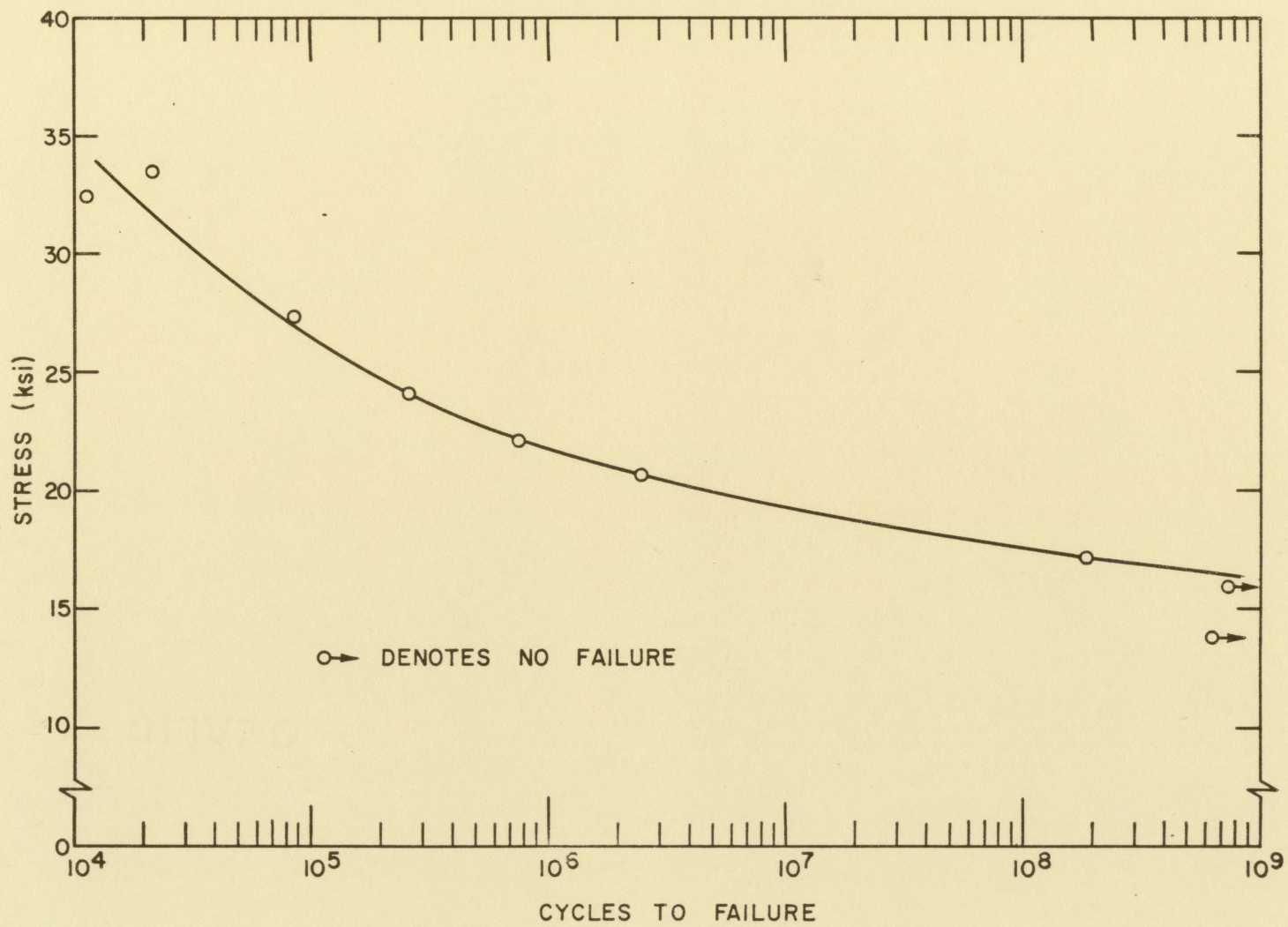


Fig. 10. S-N diagram for normal uranium at 300° C

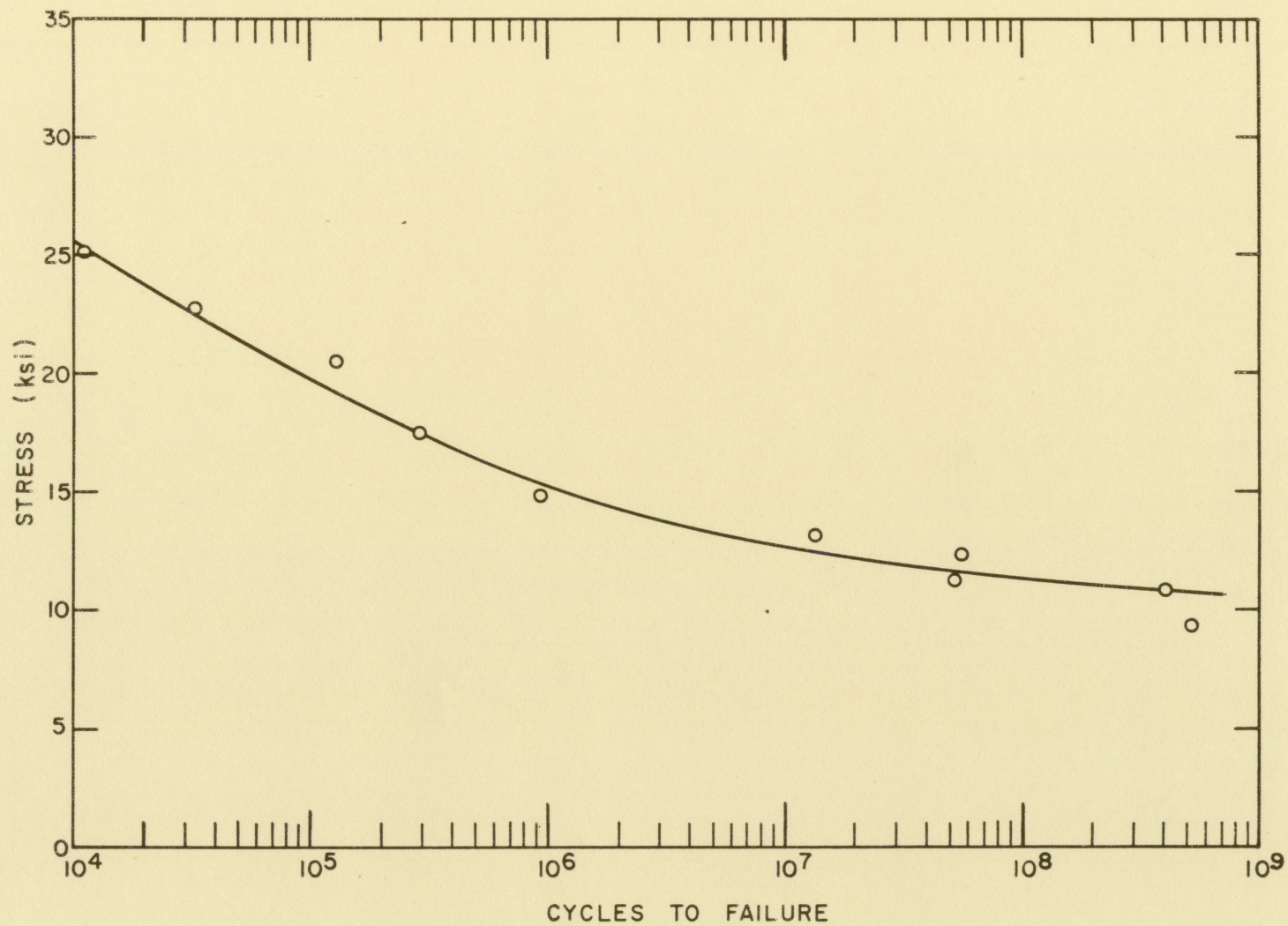


Fig. 11. S-N diagram for normal uranium at 400° C

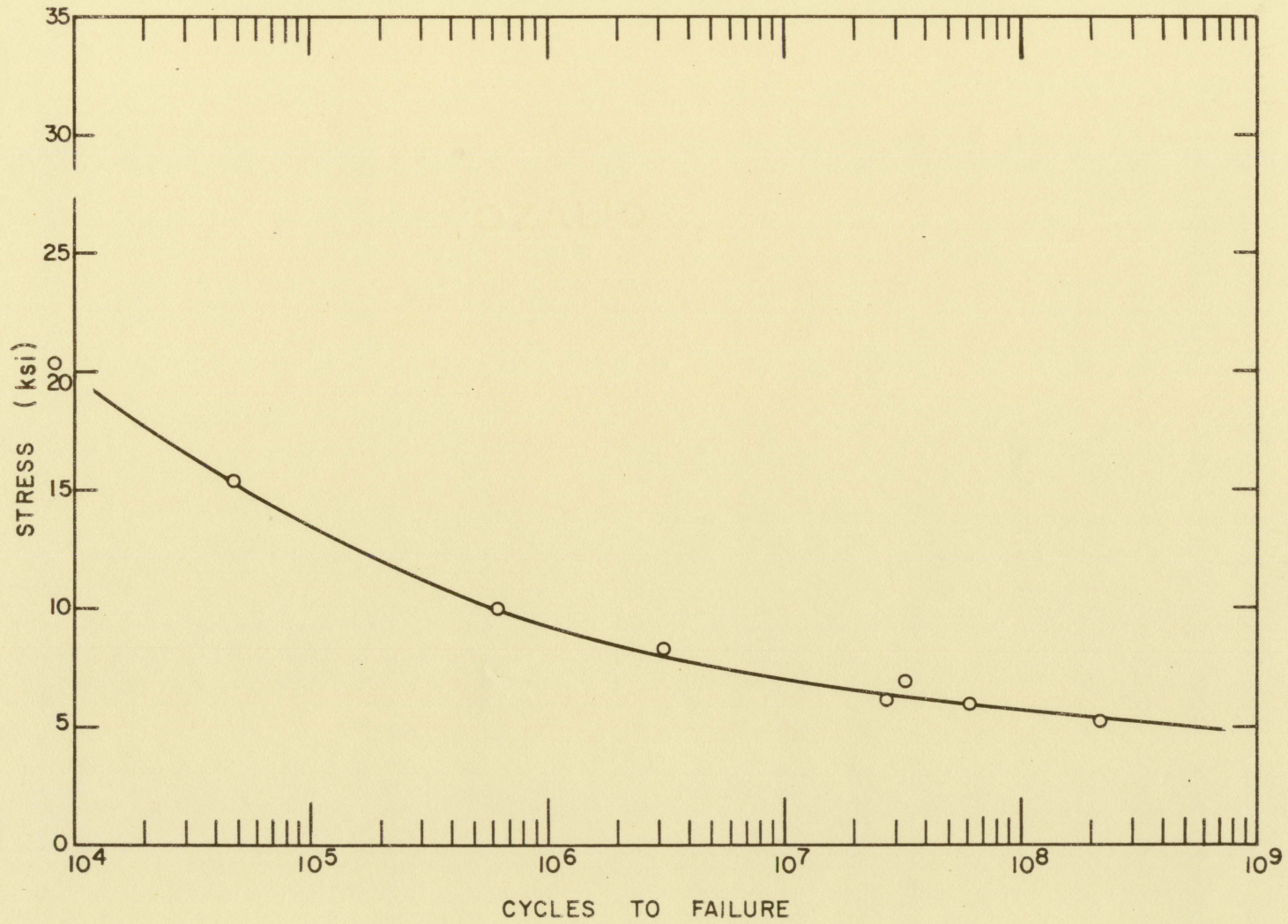


Fig. 12. S-N diagram for normal uranium at 500° C

In order to determine the effect of encapsulation on fatigue results, both encapsulated and unprotected specimens were run at room temperature to provide a comparison. Unprotected specimens were tested in cantilever type rotating beam machines, whereas encapsulated specimens tested at room temperature were subjected to the same testing procedure as elevated tests. Results are as indicated in Fig. 8.

The maximum stress which can be applied indefinitely without producing failure is commonly called the endurance limit. Here, endurance limit (S_e) is associated with the maximum stress applied for 500 (10^6) cycles without producing failure. The range of stress between the maximum stressed specimen which survived 500 (10^6) cycles, and the minimum stressed specimen which did not survive is given in Table 1 and plotted in Fig. 13.

Table 1. Endurance limits for normal uranium, 25 to 500° C

Temperature (° C)	Stress range (ksi)
25	29.3 - 30.0
150	20.1 - 22.2 ^a
300	16.0 - 17.2
400	9.4 - 10.7
500	5.1 - 5.6

^aAdjusted for continuity.

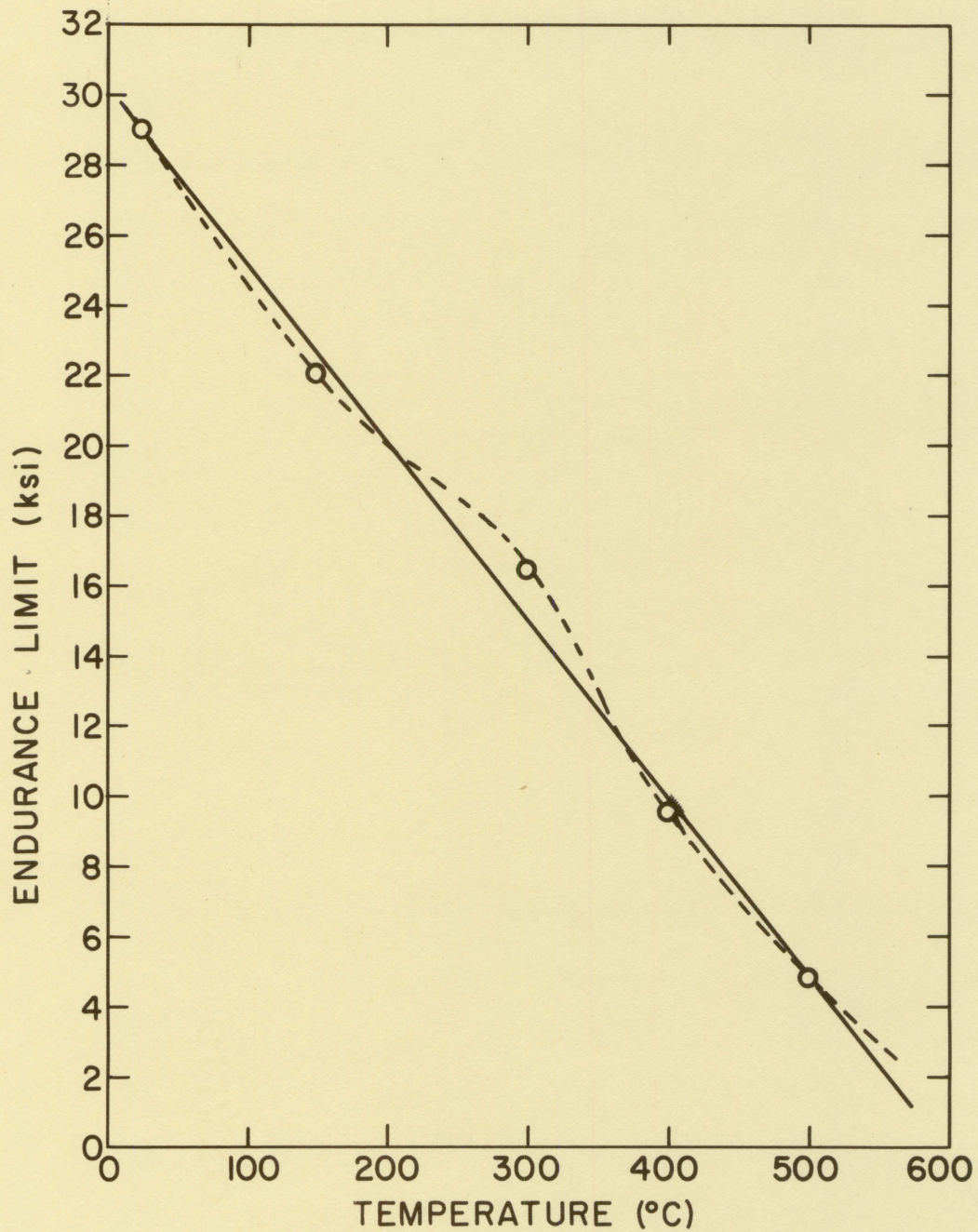


Fig. 13. Variation of endurance limit with temperature for normal uranium

2. Chromium-uranium alloy

S-N data are tabulated in Table 8 and plotted in Figs. 14 through 19.

Room temperature results were obtained from unprotected specimens in the same manner as for normal uranium. Alloyed specimens were machined from eight-inch slugs, yielding eight specimens each. There did not appear to be structural differences in alloyed slugs of such magnitude as was noted for normal uranium.

The availability of the chromium-uranium alloy was limited, which accounts for the small number of specimens tested, especially at room temperature and 400° C.

Endurance limit stress ranges are listed in Table 2 and plotted in Fig. 20.

Table 2. Endurance limits for chromium-uranium alloy

Temperature (° C)	Stress range (ksi)
25	49.0 - 50.0
150	37.4 - 39.5
300	34.0 - 34.9
400	- 20.4
500	9.0 - 10.2
600	3.6 - 4.1

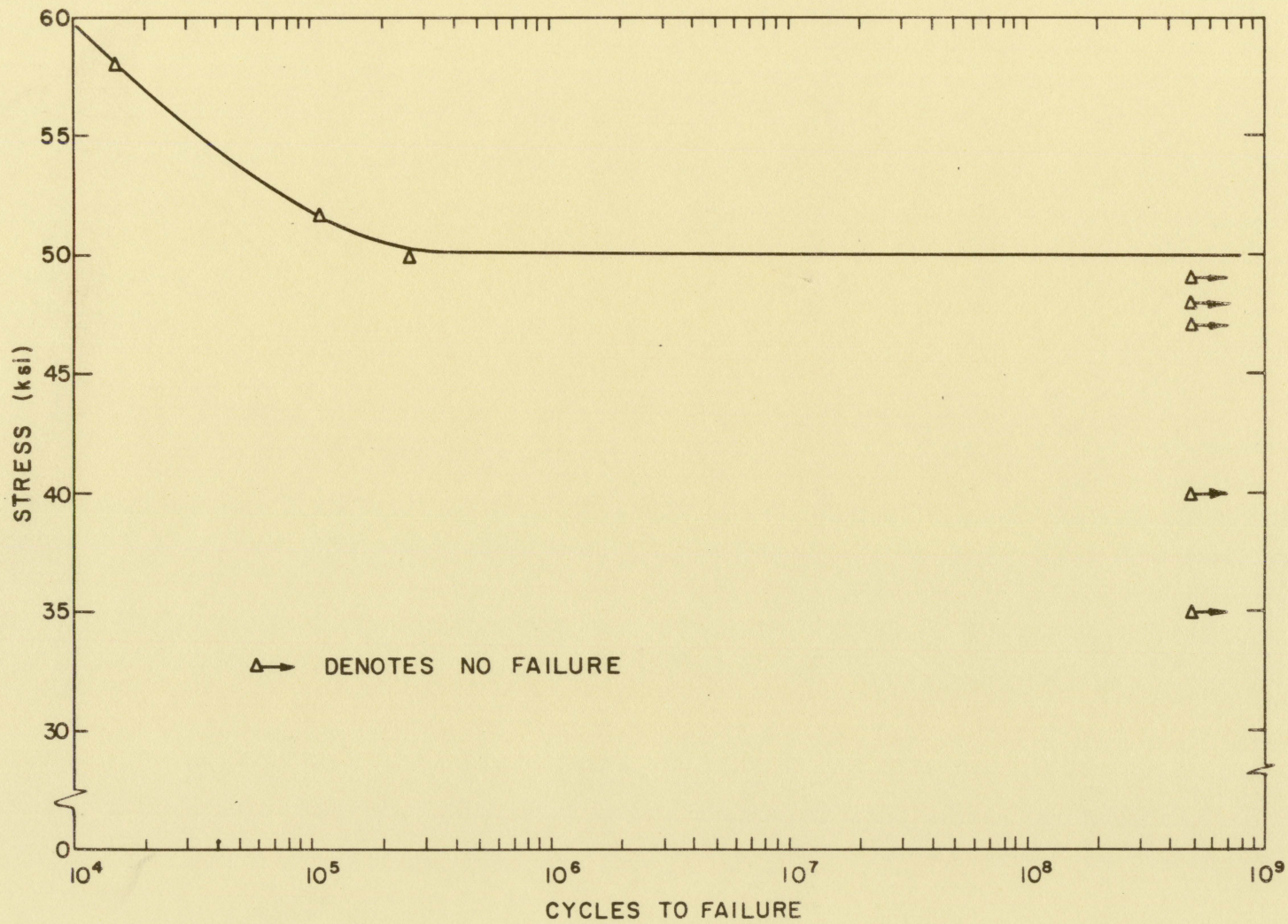


Fig. 14. S-N diagram for chromium-uranium alloy at 25° C (room temperature)

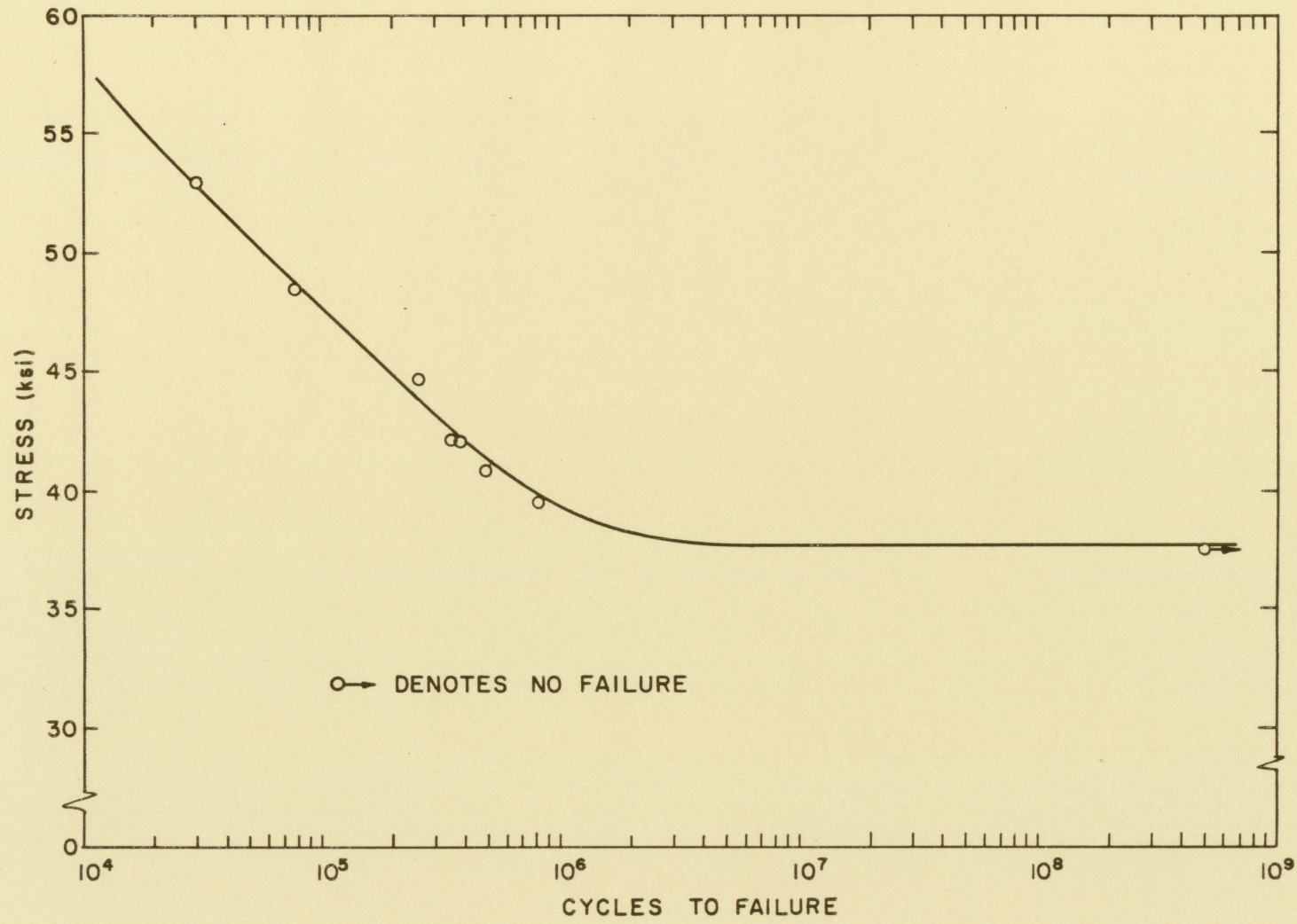


Fig. 15. S-N diagram for chromium-uranium alloy at 150° C

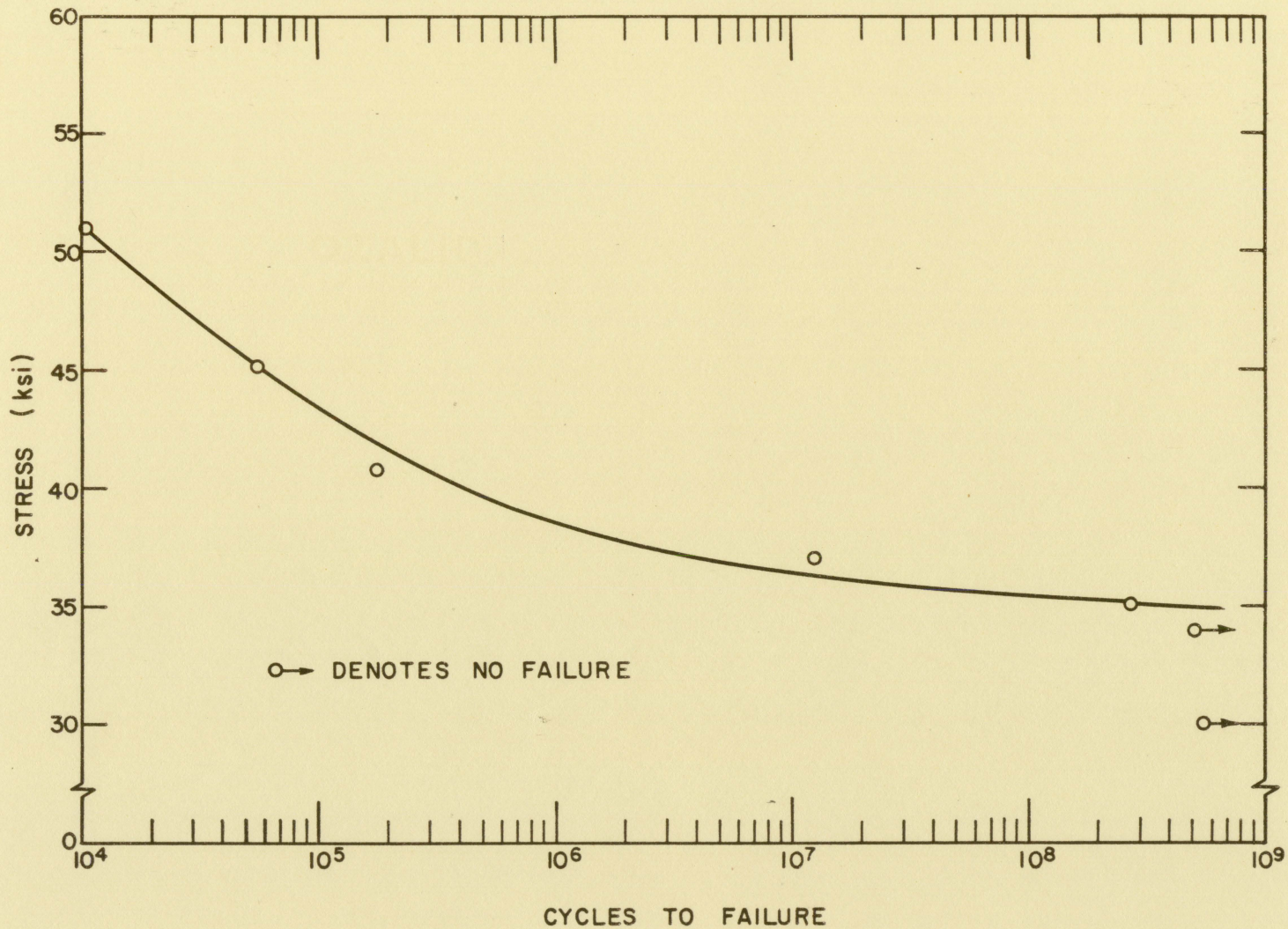


Fig. 16. S-N diagram for chromium-uranium alloy at 300° C

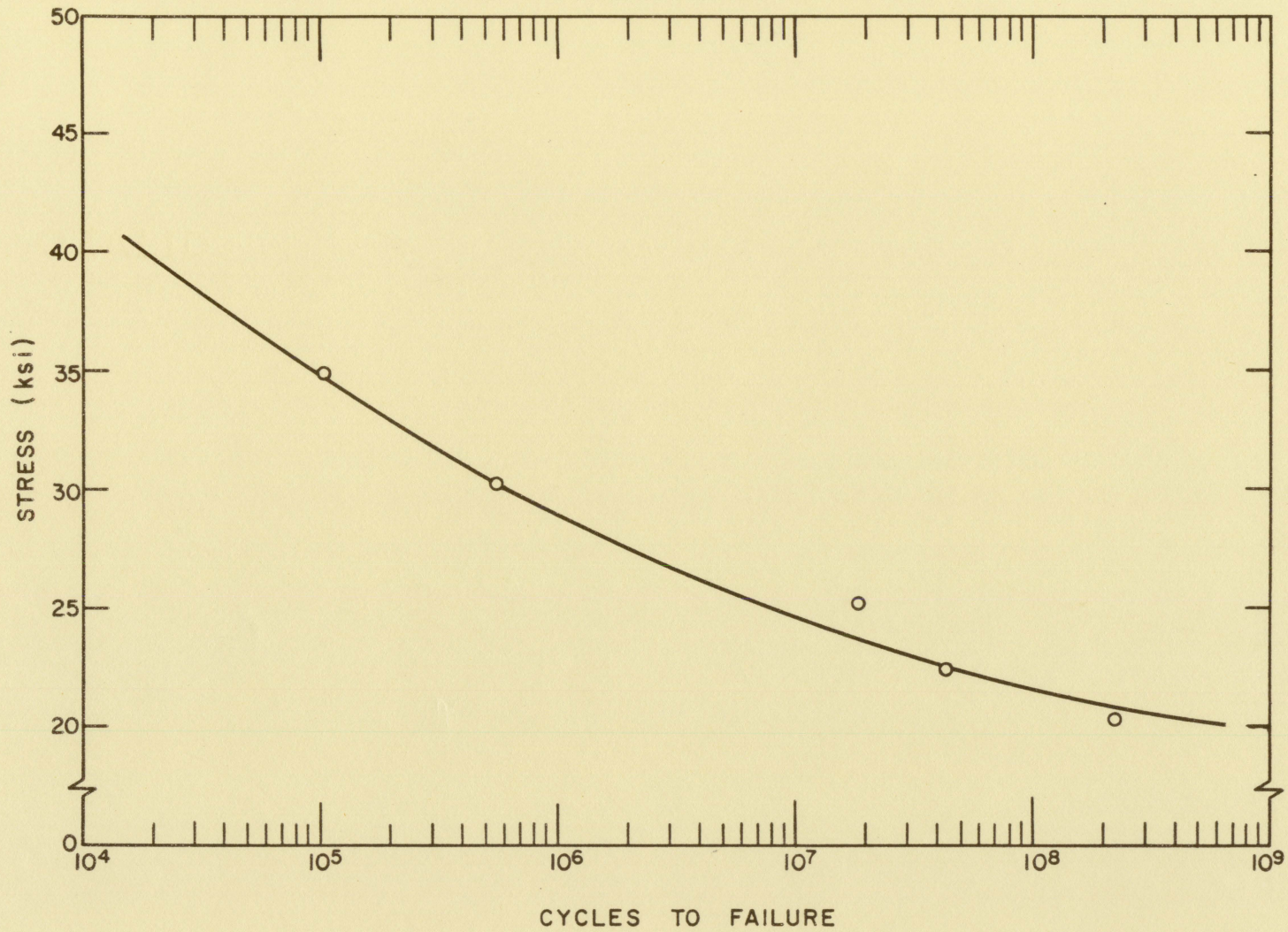


Fig. 17. S-N diagram for chromium-uranium alloy at 400° C

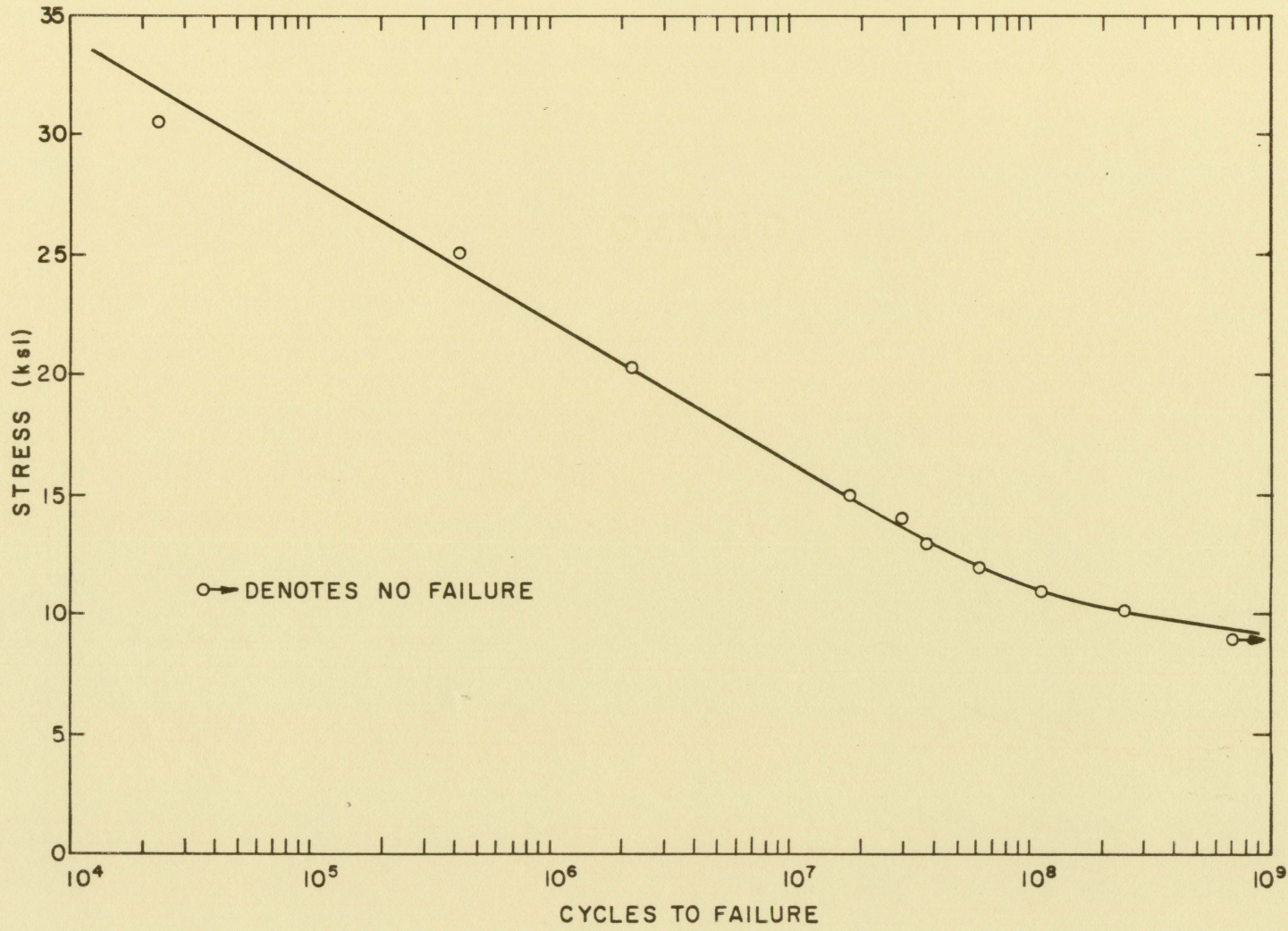


Fig. 18. S-N diagram for chromium-uranium alloy at 500° C

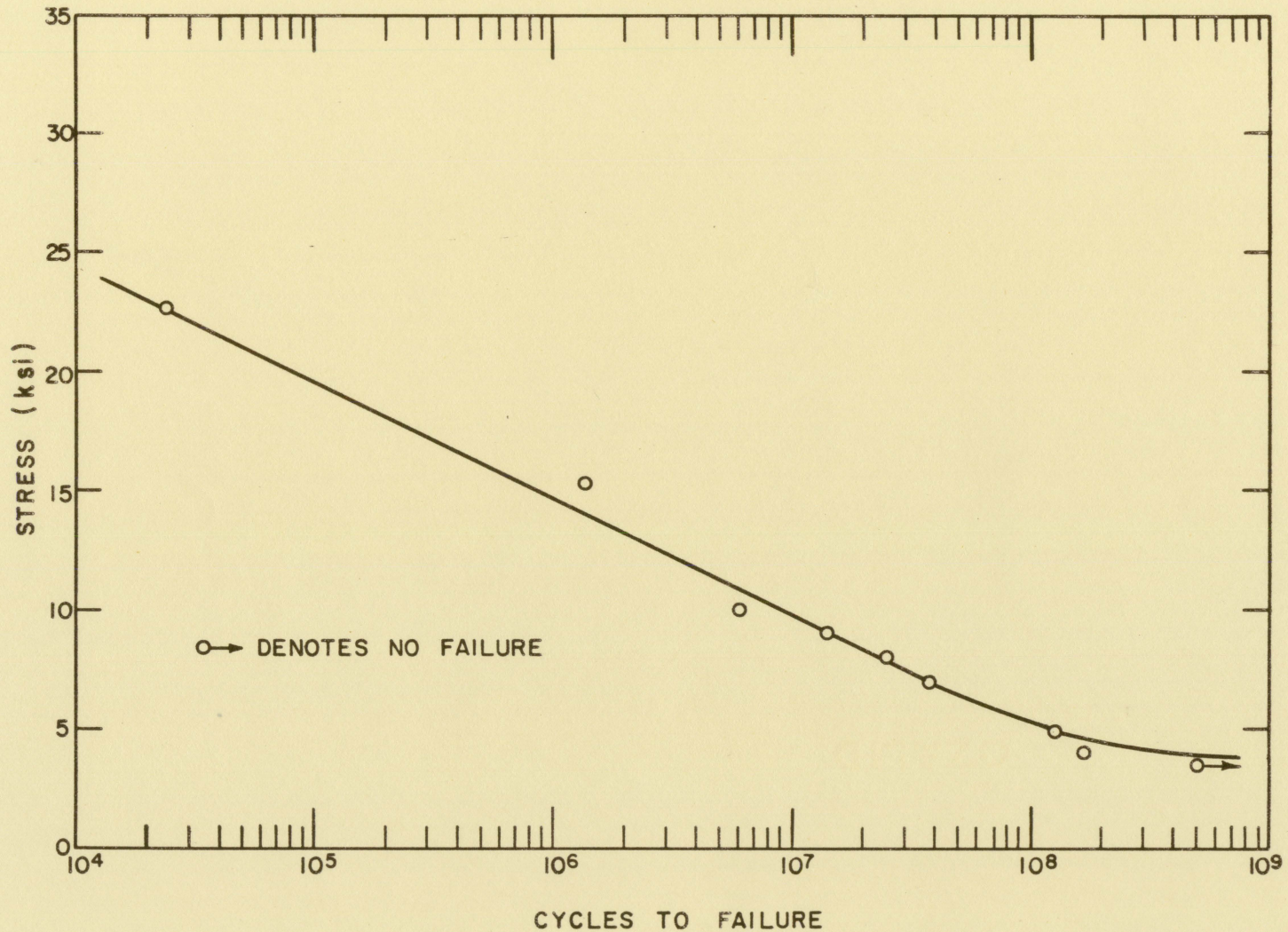


Fig. 19. S-N diagram for chromium-uranium alloy at 600° C

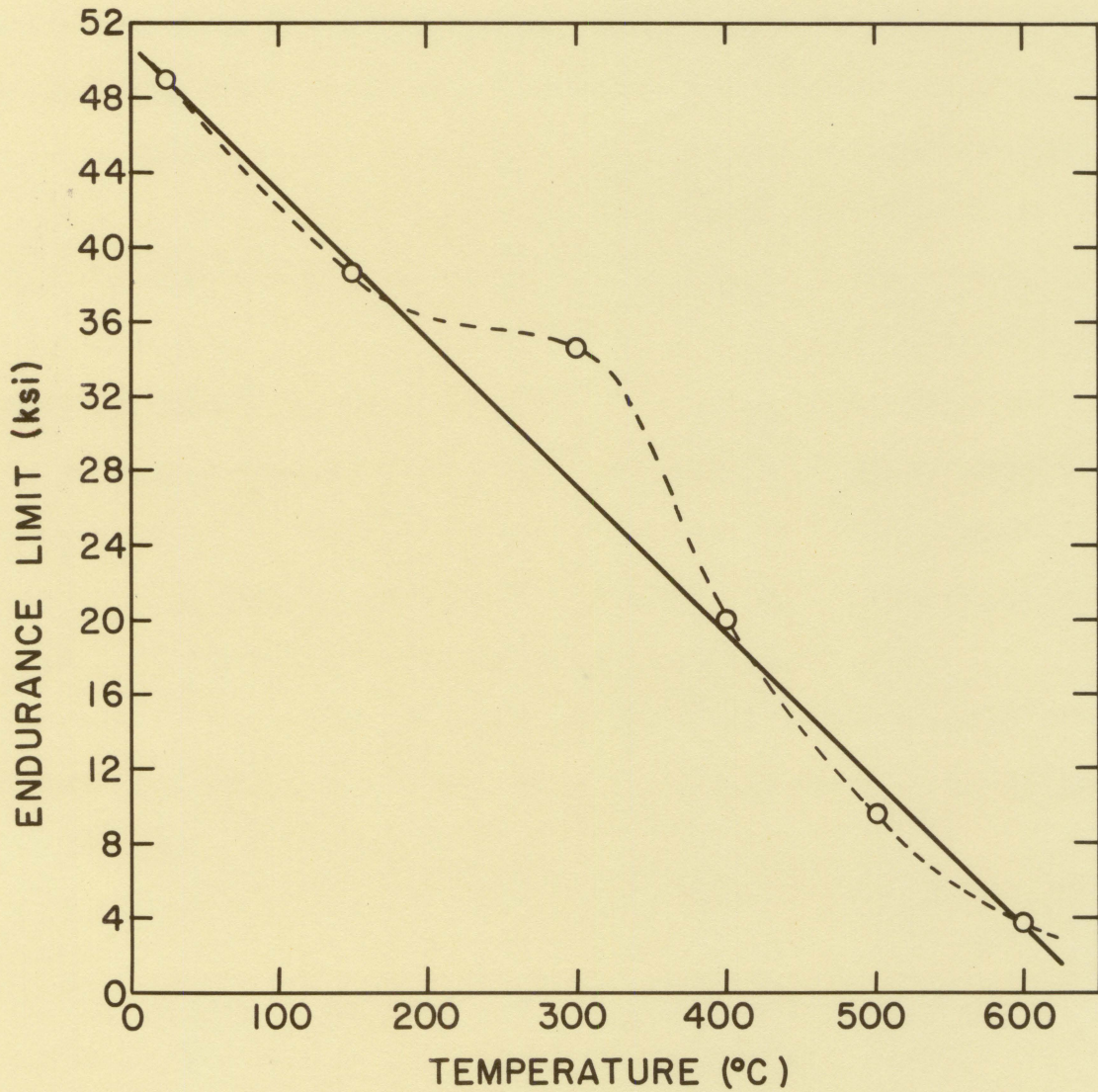


Fig. 20. Variation of endurance limit with temperature for chromium-uranium alloy

B. Statistical

In order to determine quantitatively the degree of scatter associated with the experimental testing program employed in the investigation, fourteen specimens were tested under the same conditions. The technique followed was similar to that outlined by Freudenthal (9). Table 9 lists the ordered results and the respective plotting positions of the specimens tested for scatter determination. With a limited number of specimens tested it is difficult to establish the frequency density relationships from which the calculations of errors are governed. To obtain an approximation for the frequency density of cycles to failure a cumulative distribution curve was plotted from the data, as shown in Fig. 21. The logarithm of cycles to failure was plotted versus cumulative relative frequency, X^1 , on probability paper. X^1 is given by the ratio

$$X^1 = \frac{m}{n + 1} \quad (5)$$

where m is the rank of n ordered observations. Since X^1 corresponds to the area under the normal distribution curve bounded by appropriate limits, the normal distribution curve may be obtained from the cumulative distribution curve.

$$X^1 = \int_{-\infty}^{\infty} X \, dx \quad (6)$$

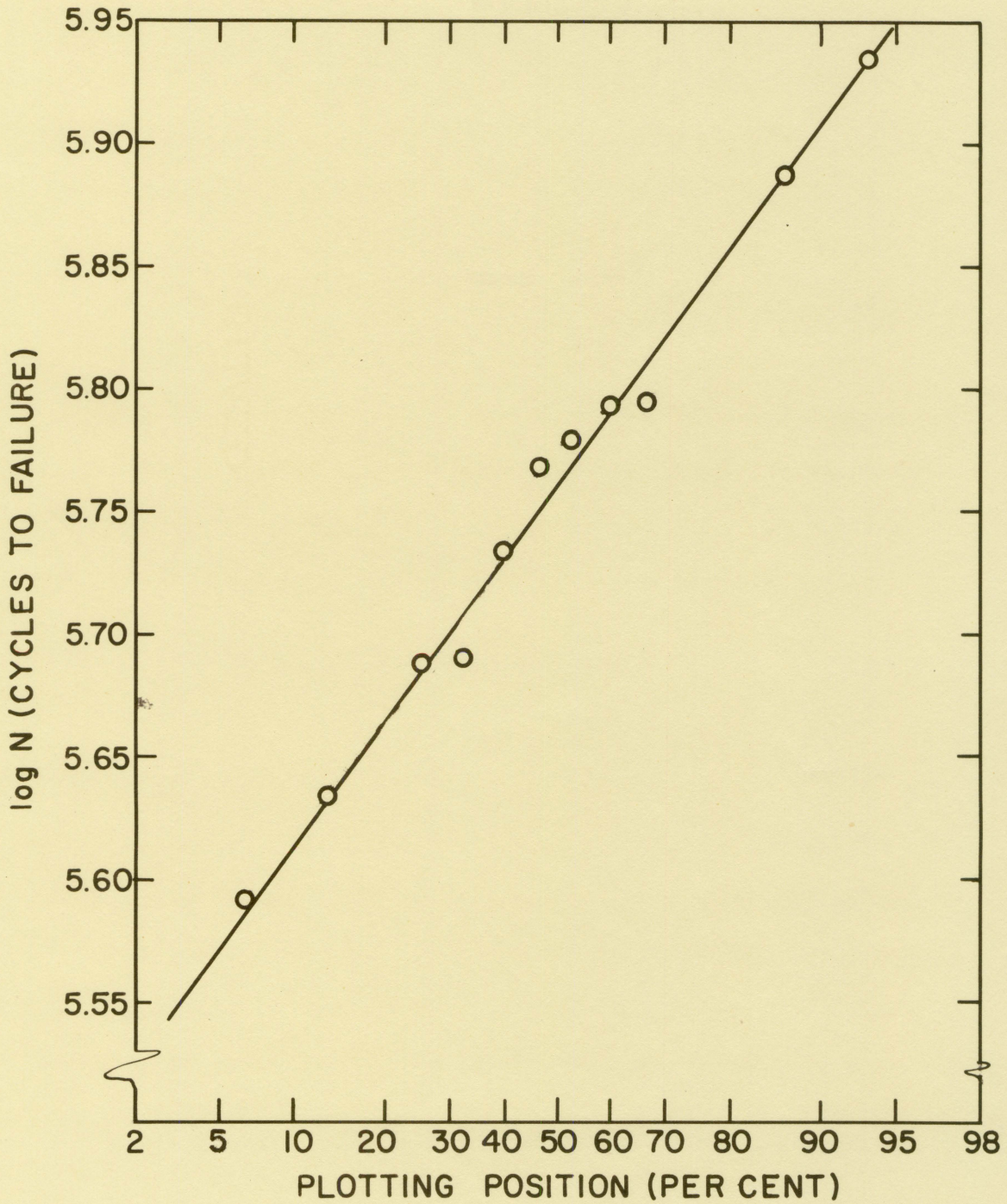


Fig. 21. Cumulative distribution of cycles to failure for normal uranium tested at 25 ksi and 300° C

The normal distribution curve is represented by

$$X = \frac{h}{\sqrt{\pi}} e^{-h^2 x^2} \quad (7)$$

where

X = frequency density

h = precision constant

$$= \frac{1}{\sigma\sqrt{2}}$$

σ = standard deviation of the mean.

Since it is desirable to express the error in terms of the standard deviation, the conditions of Eq. (7) must be satisfied, in that the distribution of the error must be Gaussian, so that from Eq. (7)

$$X = \frac{h}{\sqrt{\pi}} e^{-h^2(\log N - \overline{\log N})^2} \quad (8)$$

Fig. 22 shows the normal distribution curve obtained graphically from the cumulative distribution curve, the values plotted being taken from the straight line approximation. It follows then that the data can be represented to a fair approximation as a log-normal and the standard deviation can be calculated using

$$\sigma = \sqrt{\frac{\sum(\log N - \overline{\log N})^2}{n}} \quad (9)$$

From the data given in Table 9 in the Appendix

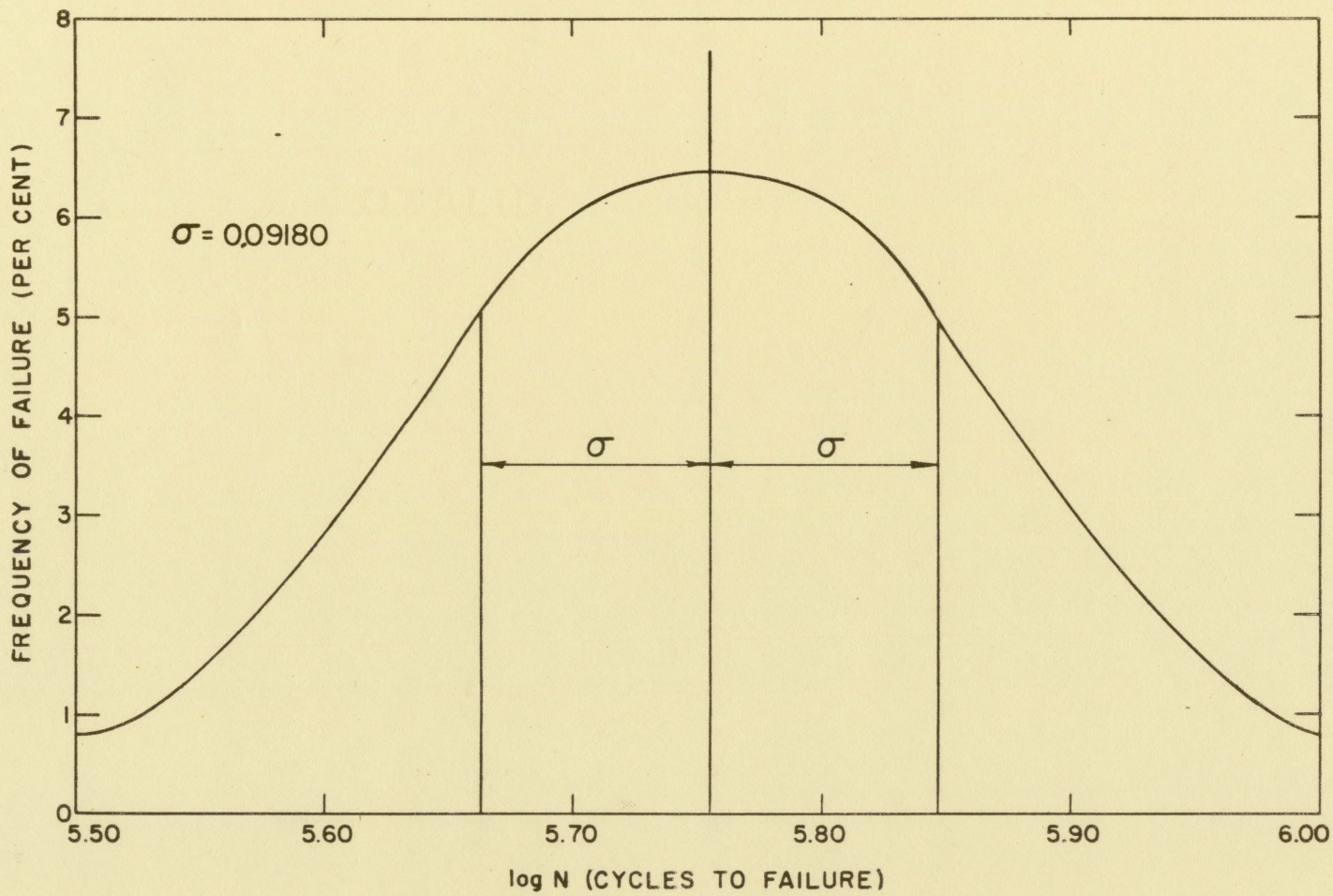


Fig. 22. Normal distribution of cycles to failure for normal uranium tested at 25 ksi and 300° C

$$\overline{\log N} = 5.75555$$

$$\sum(\log N - \overline{\log N})^2 = 0.11811$$

$$n = 14$$

$$\sigma = 0.09180$$

$$\overline{\log N} = 5.75555 \pm 0.09180 .$$

C. Micro-analytical

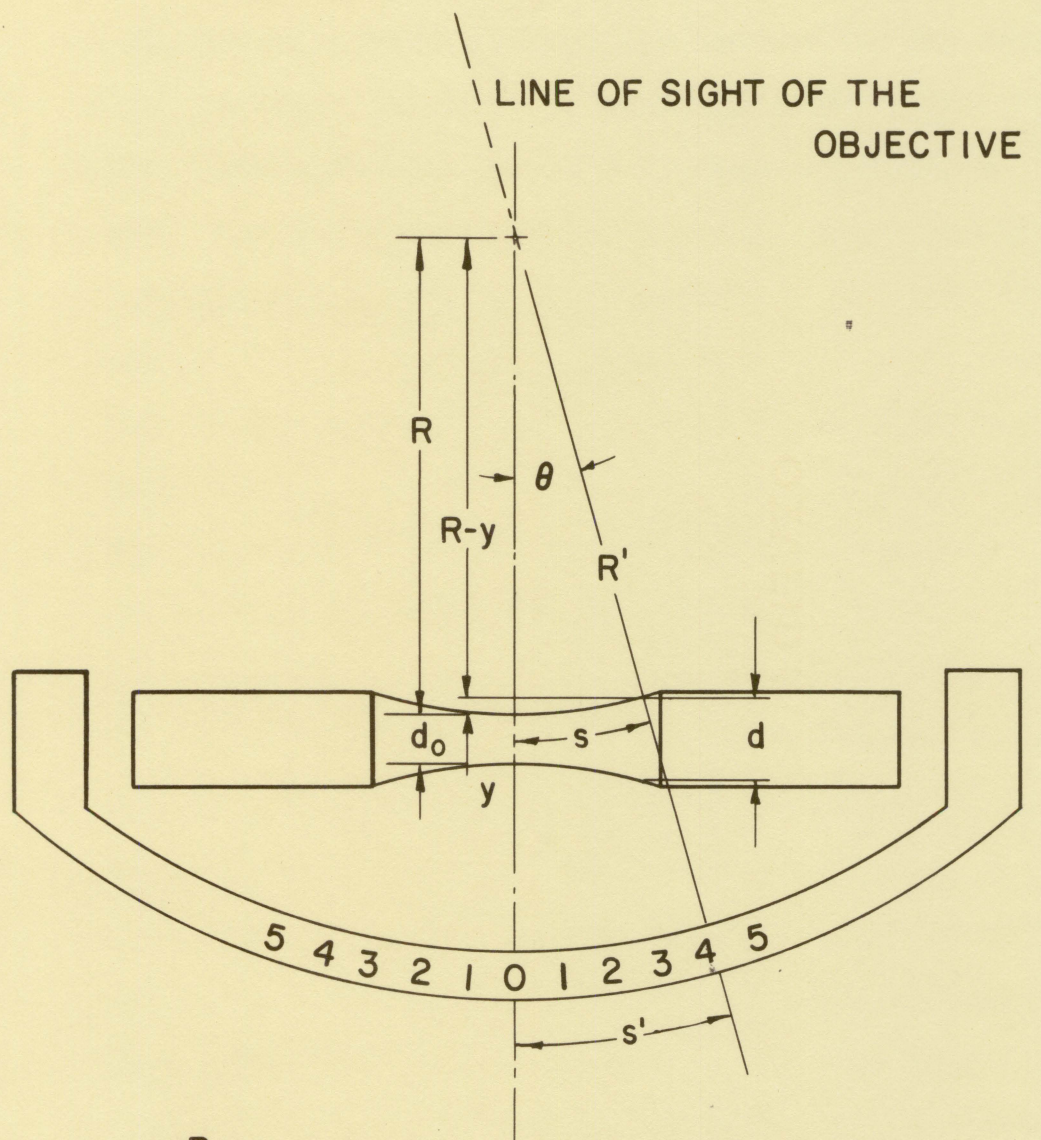
In a simply-supported rotating beam fatigue machine the specimen is subjected to a constant bending moment throughout its test section. Thus, the stress at a point on the surface of the test section varies inversely as the diameter cubed. In observing the surface of the test section microscopically, as was previously described, an area of particular interest may be referenced relative to the diameter of the specimen by means of the geometry involved, which is illustrated in Fig. 23. The relationship between viewing position and diameter is given by

$$d = d_0 + 2 R \left(1 - \cos \frac{s^1}{R^1}\right) . \quad (10)$$

Combining Eqs. (10) and (4) gives stress in terms of viewing position.

$$S = \frac{256 P}{\pi [d_0 + 2 R \left(1 - \cos \frac{s^1}{R^1}\right)]^3} . \quad (11)$$

The effects of fatigue damage on microstructure were



$$\cos \theta = \frac{R-y}{R}$$

$$\theta = \frac{S}{R} = \frac{S'}{R'}$$

$$d = d_0 + 2y$$

$$R' = 3.7 \text{ in.}$$

$$R = 2.5 \text{ in.}$$

$$d_0 = 0.252 \text{ in.}$$

$$s = \text{ARC LENGTH}$$

Fig. 23. Geometry for determining the location of fatigue damage relative to stress

studied at 150, 300, and 400° C using annealed normal uranium specimens at stresses where failure was induced in the range of 10^4 to 10^7 cycles. In order to maintain correlation between observations from one specimen to another, certain criteria were established which were somewhat analogous to the three stages of fatigue cited in Sec. II. In terms of stress, they were:

1. The lowest stress at which localized plastic deformation was detected.
2. The lowest stress at which cracks were observed.
3. The stress corresponding to fracture.

It will be noted that the preceding criteria based on microscopic observations are subject to considerable personal bias on the part of the observer. Typical reference photographs were used. Four sets of observations were made on each specimen half, at ninety degree intervals. The maximum and the minimum corresponding diameters were used to calculate stresses which seemed to establish a range or band by which the initiation of a particular phenomena is represented. Results of the tests which are given in Table 10 in the Appendix have been plotted in Figs. 24, 25, and 26.

It is observed that the band width in cycles for initiation of cracking for 300° C results shown in Fig. 25 is somewhat comparable to the scatter band for the same range of cycles to failure obtained in the test series for scatter determination.

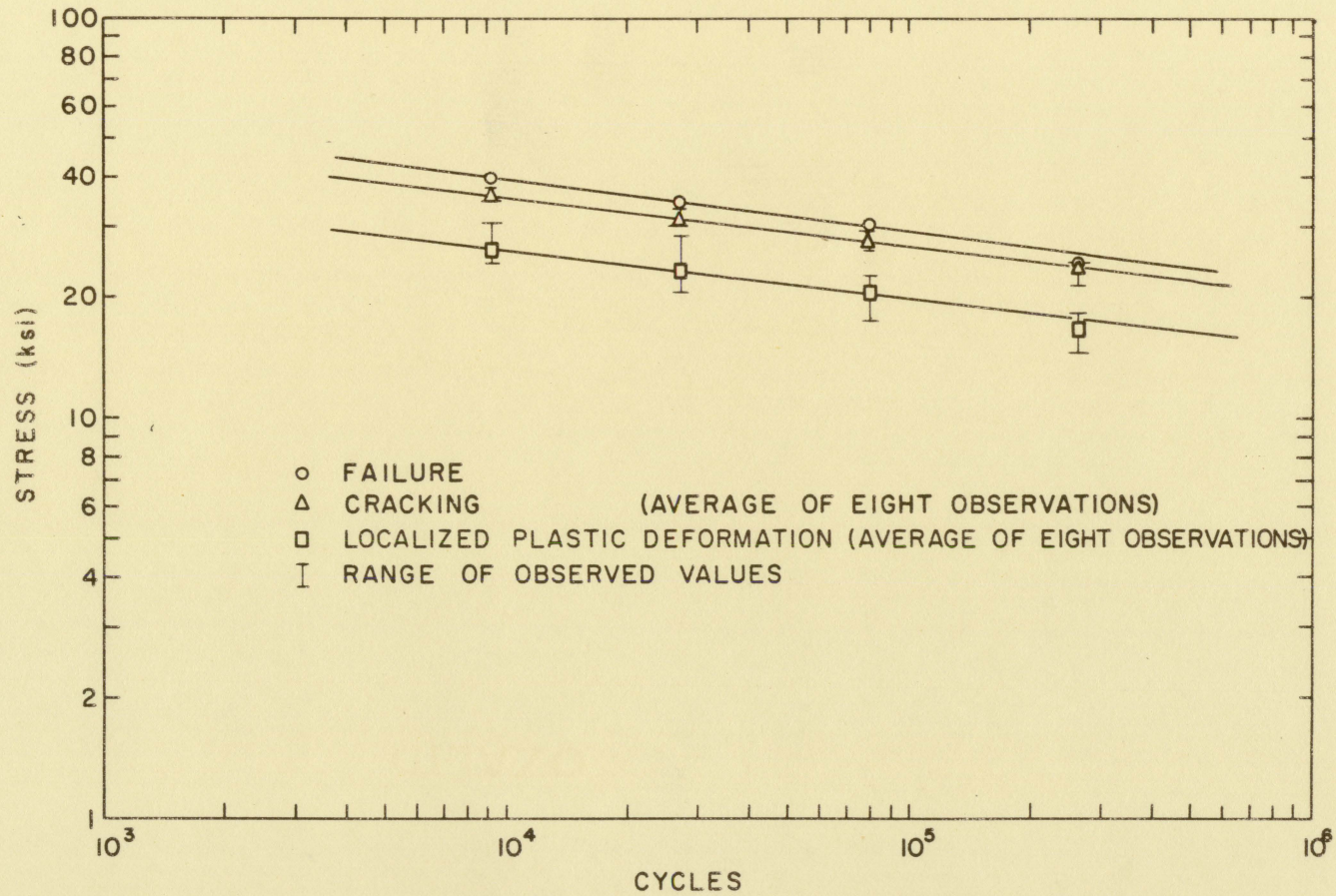


Fig. 24. Fatigue damage as a function of stress and cycles for normal uranium at 150° C

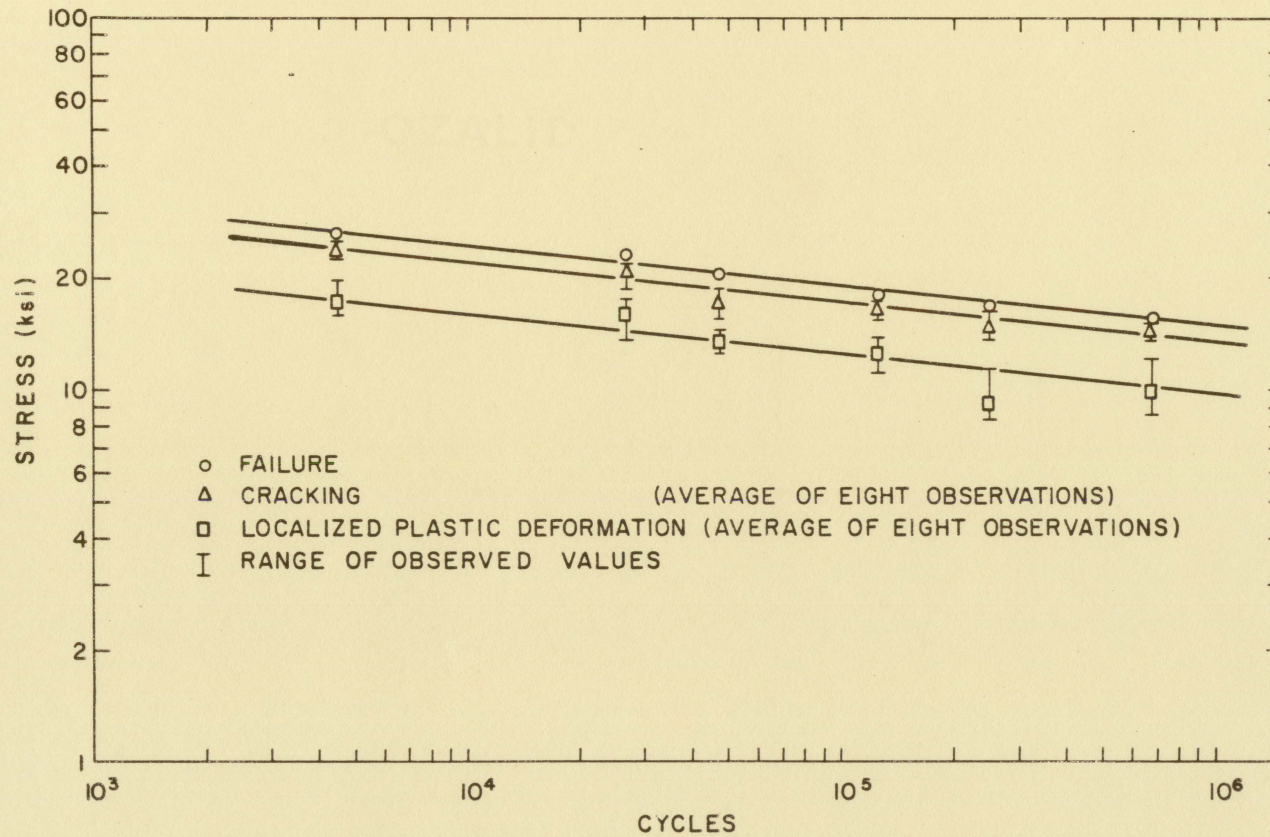


Fig. 25. Fatigue damage as a function of stress and cycles for normal uranium at 300° C

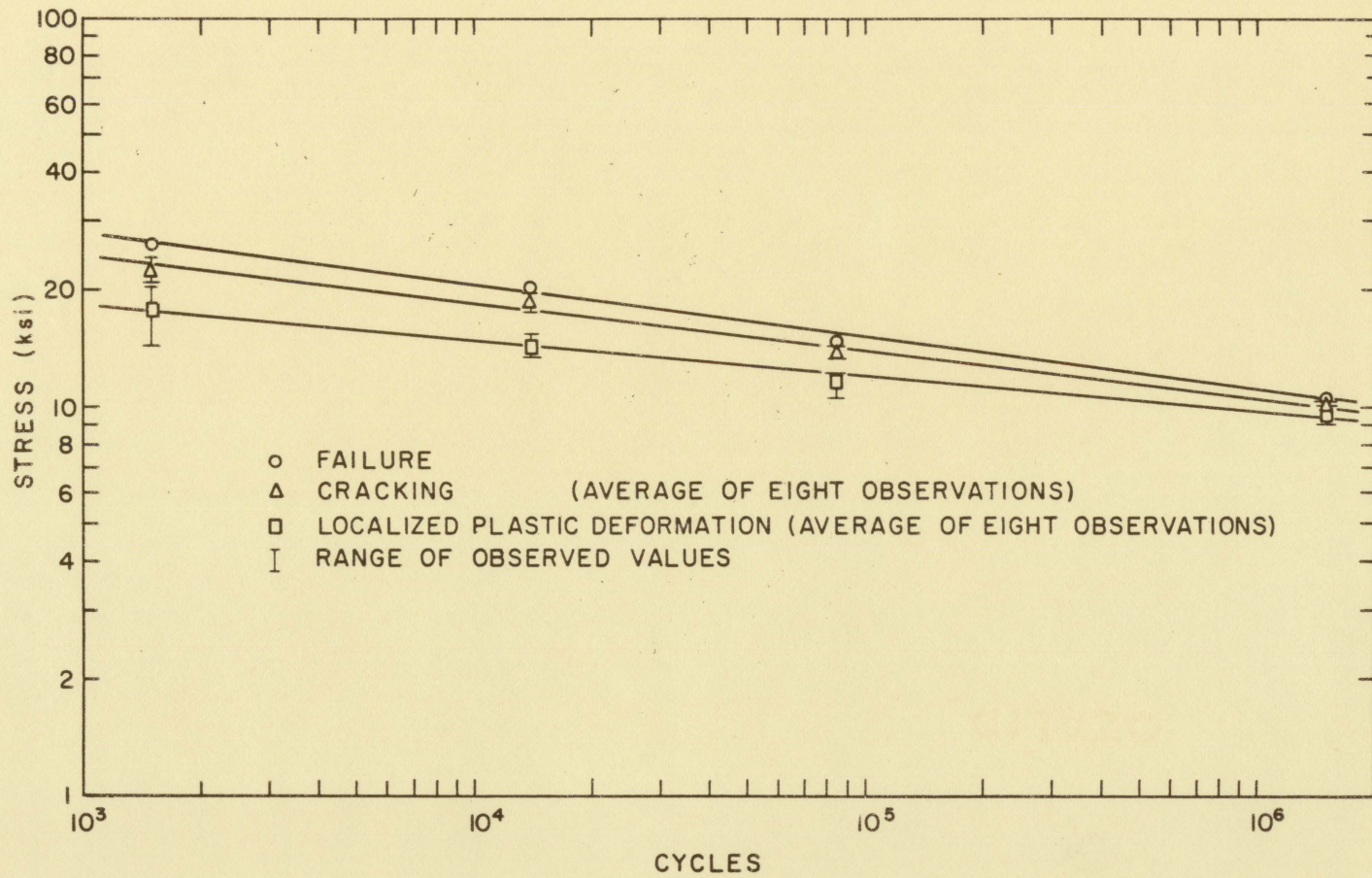


Fig. 26. Fatigue damage as a function of stress and cycles for normal uranium at 400° C

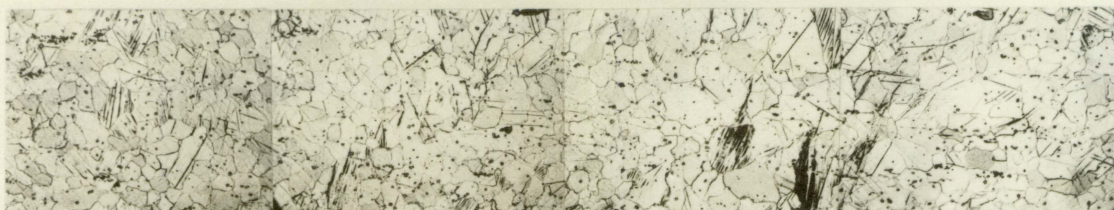
Specimens tested for micro-examination were annealed in a high vacuum apparatus at 625° C for 48 hours to eliminate as much as possible the cold working effects produced during machining. The effects of annealing and etching can be seen by a comparison of the fatigue strengths at a particular temperature as given in Figs. 24, 25, and 26 with those given in Figs. 9, 10, and 11.

Sequence photographs given in Fig. 27 show surface structure typical of that observed in scanning the test section of a specimen through a range of stress representative of no damage to fracture. These microphotographs were obtained from specimen M - 2.

It was observed that during ionic bombardment (etching), a thin film was deposited on the etched surface of the specimen. Spectrographic analysis of the film showed qualitatively the presence of aluminum, silicon, iron, copper, and small traces of other elements most of which could be attributed to various components in the discharge chamber. The film affected oxidation resistance of the etched surface, providing excellent protection from atmospheric corrosion at ambient temperatures for extended periods (several months). Subjecting the etched specimen to elevated temperature fatigue testing reduced the effectiveness of the protective film. Oxidation of the test section surfaces proceeded rapidly (in seconds) upon removing a specimen from the

66

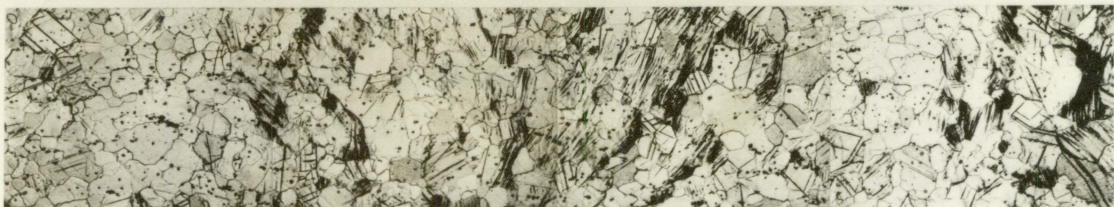
Fig. 27. Sequence photomicrograph (200X) of damage relative to stress for specimen M-2, cycled to failure in 79,800 cycles at 150° C



1 (13.05 ksi) 2

3

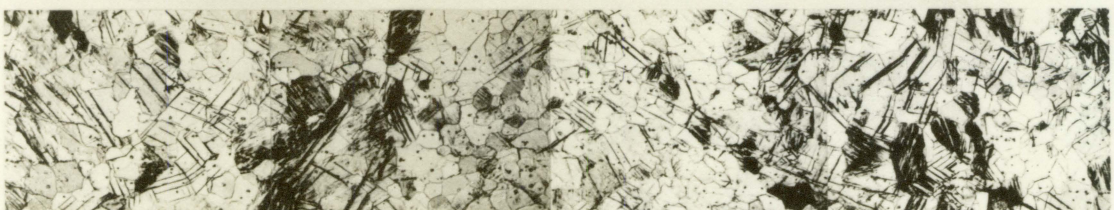
4(15.87 ksi)



5(17.26 ksi) 6

7

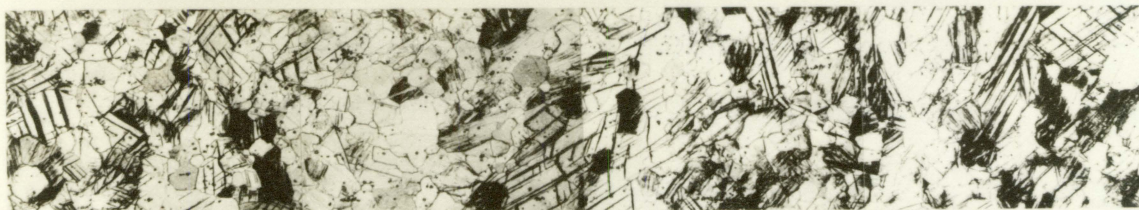
8(20.37ksi)



9(21.86 ksi) 10

11

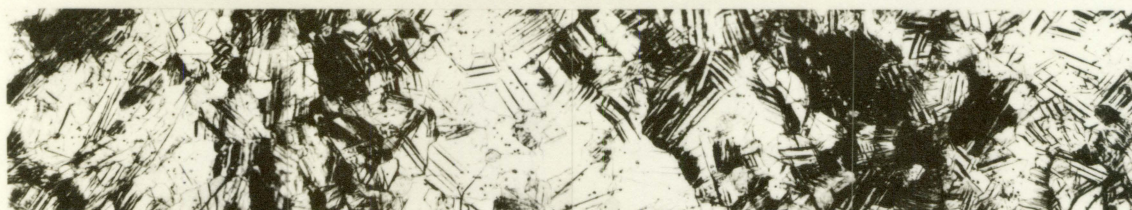
12(25.88ksi)



13(26.74ksi) 14

15

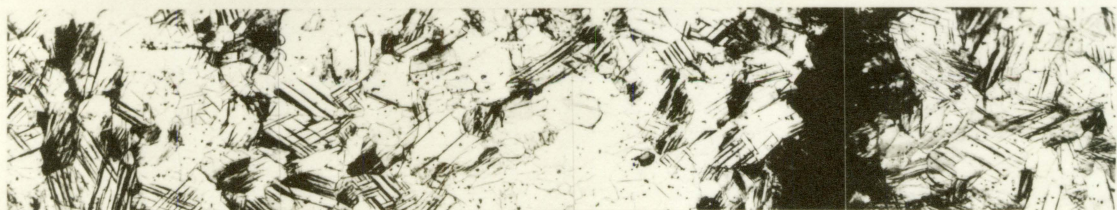
16(30.23ksi)



17(31.29 ksi) 18

19

20(33.56ksi)



21(33.96ksi) 22

23

24(34.78ksi)

flexible capsule. Microscopic examination of a test section surface showed a complete color spectrum with individual grains displaying different colors in a mosaic pattern. Representative color photomicrographs have been included in Sec. VIII.

VIII. DISCUSSION

It was desired to isolate and control as many as possible of the numerous variables associated with fatigue, with the intention that stress and temperature be the only variables adjusted in a particular determination. Diligent efforts were directed at improving the usual methods and techniques of fatigue testing to increase the representativeness of test results.

A. S-N Determination

The approach taken in S-N determinations of uranium was comparable to the commercial type fatigue tests applied to the more common structural materials. In one respect it did vary basically, hence further consideration appears noteworthy. There has not been much attention given the high temperature fatigue properties of metals which in themselves do not possess a superior ability to withstand high temperature corrosion. More consideration has been given creep and tensile properties since it is usually assumed that they control the limiting situations for failure. Elevated temperature creep and tensile properties are often compared to extrapolated room temperature fatigue properties to form the basis of design stress limits. The attitude taken toward the resistance of uranium to failure appears to be an

exception, since its poor resistance to corrosion deems it highly unsatisfactory for high temperature applications in an unprotected state. When uranium metal is used as a nuclear fuel it is invariably protected by a cladding of material having superior resistance to corrosion. It follows then that fatigue testing in a controlled atmosphere is most consistent with intended service conditions, and also results in the elimination of corrosion as a fatigue variable.

In view of the relatively few materials suitable for the needs of the many current and projected high temperature requirements, it is reasonable to assume that additional similar applications will arise in mechanical testing situations.

1. Normal uranium

Room temperature results were, for comparison, obtained using both protected (encapsulated) and unprotected specimens, as indicated in Fig. 8. A distinct variation is seen in the scatter of the data relative to the conditions of testing. Scatter in results for encapsulated specimens is extremely low, so that one might conclude that the effect of the controlled atmospheric environment was to decrease scatter even at room temperature. Discrediting this conclusion somewhat is the fact that unprotected specimens were tested in cantilever rather than in the simply supported type fatigue machines, where the possibility for variation

in the applied bending moment is greater, and could account in part for the greater scatter. Actually, the scatter observed for the unprotected specimens is relatively no greater than that seen throughout the literature for many materials.

The importance of surface structure in fatigue cannot be over-emphasized, since the stress maxima occur at the surface where fracture is initiated. Accelerated by the dissipation of plastic energy of cycling, oxidation could penetrate the surface several thousandths of an inch during the period of testing to affect a change in properties. The unusually excellent continuity in results for encapsulated specimens appears to confirm this statement.

Another interesting anomaly is evidenced by the room temperature results shown and concerns three encapsulated specimens machined from the same slug. For these specimens failure took place at a number of cycles almost ten times greater than was expected. The uniform increase in fatigue strength for these specimens would lead one to suspect that structural differences existed among the slugs of uranium from which specimens were machined. Hardness measurements made on the corresponding specimens in an effort to detect structure variations were inconclusive. Microscopic comparison of representative sectioned specimens did show an apparent variation in oxygen content. The solubility limit for oxygen in uranium is about 20 ppm, thus the precipitated oxygen

observed in the form of uranium oxide compounds provides an indication of oxygen content for the sake of comparison. The oxide particles take the form of a cubic structure as can be seen in the photomicrographs included.

Considering the mechanisms of slip and twinning associated with plastic deformation, one might suppose that oxide particles act as pinning agents at dislocation sites to decrease the operativeness of deformation systems, thereby increasing fatigue strength.

Intrinsic discontinuities were considered to exist in the S-N results starting at approximately 10^6 cycles at room temperature and continuing beyond 10^8 cycles at 500°C . This effect is often seen in S-N results for ferrous metals and is commonly referred to as the "knee" in the S-N curve. The break is usually more abrupt than that observed here, and the lowest stress at which it occurs is the endurance limit.

Fatigue tests of normal uranium were run at 600°C ; however, results were so erratic that testing was suspended. At this temperature it was suspected that heat generated within the specimen could raise the specimen temperature to the phase transformation temperature (663°C), in which case erratic results could be expected. At any rate the endurance limit would probably at most be only several hundred psi, as can be seen by extrapolating endurance limit versus temperature results given in Fig. 13.

Considering further the results of Fig. 13, one observes a slight break in the curve near 300° C. This break is inherent to a number of the physical properties of uranium, some of which are given in Sec. II. Several qualitative arguments are given regarding reasons for its presence. Earlier reference was made to the fact that high temperature slip favored the (110) slip system, where bonds are more easily severed, whereas low temperature slip requires severance of bonds on all except the (010) system. Also associated with this fact is that twinning dominates deformation at temperatures below the break temperature and slip above, however, the change in mechanism reportedly does not take place in such an abrupt transition. In addition to these facts, it is known that recrystallization takes place at about 400° C which could act to shift the discontinuity temperature, depending of course on the initial state of the material. Additional evidence of the anomaly is seen in Sec. IV. in the variation of modulus of elasticity with temperature.

Mathematical representation of the fatigue results was sought to aid in applying these findings to higher stresses, to provide a means of correlating results with other mechanical properties and to test the applicability of the various theories of fatigue. An empirical relationship was obtained which described the data in terms of S (flexure

stress), N (cycles), and T (temperature). A linear regression was applied to

$$\log N = - a \log S + A \quad . \quad (12)$$

The constants along with their respective deviations are listed below and plotted versus temperature in Figs. 28 and 29.

Table 3. Variation of slope and intercept with temperature for Eq. (12)

Temp. ° C	Slope - a	Deviation σ_a	Intercept A	Deviation σ_A
25	12.511	0.706	62.750	3.223
150	10.197	1.314	51.258	5.889
300	9.820	0.611	48.553	2.712
400	8.180	0.887	40.195	3.742
500	7.369	0.365	35.540	1.442

The method of least squares was applied to the data in Table 3, which is shown graphically in Figs. 28 and 29. The resulting empirical equation is

$$\log N = [15.2 - 1.02 \times 10^{-2} T] \log S + 77.37 - 5.41 \times 10^{-2} T \quad . \quad (13)$$

The limiting value of N at a particular temperature for which Eq. (13) is applicable is obtained by substituting the

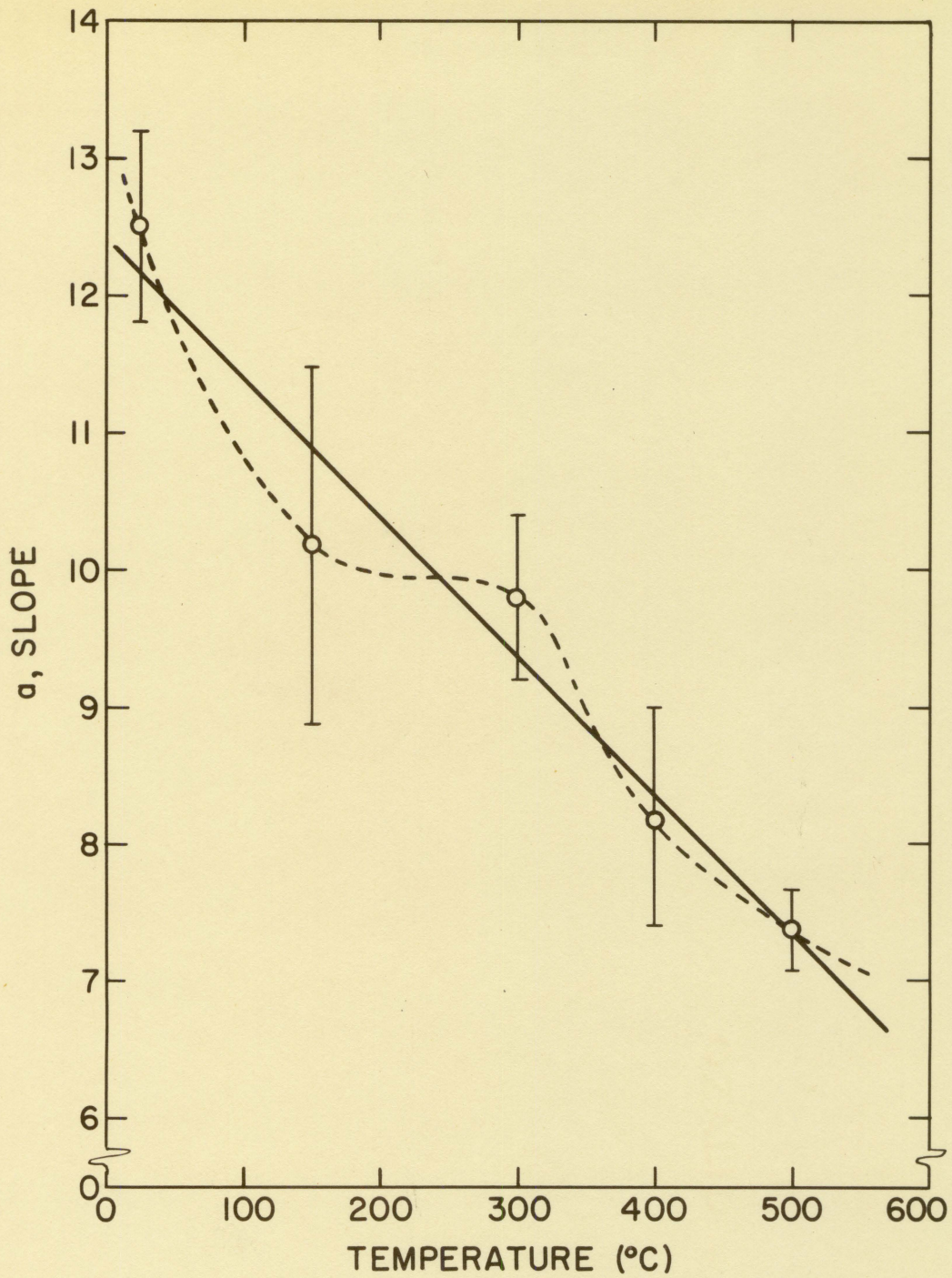


Fig. 28. Variation of slope with temperature for Eq. (12) (normal uranium)

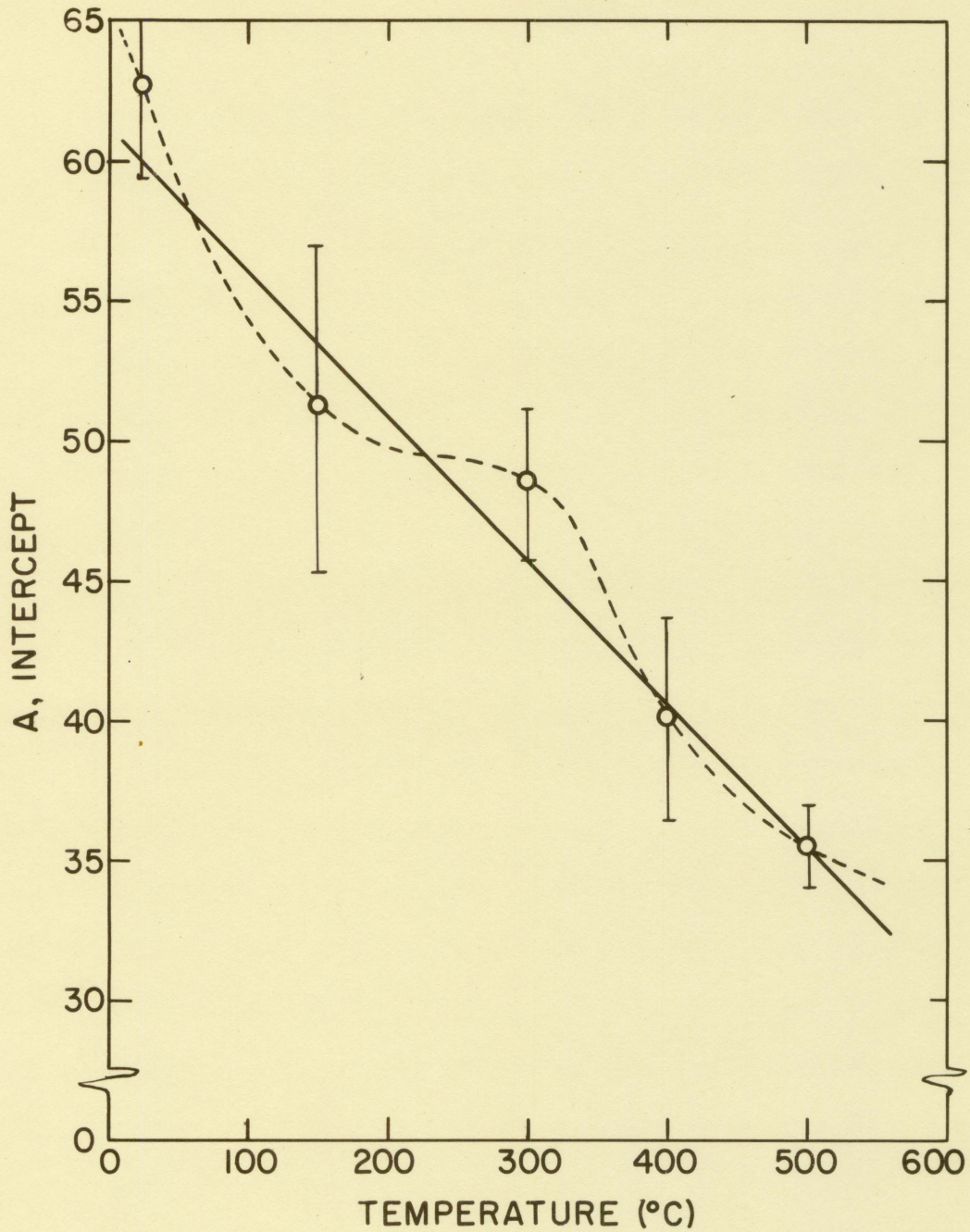


Fig. 29. Variation of intercept with temperature for Eq. (12) (normal uranium)

relationship for endurance limit;

$$S_e = 44.03 - 5.02 \times 10^{-2} T \quad (14)$$

taken from Fig. 13, into Eq. (13). Fig. 30 is a plot of Eq. (13) for the various temperatures tested indicating the range for which a fit was obtained.

A degree of correlation exists between yield strength (0.2 per cent offset) (10) and endurance limit versus temperature. Throughout the temperature range 25 to 500° C the curves for the two properties are parallel, the endurance limit curve being approximately 5 ksi less. Since yield strength is an arbitrary measurement it is not strictly a measure of elastic properties. The endurance limit has been shown to be more directly related to the proportional limit. It must of course be realized that the endurance limit carries with it the implications of work hardening and thermal softening through successive cycling, and the proportional limit does not. Also, uranium does not display a proportional range in the first cycle of stress; however, repeated cycling in tension only shows a considerable increase in yield strength (as much as 100 per cent) and also develops more of a proportional range of stress (17). It is believed that a stable form of hysteresis loop is attained after a number of completely reversed cycles.

Room temperature results for completely reversed axial

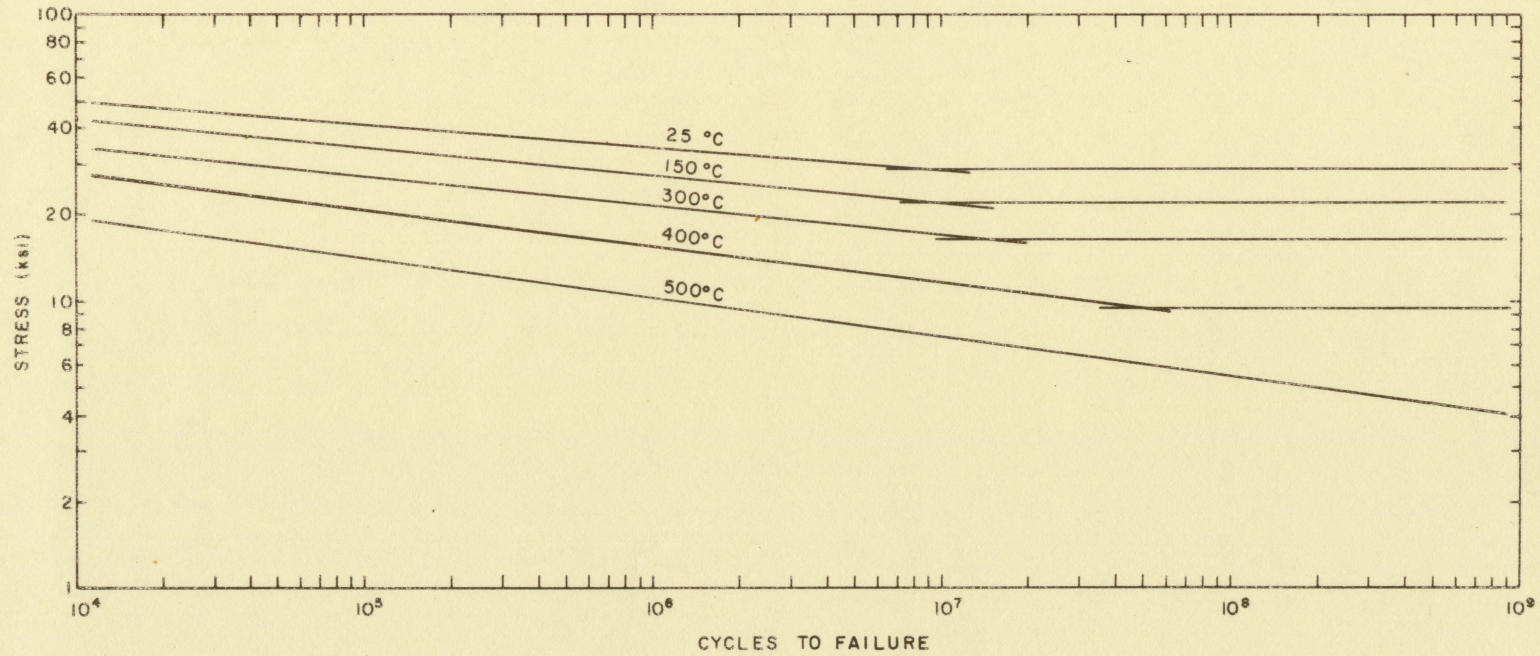


Fig. 30. Composite S-N diagram described by Eqs. (13) and (14)
(normal uranium)

tension and compression tests, shown in Fig. 31 (reproductions of the actual autographic stress-strain curve are given in Figs. 46 and 47), can be represented by

$$S = B \epsilon^b \quad (15)$$

With the exception of the first loading, only minor variations in the characteristic curve form can be observed. Variation in the tension and compression curves for a particular cycle was considered insignificant, since it was within the limits of the accuracy of the measurements. A very slight increase in slope is seen from the first through the fourth cycle, indicating the occurrence of progressive strain hardening. The constants for Eq. (15) were obtained graphically for cycles two, three, and four and are given below.

Table 4. Variation of slope and intercept with cycles for Eq. (15)

Cycle no.	Slope b	Intercept B
2	0.720	2.73×10^6
3	0.717	2.77×10^6
4	0.755	3.44×10^6

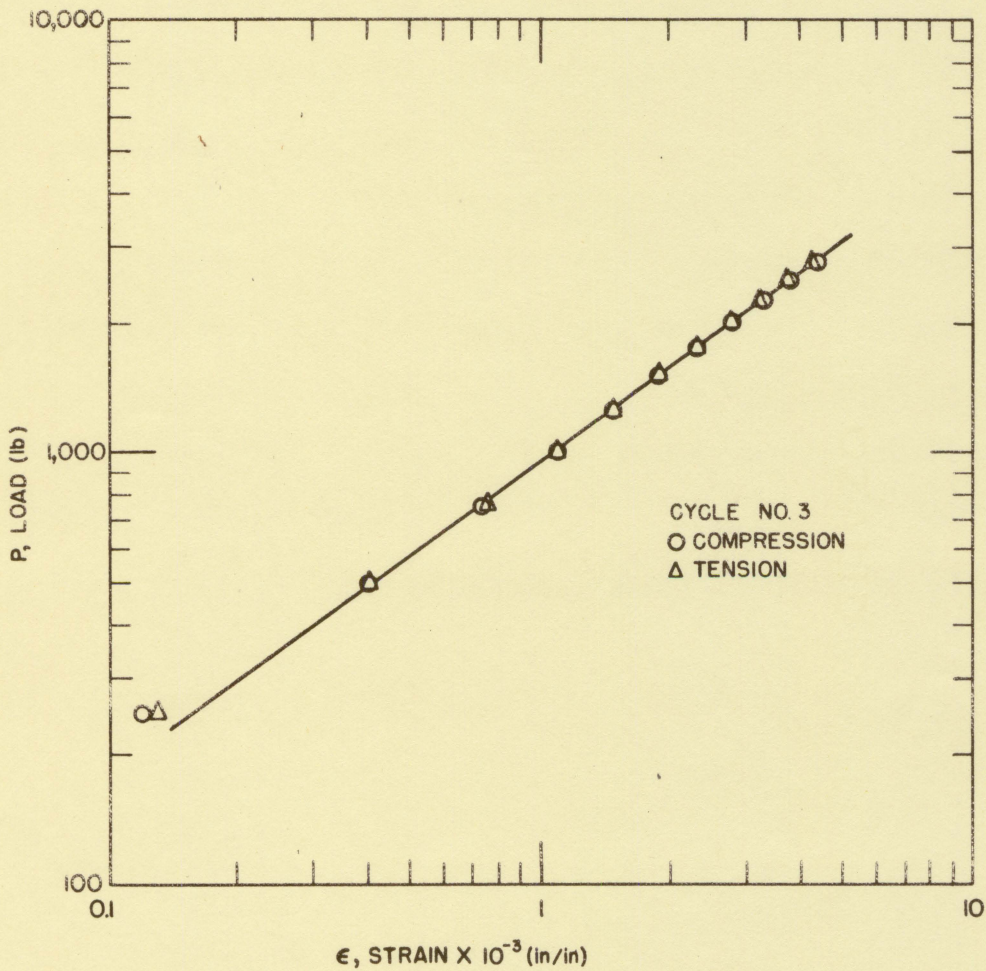
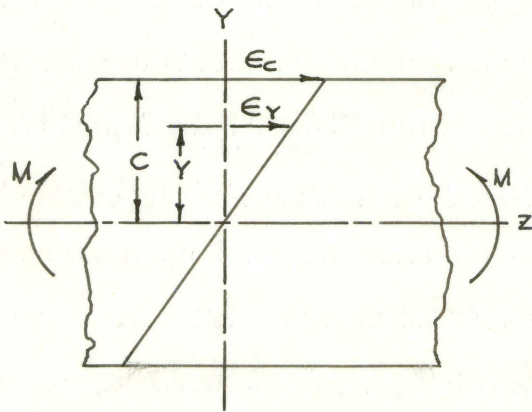


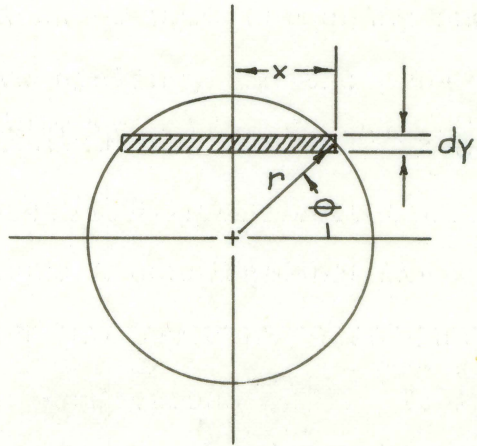
Fig. 31. Axial cyclic tension and compression load-strain curve, cycle No. 3 for normal uranium tested at room temperature

The flexure equation used to calculate bending stress in fatigue was derived for stresses in the proportional range. This fact is commonly ignored and the equation is applied to stresses above the limiting value. Because of the implications involved, the results can be considered only as an index to an engineering modulus. This approach is obviously not conducive to further correlation of properties. A second condition is the assumption that a plane section of a beam remains plane during bending. Flexural creep studies of uranium have shown that this condition is satisfied well into the plastic range of stress (22).

With the aid of Eq. (15), a more applicable form of the flexure equation can be obtained. Consider the geometry of a plane circular section of a beam in bending as follows:



$$\frac{\epsilon_c}{\epsilon_y} = \frac{c}{y}$$



$$\begin{aligned} x &= r \cos \theta \\ y &= r \sin \theta \\ dy &= r \cos \theta d\theta \\ da &= 2 x dy \\ &= 2 r^2 \cos^2 \theta d\theta \end{aligned}$$

The resisting moment developed in the differential area is given by

$$M = 2 \int_0^A S_y y da \quad (16)$$

Combining Eq. (15) with the relationship for ϵ_y obtained from geometry yields

$$S_y = B \left(\frac{\epsilon_c y}{c} \right)^b \quad (17)$$

from which

$$M = 2 \int_0^A B \left(\frac{\epsilon_c y}{c} \right)^b y da$$

and

$$= 4 B \left(\frac{\epsilon_c}{c} \right)^b \int_0^c y^{b+1} x dy$$

or

$$= 4 B \left(\frac{\epsilon_c}{c} \right)^b c^{b+3} \int_0^{\pi/2} \sin^{b+1} \theta \cos^2 \theta d\theta \quad (18)$$

where

at $y = 0$, $\theta = 0$ and at $y = c$, $\theta = \pi/2$.

The solution of the integral takes the form of a beta function

$$B(m,n) = 2 \int_0^{\pi/2} (\sin t)^{2m-1} (\cos t)^{2n-1} dt \quad (19)$$

$$= \frac{\Gamma(m) \Gamma(n)}{\Gamma(m+n)}$$

providing that $m > 0$, $n < \infty$.

Now,

$$2m - 1 = b + 1, \text{ and } 2n - 1 = 2$$

or $m = \frac{b+2}{2}$, and $n = 3/2$

such that

$$M = 2 B c^a \epsilon_c^b \left[\frac{\Gamma\left(\frac{b+2}{2}\right) \Gamma(3/2)}{\Gamma\left(\frac{b+2}{2} + 3/2\right)} \right]$$

$$= B c^a \epsilon_c^b \sqrt{\pi} \left[\frac{\Gamma\left(\frac{b+2}{2}\right)}{\Gamma\left(\frac{b+5}{2}\right)} \right] \quad (20)$$

Letting

$$k_1 = B \sqrt{\pi} c^a$$

and

$$k_2 = \left[\frac{\Gamma\left(\frac{b+2}{2}\right)}{\Gamma\left(\frac{b+5}{2}\right)} \right]$$

and

$$k = k_1 k_2$$

then

$$M = k \epsilon_c^b \quad (21)$$

Replacing ϵ_c by S from Eq. (15) gives the flexure equation in a modified form for the semi-plastic material as follows,

$$S_p = \frac{Mc}{I} \left[\frac{\sqrt{\pi} \Gamma\left(\frac{b+5}{2}\right)}{4 \Gamma\left(\frac{b+2}{2}\right)} \right] \quad (22)$$

or in terms of the elastic flexure stress

$$S_p = S_f \gamma \quad (23)$$

where

$$\gamma = \frac{\sqrt{\pi} \Gamma\left(\frac{b+5}{2}\right)}{4 \Gamma\left(\frac{b+2}{2}\right)}$$

The modification factor γ evaluated for the third cycle of the axial stress-strain results given in Table 4 is

$$\gamma = 0.85$$

Substituting the results of Eq. (22) into Eq. (12) gives the stress modified S-N relationship

$$\log N = - a \log \frac{Sp}{\tau} + A \quad (24)$$

or in terms of strain

$$\log N = - a \log \frac{B \epsilon^b}{\tau} + A \quad (25)$$

Eq. 25 is seen to be a useful means of describing the fatigue relationship in terms of strain for a given temperature and consequently providing legitimate access to the stress-strain parameters. Numerous reports on a great many materials have dealt with the applicability of equations of the form of Eq. (25) relative to constant strain amplitude fatigue tests. Results by Low (23) showed that data for several materials could be fit to a simple $\log \epsilon$ versus $\log N$ straight line plot. Thermal cyclic fatigue data are also commonly represented by the power curve of Eq. (25). This fact is noteworthy because of the similarity in stress conditions for thermal fatigue and mechanical bending fatigue. The stress gradient which occurs in bending is present in thermal stress situations and corresponds to the thermal gradient, imposed by heat transfer considerations. The consequences appear basic to the rudiments of the problem of determining the resistance to failure of uranium through mechanical tests.

It is interesting to note that if the results given in Eq. (24) are extrapolated to one quarter of a cycle ($N = 0.25$)

a stress of 98.5 ksi is obtained for room temperature, which is within the range of values listed for the ultimate tensile strength. However, the modified flexure equation was derived for stress-strain characteristics other than those of the first loading, thus it may be more reasonable to extrapolate to $N = 0.75$ where close proximity did exist with the successive cycles. At this value of N the resulting stress is 90.3 ksi.

2. Chromium-uranium alloy

Inspection of the S-N diagrams from 25 to 600° C shows several characteristic curve shapes. Room temperature and 150° C semi-logarithmic plots display two discontinuous straight line segments characterized by the "knee" mentioned previously. The curves for 300 and 400° C closely resemble the normal uranium results, in that they do not show an abrupt break on the semi-logarithmic plot. Five hundred and 600° C results are of the same form as those for 25 and 150° C, although they have less abrupt discontinuities at a far greater number of cycles (10^8 cycles), if at all.

In an attempt to obtain an empirical representation of the data, several forms of power equations were employed with only limited success. It was found that the best overall representation could be obtained by fitting the data to the relationship

$$\log N = -gS + G \quad . \quad (26)$$

The slopes and intercepts along with their deviations are listed in Table 5 and plotted in Figs. 32 and 33. No attempt was made to obtain expressions for their variation with temperature due to their discontinuous nature. The limited data available for the method of least squares at 25° C plus the questionable applicability of the exponential model at 300 and 400° C would obviously discredit any conclusions drawn regarding the presence of this discontinuity. The fact still remains that this anomaly is typical of a great number of properties of uranium. The discontinuity seen in the normal uranium was near 300° C, but with chromium-uranium alloy it is closer to 400° C. This is consistent with the corresponding increase in endurance limit versus temperature for the chromium-uranium alloy. Since progressive strain hardening and strain aging are believed to be fundamental in the mechanism of fatigue, it follows that the break in the curve could arise from a gradual transition from one of these rate controlling processes to another. Further evidence of this fact may be seen in the variation in endurance limit versus reciprocal temperature (°K) shown in Fig. 34, where for temperatures above approximately one-half the melting point (T_m) the rate of change is constant. It is a generally accepted fact that for most materials the activation energy for self diffusion is constant above

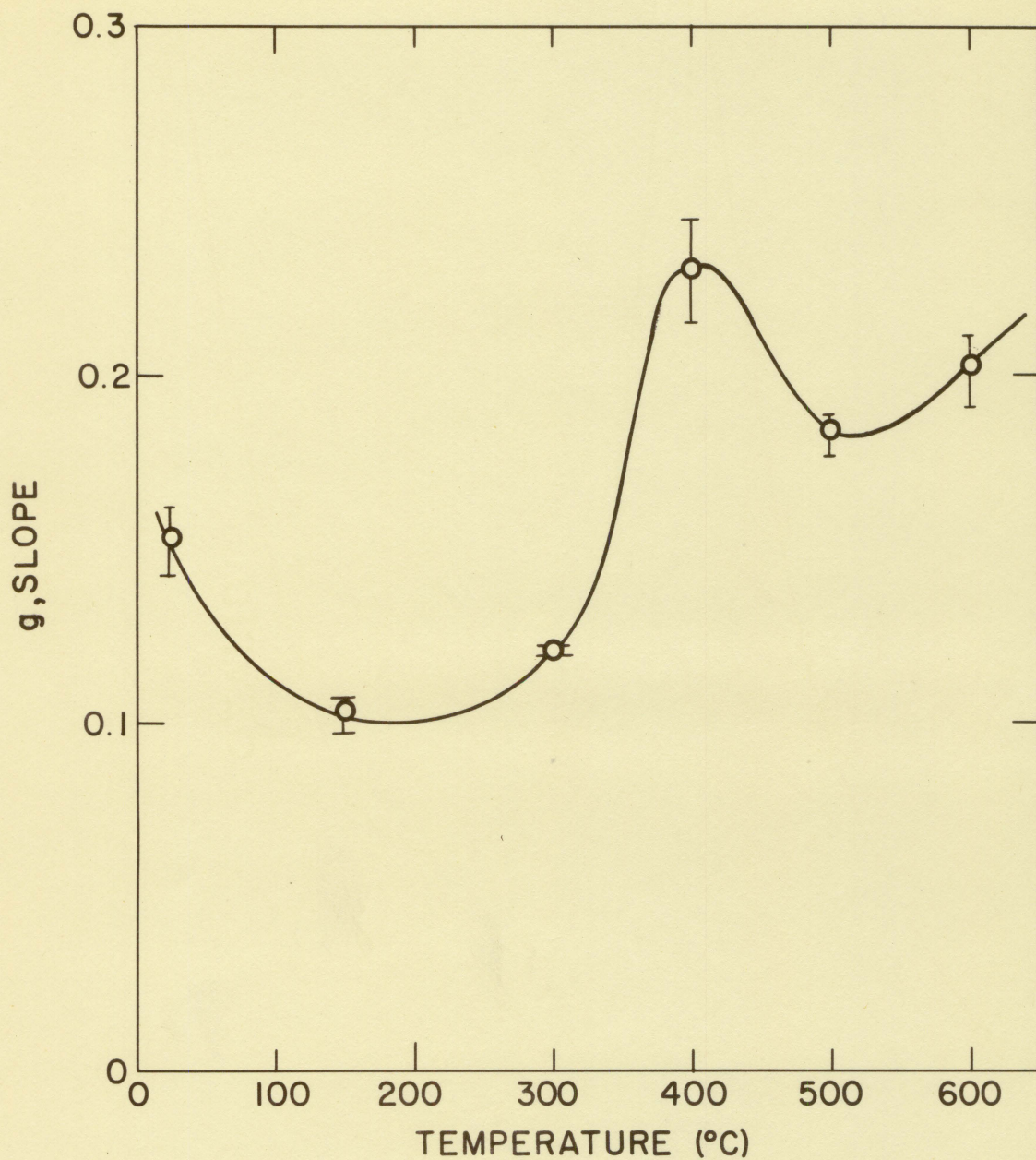


Fig. 32. Variation of slope with temperature for Eq. (26) (chromium-uranium alloy)

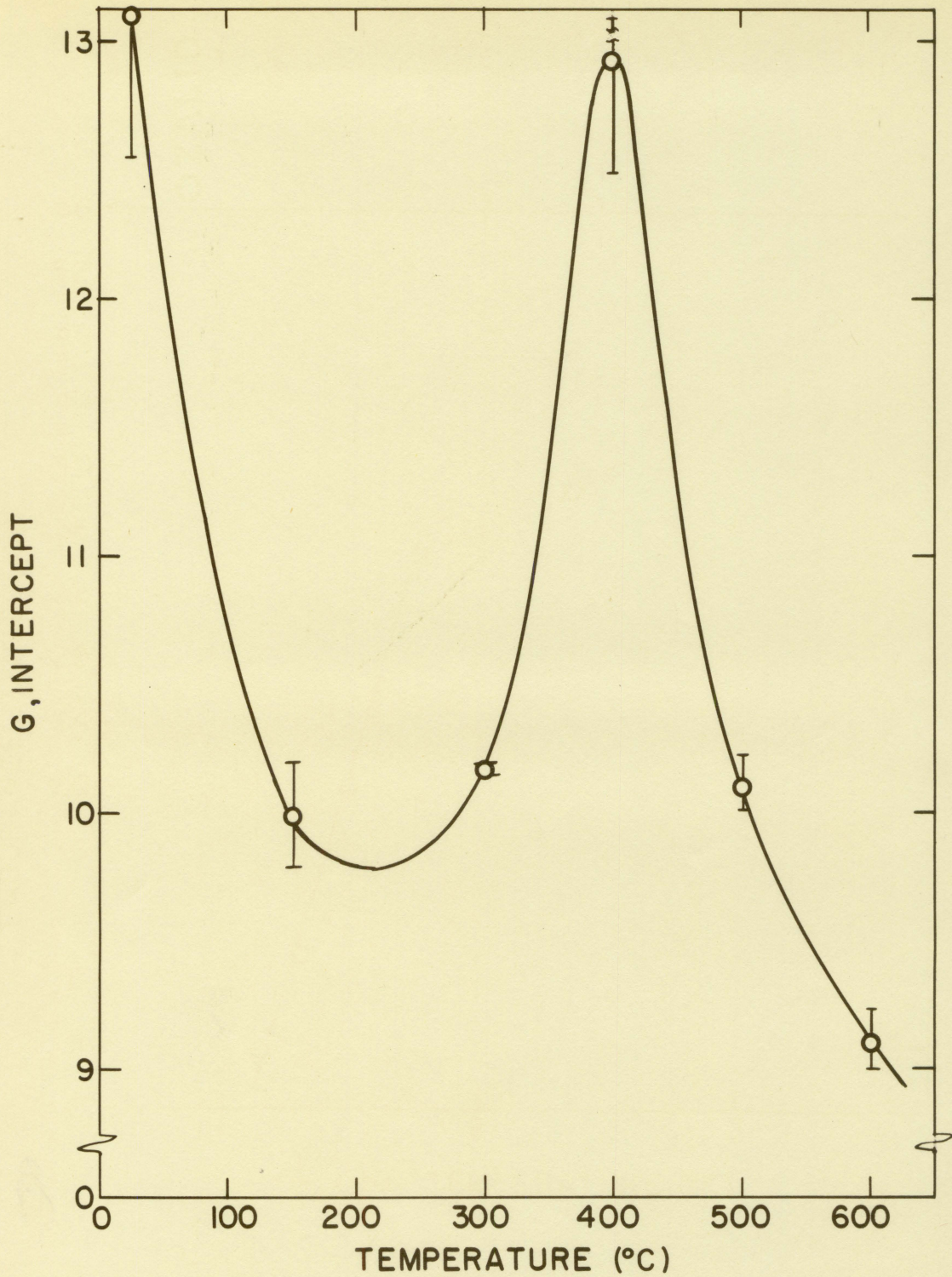


Fig. 33. Variation of intercept with temperature for Eq. (26) (chromium-uranium alloy)

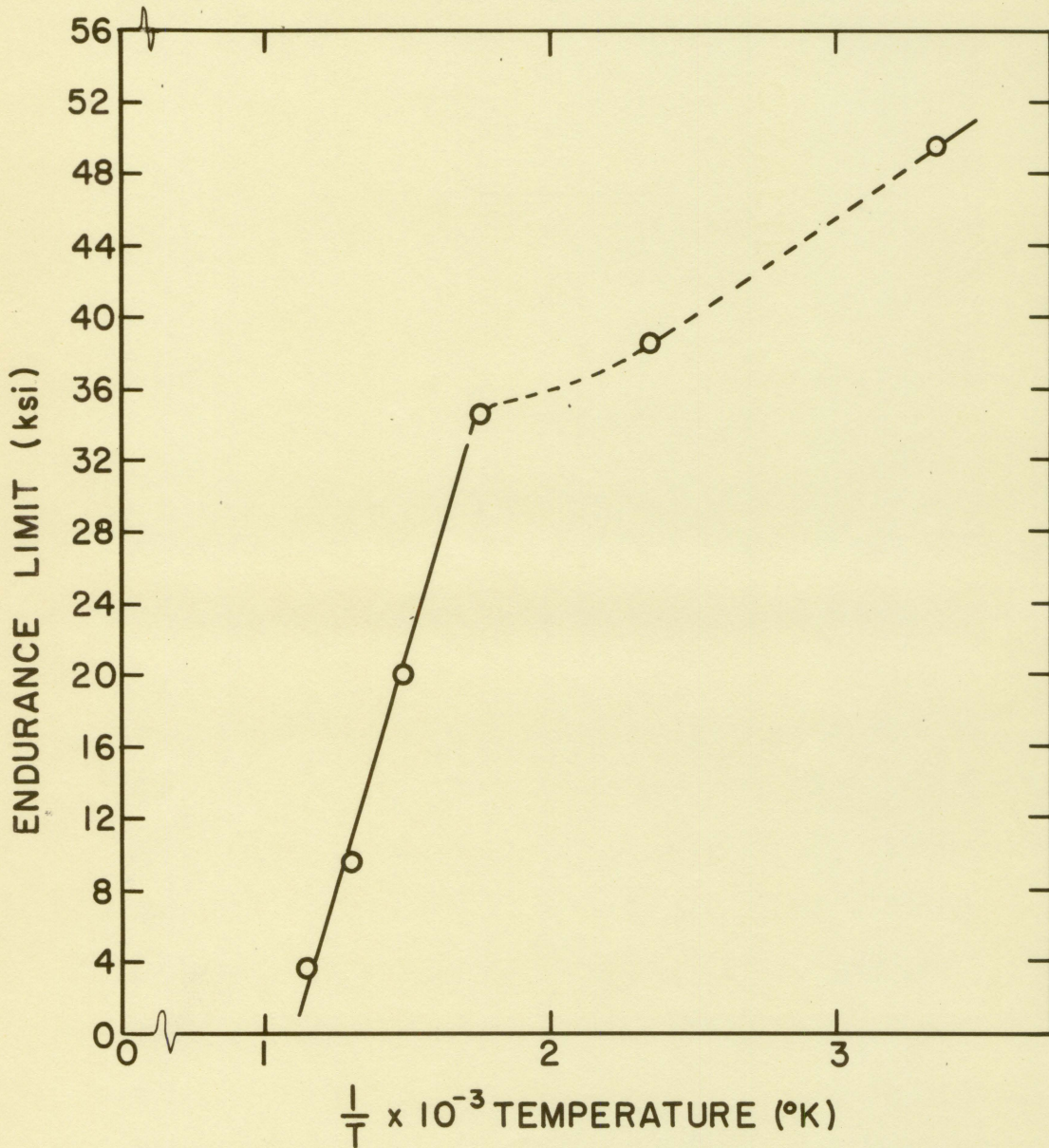


Fig. 34. Variation of endurance limit with temperature for chromium-uranium alloy

Table 5. Variation of slope and intercept with temperature for Eq. (26) (chromium-uranium alloy) (S in ksi)

Temperature °C	Slope - g	Deviation σ_g	Intercept g	Deviation σ_g
25	0.153	0.023	13.069	0.559
150	0.103	0.011	9.931	0.211
300	0.121	0.002	10.164	0.028
400	0.231	0.034	12.938	0.446
500	0.184	0.014	10.091	0.101
600	0.203	0.023	9.104	0.118

one half the melting point. This appears significant since the strain aging phenomenon is so directly associated with diffusion.

The stress-strain characteristics from completely reversed axial tests of the chromium-uranium are also found to obey the $\log S - \log \epsilon$ relationship except for the first loading. Just as with normal uranium, only slight variations can be observed in the successive load cycles for chromium-uranium. Reproductions of the original autographic load-strain curves are shown in Figs. 48 and 49. $\log P$ versus $\log \epsilon$ for the fourth cycle is plotted in Fig. 35 along with the comparable results of normal uranium. It is noted that a degree of parallelism exists between the two results. The

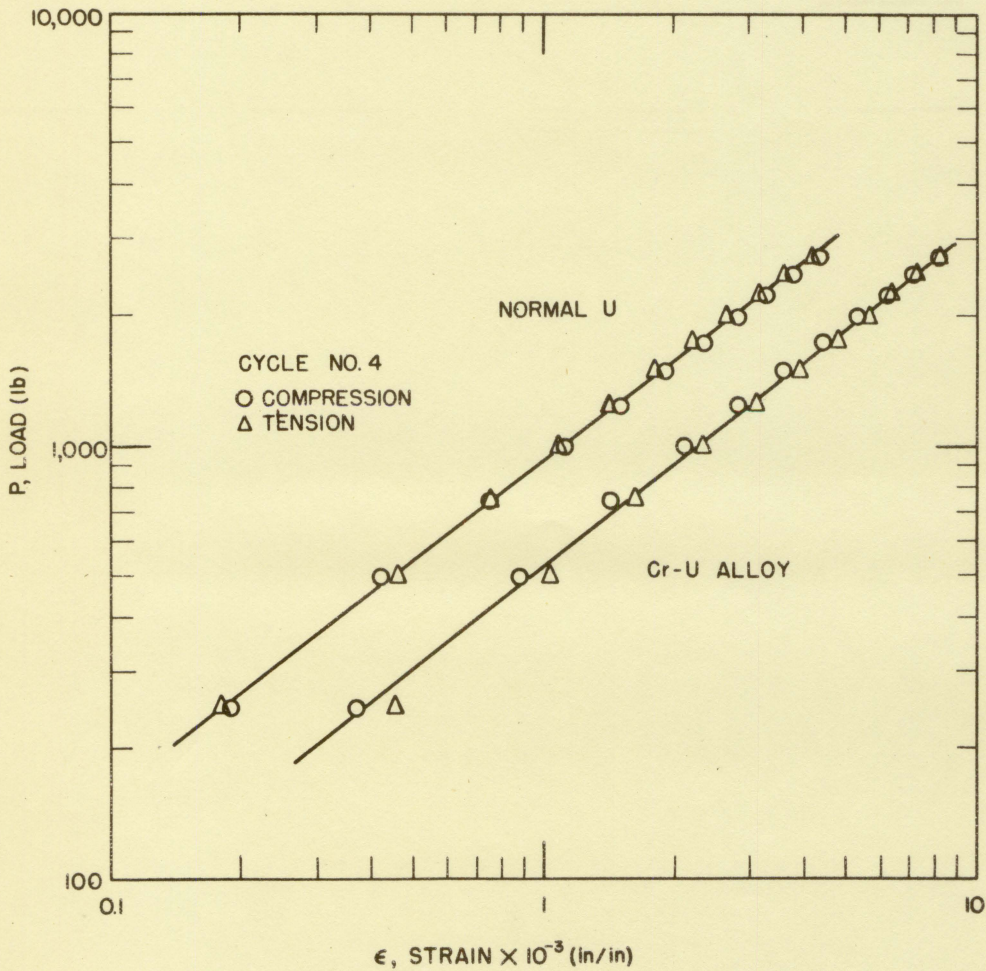


Fig. 35. Axial cyclic tension and compression load-strain curves, cycle No. 4 for normal uranium and chromium-uranium alloy tested at room temperature

S- ϵ relationship evaluated for the alloy from Fig. 35 is

$$S = 2.33 (10^6) \epsilon^{0.78} . \quad (27)$$

The flexure modification factor γ evaluated for $b = 0.78$ is $\gamma = 0.87$ such that

$$S_p = 0.87 S_f . \quad (28)$$

Extrapolating Eq. (26) for room temperature data given in Table 5 gives a value of stress much less than the value for ultimate tensile stress in axial tension. Insufficient S-N results in the finite life region of stress at 25° C disqualifies further discussion.

B. Damage

In this investigation it was desired to determine the effects of fatigue damage on microstructure. This is considered important for several reasons. First, from a phenomenological point of view in support of the laboratory attitude taken in fatigue testing, it is desirable to make fundamental observations to support basic studies which may ultimately satisfy the quest for the basic mechanisms of fatigue. Second, for purposes of design application of fatigue data it is important to know more of the action of fatigue than the stress which can be applied indefinitely without producing fracture, since obviously design components

are usually not intended to last indefinitely. For this reason the finite life range of stress should be given more attention than the mere determination of cycles to failure as a function of stress.

The conventional method of determining the safe design limits in the finite stress range is involved and time consuming. It requires first the complete determination of the S-N curve. Then a number of specimens are run at a given stress for various fractions of their life, estimated from the S-N curve obtained. Each specimen is then rerun at the endurance limit. Specimens which suffered damage in the prestress tests will fail before the endurance number of cycles; those not suffering damage will not fail. Thus the highest fraction of cycles to failure corresponding to a specimen unfractured in the endurance limit retest is considered to be the "damage point". This process is repeated for various stress levels from which a "damage line" can eventually be obtained. The stress corresponding to a particular number of cycles to damage may then be considered for design application.

The same information was sought in this investigation using microscopic observations of damage to evaluate the "damage line". This technique does not require specimens other than those used in the S-N determination. Its greatest disadvantage stems from the uncertainty of optical

crack detection and the resulting arduous task of scanning. This disadvantage is somewhat lessened by the use of two criteria for damage, localized plastic deformation and cracking, which may be reasonably considered as the limits of damage. The technique requires further that the microstructure initially be as free as possible from the effects of cold-working, which would usually imply annealing. In addition there is the necessity of etching which could possibly introduce additional undesired variables. It was felt that the method of etching employed in this investigation provided a minimum situation, and no attempt was made to study its affect.

Straight line logarithmic representation is given the results shown in Figs. 24, 25, and 26. Note the parallelism at 150 and 300° C, and the convergence at 400° C. The latter might be interpreted in terms of the action of recrystallization which begins near 400° C. Further evidence of this effect can be seen in the photomicrographs included. Scatter in the damage data plotted is fairly consistent with that observed for fracture. The ranges of observed values for damage were included to provide an index of the symmetry of deformation relative to the minimum test section diameter of the specimen.

The mode of fatigue deformation is seen to vary with temperature for the range of temperatures investigated.

This fact is evidenced in the following color photomicrographs.

At 150° C cracking follows the paths of deformation marking, and is therefore observed to take place on an intracrystalline basis. Fig. 36 is illustrative of this point and further typifies the results of the sequence photomicrographs shown in Fig. 27 where the presence of cracks is not readily apparent. The individual coloration of the crystals provides a definite record of crystal boundaries and thus an accurate means of tracing deformation otherwise lost in the photomicrographs due to the limited depth of field in areas of highly disrupted crystal structure. Note the well defined deformation marks at 150° C. They are observed to become less distinct as the test temperature is increased. Fig. 37 shows the termination of a crack within a crystal and indicates the operativeness of many deformation systems as it branches to form a "Y". This is also evidenced in Fig. 38 where a crack has traversed a portion of a crystal in an irregular path, following the direction of deformation marking.

Fig. 39 has been included to illustrate the typical undamaged microstructure of specimens used in this investigation. The residual plastic deformation seen here could not readily be eliminated, and is probably due to the anisotropy of thermal expansion in uranium causing plastic flow during

Fig. 36. Fatigue damage in normal uranium tested at 150° C, showing intracrystalline cracking and well defined deformation marking (200X)

Fig. 37. Termination of a fatigue crack in normal uranium tested at 150° C (500X)

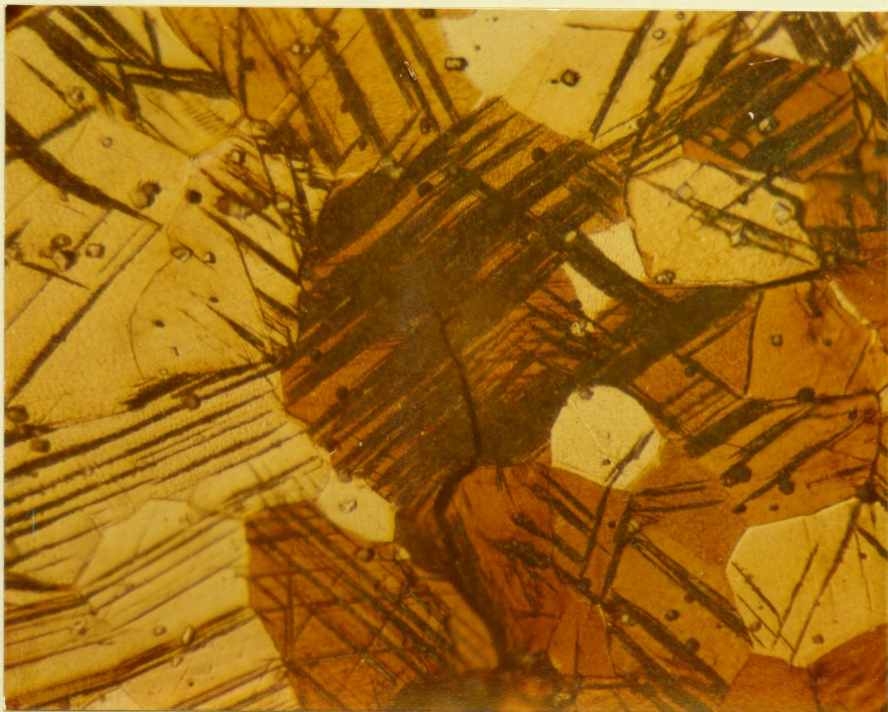
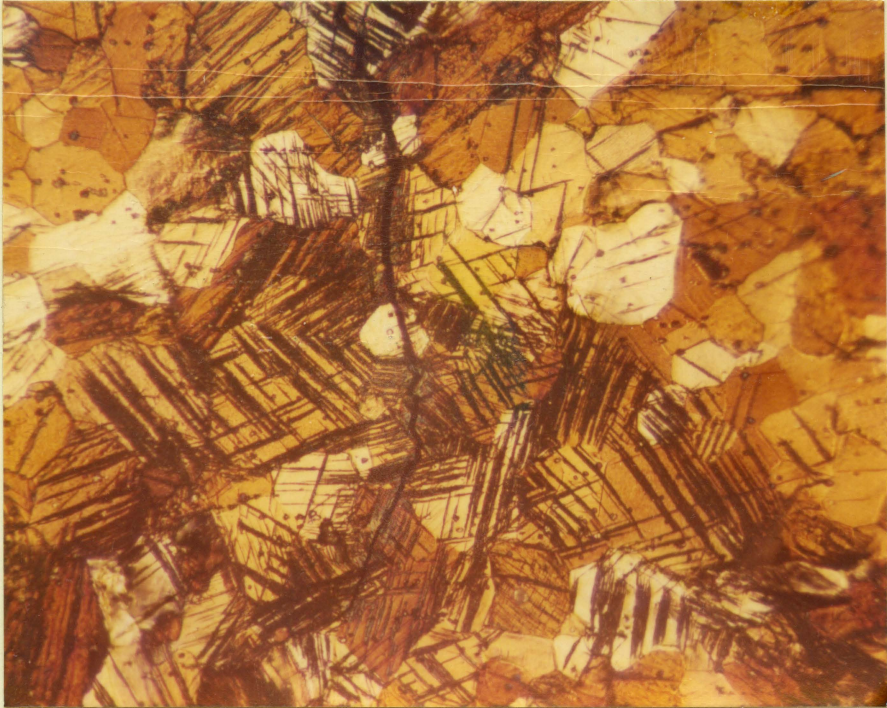
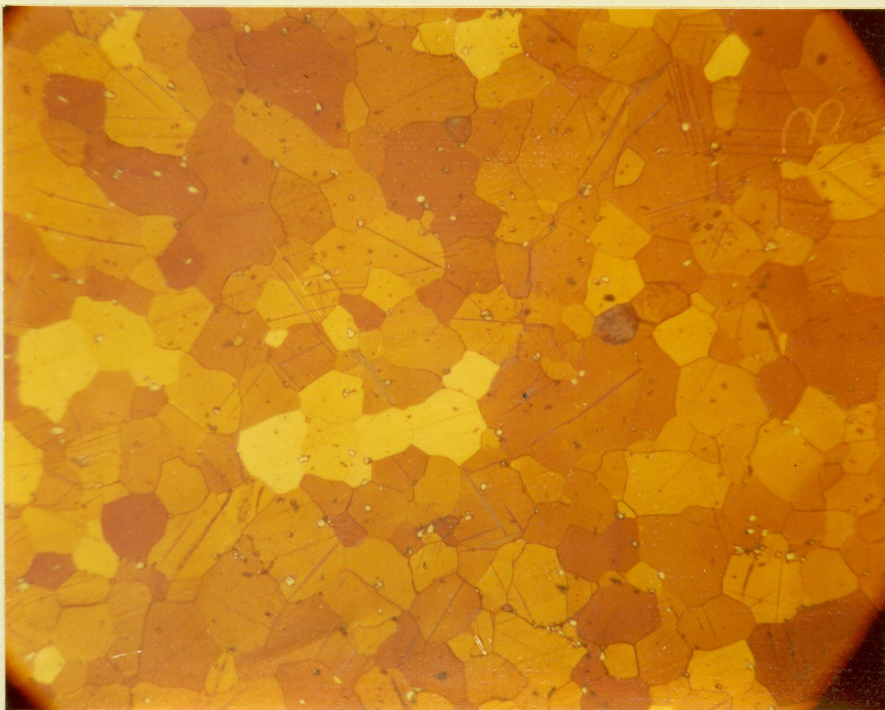


Fig. 38. The irregular path of a crack in normal uranium tested at 150° C (1000X)

Fig. 39. Typical undamaged microstructure of normal uranium (200X)



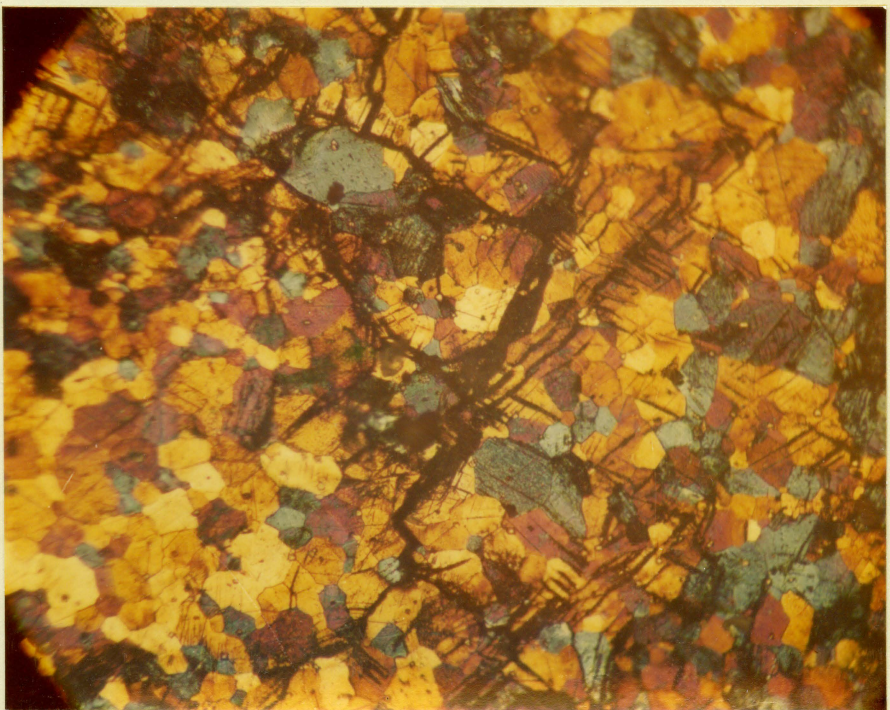
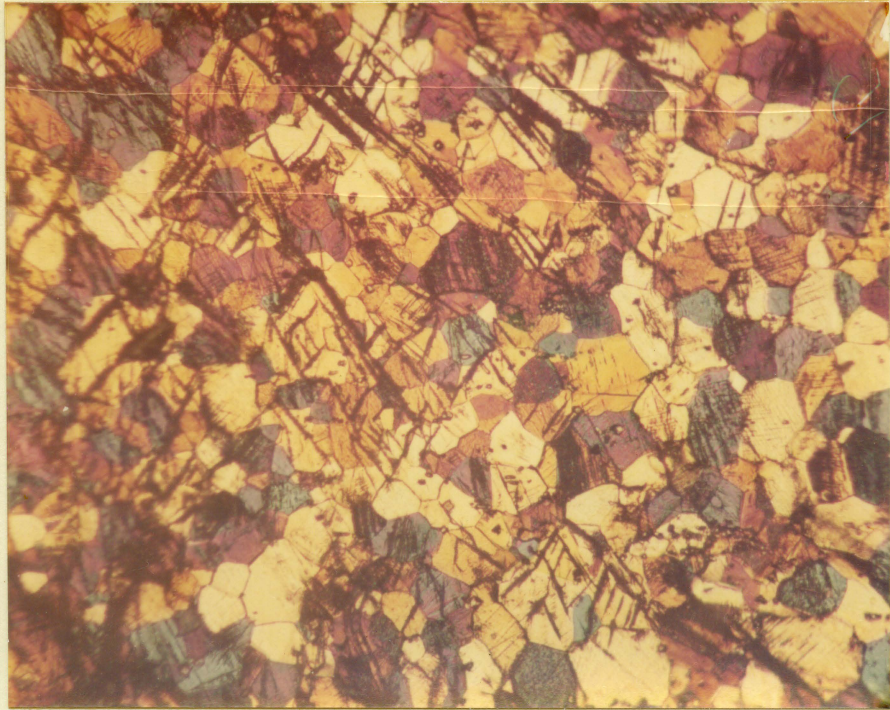
cooling from the annealing temperature.

At 300° C the same general characteristics observed at 150° C are present, as may be seen in Figs. 40 and 41. Deformation marks are still fairly distinct, although in some crystals an increased amount of more uniform local deformation is observed. This might be attributed to the increasing number of active deformation systems operating, requiring less activation energy at this temperature and/or to the effects of annealing and recrystallization induced by localized plastic energy dissipation in the form of heat. It is interesting to note the apparent disregard for crystal boundaries that deformation takes in progressing from one crystal to another, which is still further evidence of additional deformation systems acting with increasing temperature. Cracking at 300° C, as illustrated in Fig. 41, progresses in both an intercrystalline and intracrystalline manner, but to a greater extent by the latter.

Plastic deformation at 400° C, shown in Fig. 42, takes place almost exclusively in the manner mentioned for 300° C as an exception. Deformation marking is not distinct, but appears rather as a more or less uniform fragmentation of the crystal surface. The fine light-colored deformation lines seen are thought to be a result of plastic flow occurring during cooling from the test temperature, and/or during the handling involved in removing a specimen from

Fig. 40. Fatigue damage in normal uranium tested at 300° C (200X)

Fig. 41. Fatigue cracks in normal uranium tested at 300° C (200X)



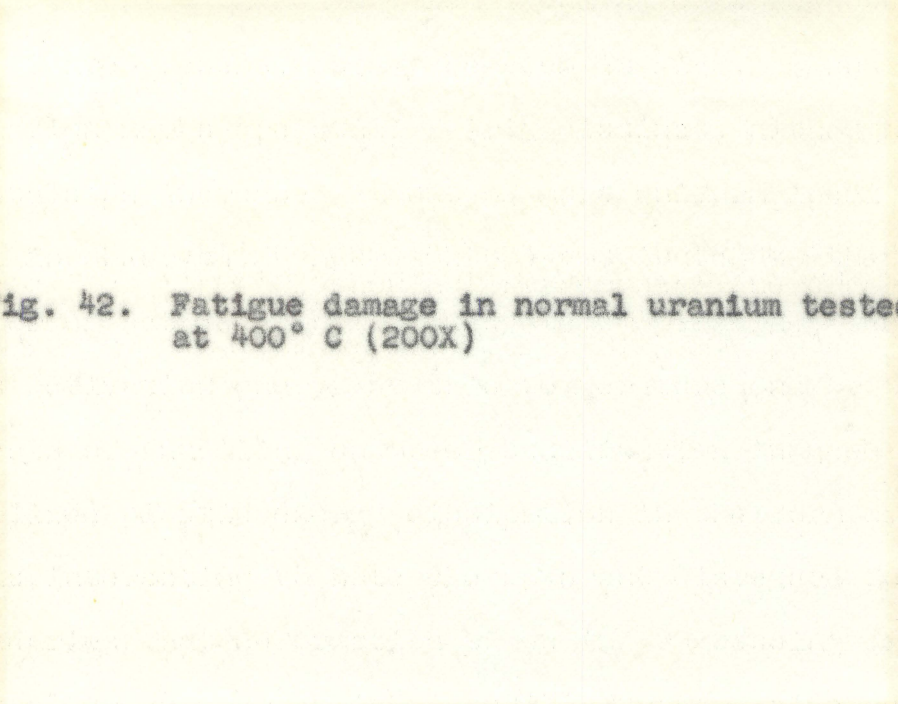


Fig. 42. Fatigue damage in normal uranium tested at 400° C (200X)

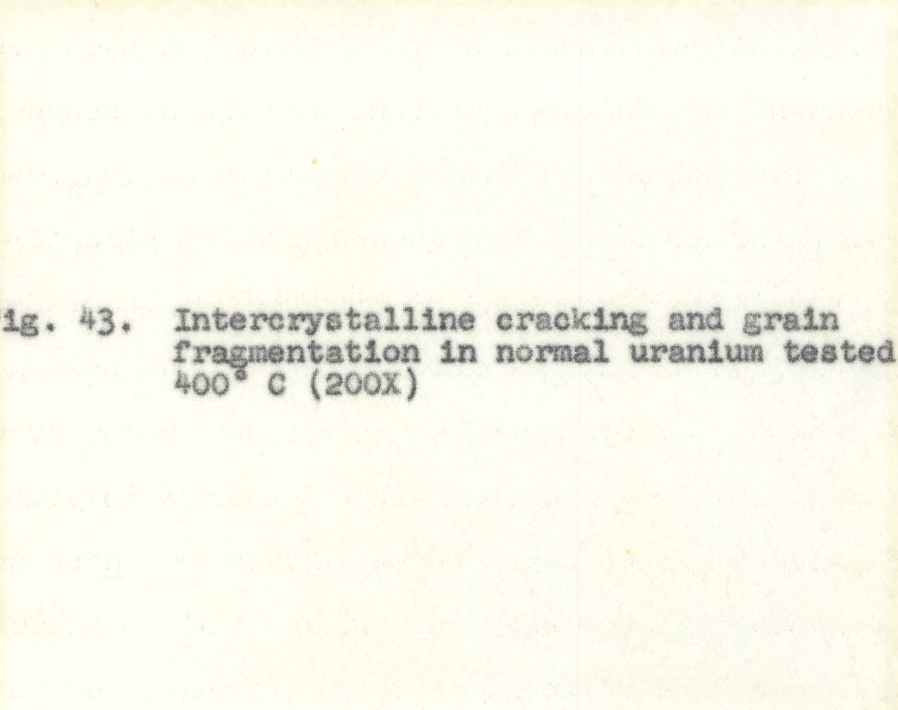
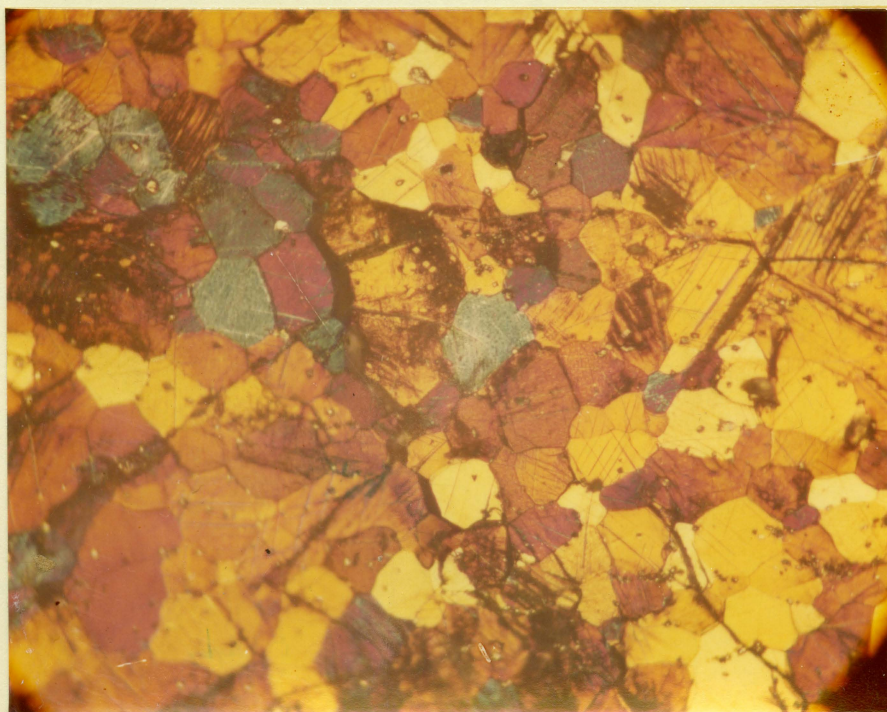


Fig. 43. Intercrystalline cracking and grain fragmentation in normal uranium tested at 400° C (200X)

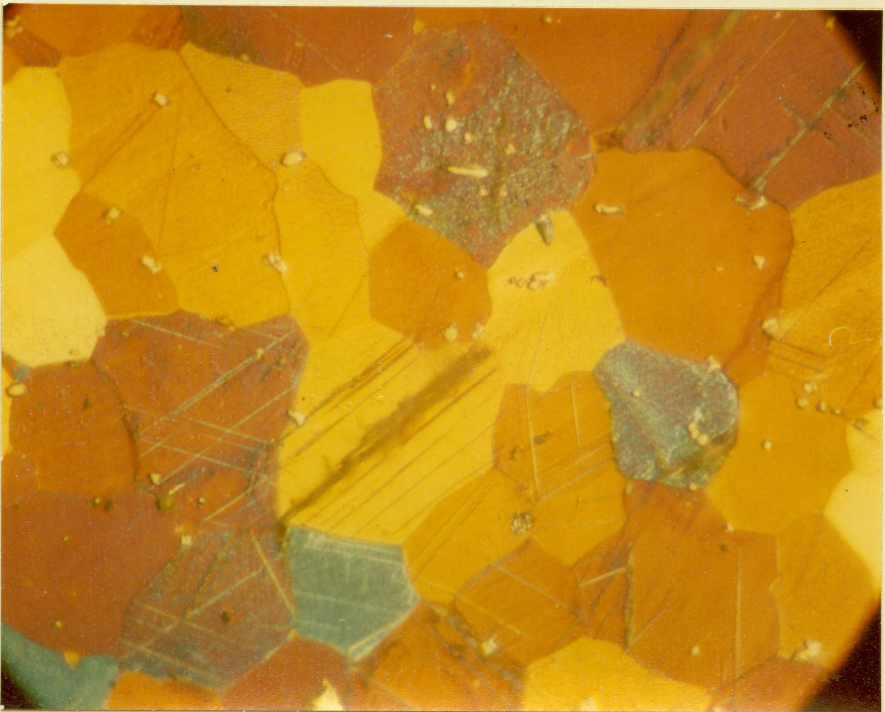
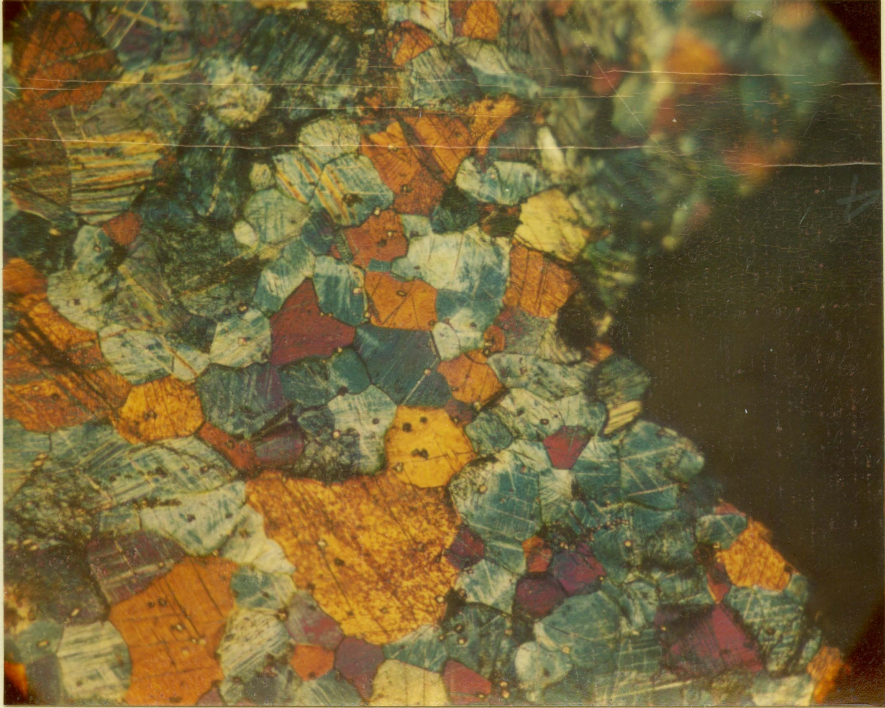


its capsule. Cracking at 400° C takes place predominantly along the boundaries as can be observed in Fig. 43. Cracks which developed in specimens used in cyclic temperature growth studied for uranium at the same temperature were also observed to progress in this manner (24). The term grain boundary melting was associated with this phenomena. In addition it was noted that thermal cycling below 300° C produced only negligible growth, whereas above 400° C substantial growth was observed. This may be regarded as additional support for the reasons given previously in discussing the discontinuity in results in the 300 to 400° C temperature range. Fig. 44 shows microstructural damage typical of fracture at 400° C, and indicates a lesser degree of localization of deformation at this temperature as compared with 150 and 300° C. The overall crystal structure shown here may be characterized by the effects of thermal softening.

Asperities such as seen in Fig. 45 were observed occasionally in the microstructure of 400° C test specimens. Careful examination at high magnification shows evidence of an extruding action where thin sheets of material have oozed out of the deformation bands. These thin sheets are very fragile and can easily be shaken loose, which could account for their infrequent detection in this investigation. Unaccounted for metallic particles were often found in the bellows during the removal of specimens from their capsules.

Fig. 44. Fatigue deformation at fracture in normal uranium tested at 400° C (200X)

Fig. 45. Asperities extruded from deformation bands in normal uranium tested at 400° C (500X)



Their presence might be attributed to this phenomenon. This extruding action was observed in fatigue studies of aluminum by Forsyth (25) who termed the action described as "slip band extrusion". The phenomenon was considered of interest from the standpoint of supporting evidence for conclusions drawn involving the processes of localized thermal softening. It is suggested that this process plays an important role relative to the initiation of cracks in fatigue.

IX. SUMMARY AND CONCLUSIONS

Rotating beam type fatigue tests were run on natural and alloyed uranium in the temperature range 25 to 600° C. From S-N data and information obtained from allied experiments a number of conclusions may be drawn regarding the fatigue characteristics of uranium.

The method of encapsulation was found to be an effective means of providing specimen oxidation protection for elevated temperature fatigue testing. Scatter in normal uranium room temperature data was markedly reduced using encapsulated specimens.

Apparent structural variations in the virgin material affected a large variation (10 per cent) in the fatigue strength of normal uranium. Experimental support for this statement is based on microscopically observed variations in oxygen content. S-N curves for normal uranium in the finite life range of stress can be represented by the power curve relationship

$$N = A' S^{-a}$$

where both the slope and intercept are shown to be temperature dependent. Their variation with temperature is approximately linear as is also the case for the variation of endurance limit with temperature. A discontinuity in the

variation of these parameters with temperature near 300° C was observed. This effect is typified by similar observations involving temperature variation of numerous other mechanical and physical properties of the same material.

The fatigue strength of a low chromium-uranium alloy was found to be superior to that of normal uranium. The affected increase is greater at low temperatures than at high temperatures and can be illustrated by a comparison of endurance limits. The respective values for normal and alloyed uranium are approximately 29 and 48 ksi at 25° C, and 5 and 10 ksi at 500° C. S-N results for the chromium-uranium alloy in the finite life range of stress may be described by the exponential relationship

$$N = G' e^{-GS}$$

where the slope and intercept are again temperature dependent.

The frequency distribution for cycles to failure is to a fair approximation log-normal for normal uranium at 25 ksi and 300° C.

The microscopic technique used to determine fatigue damage criteria for normal uranium is effective as described. Results obtained for cracking and fracture as criteria for failure are parallel on log S-log N plots below 300° C, and above this temperature they converge as a function of cycles. Fatigue damage at 150° C appears in the form of distinct

deformation bands (slip and twinning bands). At 400° C deformation takes the form of striated crystal surfaces. A combination of both forms of damage is seen at 300° C. Intracrystalline cracking predominates below 350° C and intercrystalline cracking above this temperature.

The stress-strain characteristics for successive cycles of completely reversed axial loading of normal and chromium-alloyed uranium may be represented by

$$S = B\epsilon^b$$

with the exception of the first loading. This relationship was verified experimentally at room temperature and for stresses up to approximately 60 ksi for four cycles. A modification of the flexure equation can be formulated which is applicable to semi-plastic materials which possess straight line log $S-\epsilon$ characteristics. Extrapolation of normal uranium room temperature fatigue data to a fraction of a cycle, on the basis of the modified flexure stress, yields results comparable to the ultimate tensile strength of the material.

X. SUGGESTIONS FOR FURTHER INVESTIGATION

It is felt that additional information relative to the effects of corrosion on the fatigue properties of metals would be desirable. Many super alloys have been developed to resist failure under extreme temperature and environmental conditions. It would be of more than academic interest to determine whether resistance to failure is brought about by the increase in resistance to corrosion or by an overall improvement in resistance to deformation, or both. Such information should certainly stimulate the advances of high temperature metallurgy in developing new materials. Extended application of the methods developed for corrosion protection in the course of this investigation is suggested.

Since it was seen that the fatigue properties of uranium at room temperature can be related to the corresponding stress-strain characteristics, it would appear worthwhile to determine if the correlation existed at elevated temperatures. This would require that elevated temperature axial cycle tension and compression tests be conducted. Suitable controlled atmosphere testing facilities for both axial tension and compression are non-existent; however, it is believed that an appropriate encapsulation technique could be effectively employed. Further verification of correlation might be evaluated by running constant strain amplitude

fatigue tests to obtain results for comparison with the constant moment tests. Such a comparison could provide access to the behavior of progressive strain hardening through successive cycling in fatigue.

XI. LITERATURE CITED

1. Ewing, J. A. and Humphrey, J. W. C. The fracture of metals under repeated alterations of stress. Philosophical Transactions A 200:241. 1902.
2. Dener, L. J. Fatigue crack detection methods. Wright Air Development Center Technical Report 55-86. 1955.
3. Gough, H. J. and Hanson, D. The behavior of metals subjected to repeated stresses. Proceedings of the Royal Society of London A 104:538. 1923.
4. Crowan, E. Theory of the fatigue of metals. Proceedings of the Royal Society of London A 171:79. 1939.
5. Machlin, E. S. Dislocation theory of the fatigue of metals. National Advisory Committee for Aeronautics Technical Note 1489. 1946.
6. Norwick, A. S. and Machlin, E. S. Quantitative treatment of creep of metals by dislocation and rate-process theories. National Advisory Committee for Aeronautics Technical Note 1039. 1946.
7. American Society for Testing Materials. Manual on fatigue testing. American Society for Testing Materials Special Technical Publication 19:31. 1951.
8. Cramer, H. Mathematical methods of statistics. Princeton University Press. Princeton, New Jersey. 1946.
9. Fruedenthal, A. M. Planning and interpretation of fatigue tests. American Society for Testing Materials Special Technical Publication 121:3. 1951.
10. Holden, A. N. Physical metallurgy of uranium. Addison-Wesley. Reading, Massachusetts. 1958.
11. McCutchan, D. A. and Murphy, Glenn. The stress-strain characteristics of uranium. U. S. Atomic Energy Commission Report ISC-700. [Iowa State University of Science and Technology.] 1955.

12. Laquer, H. L. The elastic constants of uranium. American Society for Metals Transactions 42:771. 1950.
13. Maringer, R. E. Battelle Memorial Institute. 1954. Unpublished work (Original not available for examination; cited in Holden, A. N. Physical metallurgy of uranium. pp. 63-64. Addison-Wesley. Reading, Massachusetts. 1958.)
14. Chubb, W. A method of measuring the contribution of crystal structure to the hardness of metals. U. S. Atomic Energy Commission Report BMI X-112. [Battelle Memorial Institute] 1953.
15. Shober, F. R. Battelle Memorial Institute. 1955. Unpublished work (Original not available for examination; cited in Holden, A. N. Physical metallurgy of uranium. pp. 73-74. Addison-Wesley. Reading, Massachusetts. 1958.)
16. Coffin, E. F. The effect of cyclic strain on the fatigue resistance of alpha-rolled uranium. U. S. Atomic Energy Commission Report KAPL-1019. [Knolls Atomic Power Laboratory] 1953.
17. Lewis, R. W. The tensile properties of metals in the elastic range of stress. Unpublished M.S. Thesis. Ames, Iowa. Library, Iowa State University of Science and Technology. 1956.
18. Hunter, D. and Murphy, Glenn. Thermal stress analysis of a cylinder of semi-plastic material. U. S. Atomic Energy Report ISC-839. [Iowa State University of Science and Technology] 1956.
19. Bohn, J. R. and Murphy, Glenn. High-temperature fatigue testing with application to uranium. American Society for Testing Materials Bulletin 234:57. 1958.
20. Carlson, A. J., Williams, J. T., Rogers, B. A. and Manthos, E. J. Etching metals by ionic bombardment. U. S. Atomic Energy Commission Report ISC-480. [Iowa State University of Science and Technology] 1954.
21. Murphy, Glenn. Mechanics of materials. Ronald Press. New York, New York. 1948.

22. Danofsky, R. and Murphy, Glenn. Ames, Iowa. Private communication. 1959.
23. Low, A. C. Short endurance fatigue. International Conference on fatigue of metals. London, England. Session 2, Paper 15. 1956.
24. Mayfield, R. M. Effect of cyclic variables upon growth-rate of 300° C rolled uranium. American Society for Metals Transactions 50:926. 1958.
25. Forsyth, P. J. E. The basic mechanism of fatigue and its dependence on the initial state of a material. International Conference on fatigue of metals. London, England. Session 2, Paper 5. 1956.

XII. ACKNOWLEDGMENTS

Sincere appreciation is extended Dr. Glenn Murphy, Head of the Department of Theoretical and Applied Mechanics, for his helpful guidance and continued support throughout the extended period of this investigation.

Many thanks are directed to the members of Nuclear Engineering Group I for their able assistance, and especially to Myron Willey for his tireless efforts in preparing specimens. The author also wishes to thank Dr. David Peterson and Ardis Johnson for their suggestions and assistance during the early stages of development of the welding techniques used in this investigation.

XIII. APPENDIX

XIII. APPENDIX

A. Tabulated Data

Table 6. S-N data for normal uranium (protected specimens)

Specimen no.	Temperature (°C)	Material designation	Minimum test section diameter (in)	Flexure stress (ksi)	Cycles to failure (x10 ⁶)	
1	25	Q-1	0.252	28.00	500.	a
2	25	Y-1	0.252	29.29	500.	a
3	25	L-1	0.250	29.99	6.6721	
4	25	L-1	0.251	33.50	1.2700	
5	25	Y-1	0.252	36.92	0.3300	
6	25	Y-1	0.252	40.74	0.1045	
7	25	Y-1	0.253	45.29	0.0395	
8	150	I-1	0.251	23.19	750.	a
9	150	C-1	0.251	20.10	505.	a
10	150	Y	0.252	22.15	302.9209	
11	150	C-1	0.250	21.12	196.3309	
12	150	Y	0.250	25.29	3.2776	
13	150	C-1	0.245	23.00	2.6246	
14	150	O-1	0.251	28.34	1.4023	
15	150	O-1	0.252	30.55	0.3314	
16	150	O-1	0.249	35.63	0.1000	
17	150	M-1	0.252	42.01	0.0075	
18	300	X	0.252	16.04	750.	a
19	300	Q	0.250	13.82	640.	a
20	300	T	0.250	17.21	186.8045	
21	300	X	0.252	18.59	102.2063	
23	300	Q	0.249	20.06	2.4695	
24	300	T	0.248	22.17	0.7432	
25	300	X	0.250	24.25	0.3080	
26	300	X	0.252	25.97	0.1280	
27	300	K-1	0.250	27.38	0.0848	
29	300	K-1	0.251	33.50	0.0215	
30	300	K-1	0.248	32.59	0.0112	
31	300	K-1	0.251	37.36	0.0048	

^aDenotes no failure.

Table 6 (continued)

Specimen no.	Temperature (°C)	Material designation	Minimum test section diameter (in)	Flexure stress (ksi)	Cycles to failure (x10 ⁶)
32	400	H-1	0.248	9.35	508.0055
33	400	H-1	0.248	10.68	398.8400
34	400	G-1	0.249	13.20	13.3910
35	400	G-1	0.252	11.97	5.5642
36	400	A-1	0.236	11.16	5.1124
37	400	A-1	0.249	14.78	0.9211
38	400	H-1	0.249	17.42	0.2825
39	400	P-1	0.251	20.61	0.1281
40	400	P-1	0.252	22.91	0.0321
41	400	P-1	0.250	25.03	0.0110
42	500	I-1	0.243	5.11	222.1862
43	500	I-1	0.250	5.60	62.3542
44	500	F-1	0.251	6.96	30.6250
45	500	I-1	0.248	6.14	26.7240
46	500	F-1	0.248	8.01	3.0635
47	500	F-1	0.246	10.40	0.6117
48	500	M-1	0.251	15.46	0.0468
49	500	M-1	0.252	20.37	0.0080

Table 7. S-N data for normal uranium (room temperature unprotected specimens)

Specimen no.	Material designation	Minimum test section diameter (in)	Bending moment (in-lb)	Flexure stress (ksi)	Cycles to failure ($\times 10^6$)
1	C	0.252	39.3	25.0	501.2303 ^a
2	A	0.250	41.3	27.0	502.6620 ^a
3	B	0.248	40.3	27.0	7.0559
4	M	0.254	44.3	27.5	17.4085
5	D	0.252	44.0	28.0	2.1529
6	J	0.247	41.4	28.0	504.1130 ^a
7	K	0.249	43.8	29.0	7.9008
8	L	0.252	45.5	29.0	47.8751
9	A	0.251	46.5	30.0	5.1954
10	C	0.252	48.7	31.0	191.6250
11	J	0.252	48.7	31.0	12.3018
12	K	0.250	47.4	31.0	65.6434
13	A	0.250	49.0	32.0	1.2665
14	D	0.253	50.4	32.0	9.4150
15	A	0.252	55.2	35.0	1.0389
16	I	0.252	54.9	35.0	2.6678
17	D	0.252	59.8	38.0	0.4933
18	L	0.251	58.9	38.0	1.5448
19	B	0.248	59.9	40.0	1.3654
20	K	0.244	58.2	41.0	0.1284
21	J	0.248	63.0	42.0	0.0960
22	I	0.251	65.1	42.0	0.0675
23	I	0.244	61.0	43.0	0.0510
24	G	0.252	70.6	45.0	0.0560
25	M	0.251	72.8	47.0	0.0228
26	L	0.250	75.0	49.0	0.0141
27	B	0.252	78.5	50.0	0.1632
28	J	0.252	81.7	52.0	0.0054
29	G	0.253	87.5	55.0	0.0050
30	D	0.254	96.7	60.0	0.0034
31	L	0.248	97.5	65.0	0.0037
32	N	0.227	80.4	70.0	0.0040
33	M	0.250	114.8	75.0	0.0008
34	M	0.248	136.0	90.0	0.0003

^aDenotes no failure.

Table 8. S-N data for chromium-uranium alloy

Specimen no.	Temperature (°C)	Material designation	Minimum test section diameter (in)	Flexure stress (ksi)	Cycles to failure (x10 ⁶) ^a
1	25 ^b	A	0.253	40.0	500. a
2	25	A	0.252	47.0	500. a
3	25	A	0.252	48.0	500. a
4	25	D	0.252	49.0	500. a
5	25	A	0.253	50.0	0.2682
6	25	B	0.254	52.0	0.1090
7	25	D	0.253	58.0	0.0158
8	150	I	0.252	37.43	500. a
9	150	I	0.252	39.50	0.8012
10	150	I	0.252	40.74	0.4889
11	150	I	0.252	42.01	0.3852
12	150	I	0.252	42.01	0.3499
13	150	I	0.252	44.55	0.2599
14	150	I	0.252	48.37	0.0788
15	150	I	0.253	52.84	0.0310
16	300	E	0.252	30.04	537. a
17	300	E	0.253	33.97	504. a
18	300	E	0.252	34.88	270.7420
19	300	E	0.252	37.17	12.4236
20	300	G	0.252	40.74	0.1707
21	300	G	0.253	45.29	0.0548
22	300	G	0.252	50.92	0.0102
23	400	H	0.252	20.37	214.3142
24	400	H	0.254	22.38	42.3772
25	400	H	0.249	25.07	18.7526
26	400	H	0.253	30.19	0.5421
27	400	H	0.254	34.81	0.1049
28	500	F	0.249	8.97	729. a
29	500	F	0.249	10.15	248.3112
30	500	F	0.250	10.95	112.2384
31	500	E	0.252	11.97	73.4816
32	500	E	0.250	12.98	38.2312

^aDenotes no failure.

^bCantilever tests on unprotected for 25° C.

Table 8 (continued)

Specimen no.	Temperature (°C)	Material designation	Minimum test section diameter (in)	Flexure stress (ksi)	Cycles to failure ($\times 10^6$)
33	500	E	0.252	14.00	30.6028
34	500	E	0.252	15.02	18.8092
35	500	F	0.252	20.37	2.2380
36	500	H	0.253	25.16	0.4348
37	500	H	0.252	30.55	0.0240
38	600	G	0.252	3.56	516. ^a
39	600	G	0.252	4.07	167.2004
40	600	G	0.252	4.84	128.5220
41	600	F	0.250	7.04	37.5705
42	600	F	0.252	8.15	24.9075
43	600	F	0.250	9.13	14.1457
44	600	F	0.251	10.31	5.9950
45	600	G	0.252	15.28	1.3642
46	600	H	0.253	22.64	0.0237

Table 9. Frequency distribution for normal uranium at
25 ksi and 300° C

Specimen no.	Cumulative relative frequency per cent	Cycles to failure, N ($\times 10^6$)	log N	log N - $\overline{\log N}$
1	6.67	0.3902	5.59129	-0.16426
2	13.33	0.4299	5.63337	-0.12218
3	19.99	0.4600	5.66276	-0.09279
4	26.66	0.4887	5.68904	-0.06651
5	33.33	0.4890	5.68931	-0.06624
6	39.99	0.5412	5.73336	-0.02219
7	46.66	0.5874	5.76893	0.01338
8	53.33	0.6003	5.77837	0.02282
9	59.99	0.6190	5.79169	0.03614
10	66.66	0.6233	5.79470	0.03915
11	73.33	0.6419	5.80447	0.05192
12	79.99	0.6445	5.82249	0.06694
13	86.66	0.7605	5.88110	0.12555
14	93.33	0.8588	5.93389	0.17834

Table 10. Effect of fatigue damage on the microstructure of uranium

Specimen no.	Temperature (°C)	Type of deformation ^a	Reference diameter (in)	Per cent of maximum stress	Stress (ksi)	Cycle to failure (x10 ⁶)
1	150	LPD	0.286	65.99	26.12	0.0092
1	150	C	0.258	89.89	35.59	0.0092
1	150	F	0.249	100.00	39.59	0.0092
2	150	LPD	0.286	67.59	23.51	0.0272
2	150	C	0.260	89.97	31.29	0.0272
2	150	F	0.251	100.00	34.78	0.0272
3	150	LPD	0.284	67.40	20.46	0.0798
3	150	C	0.256	92.02	27.93	0.0798
3	150	F	0.249	100.00	30.35	0.0798
4	150	LPD	0.285	67.50	16.72	0.2628
4	150	C	0.252	97.64	24.19	0.2628
4	150	F	0.250	100.00	24.77	0.2628
5	300	LPD	0.292	65.04	9.82	0.6762
5	300	C	0.258	94.29	14.24	0.6762
5	300	F	0.253	100.00	15.10	0.6762
6	300	LPD	0.299	55.01	9.14	0.2500
6	300	C	0.256	87.65	14.57	0.2500
6	300	F	0.245	100.00	16.62	0.2500
7	300	LPD	0.285	69.13	12.32	0.1269
7	300	C	0.260	91.05	16.23	0.1269
7	300	F	0.252	100.00	17.82	0.1269
8	300	LPD	0.290	66.40	13.37	0.0475
8	300	C	0.268	83.97	16.90	0.0475
8	300	F	0.253	100.00	20.13	0.0475
9	300	LPD	0.285	69.13	15.84	0.0266
9	300	C	0.261	90.01	20.62	0.0266
9	300	F	0.252	100.00	22.91	0.0266

^aLPD = localized plastic deformation.
C = cracking.
F = fracture.

Table 10 (continued)

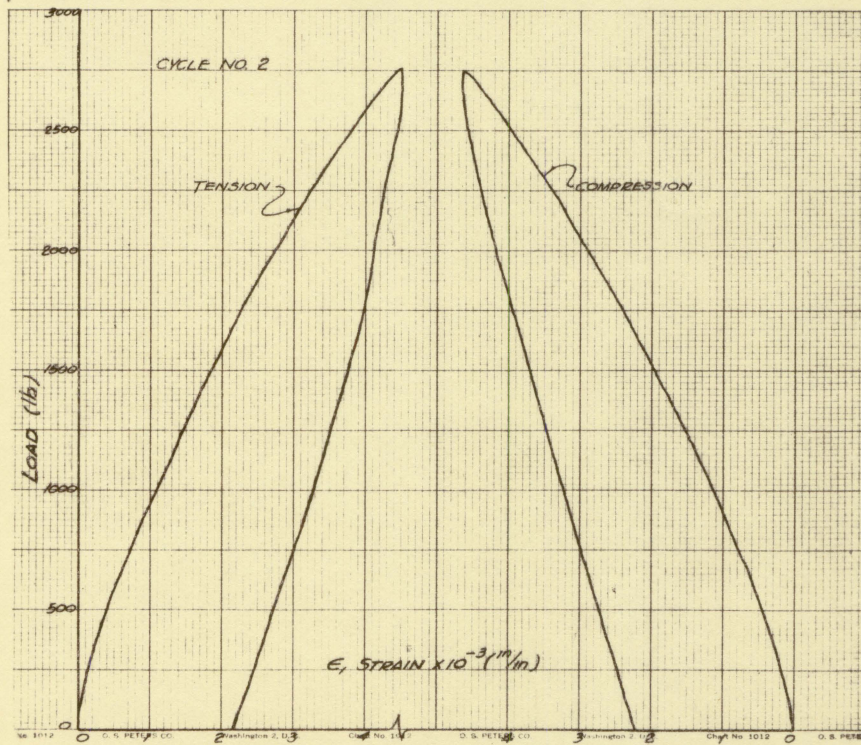
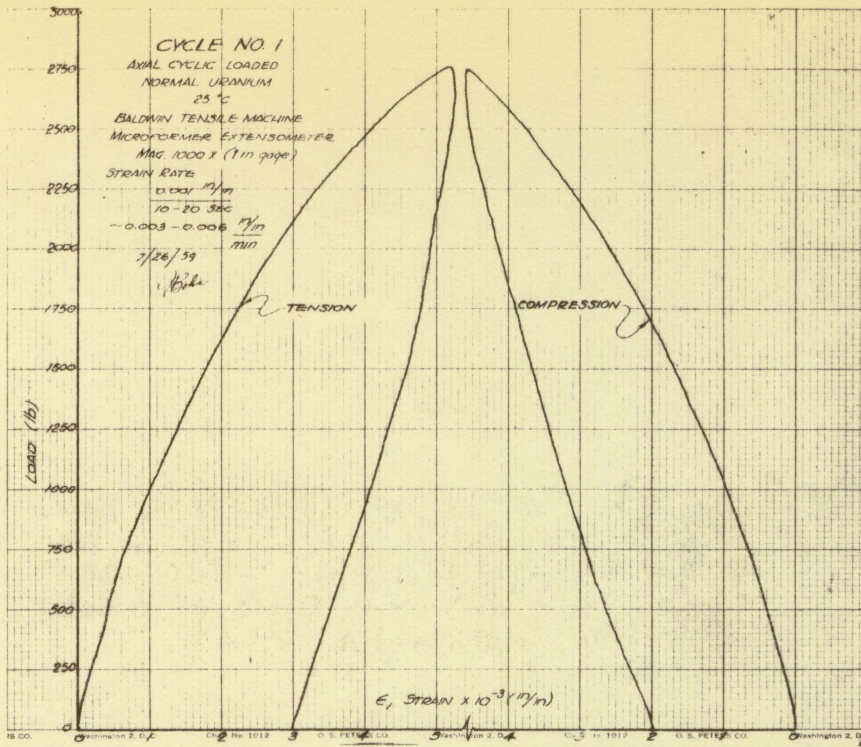
Specimen no.	Temperature (°C)	Type of deformation ^a	Reference diameter (in)	Per cent of maximum stress	Stress (ksi)	Cycle to failure (x10 ⁶)
10	300	LPD	0.292	65.04	17.02	0.0045
10	300	C	0.261	91.08	23.84	0.0045
10	300	F	0.253	100.00	26.17	0.0045
11	400	LPD	0.256	93.13	9.71	1.5410
11	400	C	0.251	98.81	10.31	1.5410
11	400	F	0.250	100.00	10.43	1.5410
12	400	LPD	0.267	80.14	11.77	0.0840
12	400	C	0.253	94.19	13.84	0.0840
12	400	F	0.248	100.00	14.69	0.0840
13	400	LPD	0.279	70.23	14.06	0.0140
13	400	C	0.253	94.19	18.86	0.0140
13	400	F	0.248	100.00	20.03	0.0140
14	400	LPD	0.284	68.25	17.84	0.0015
14	400	C	0.264	84.90	22.30	0.0015
14	400	F	0.250	100.00	26.08	0.0015

Table 11. Position reference to stress for sequence photo-micrograph of specimen M-2 tested at 150° C for 0.0798×10^6 cycles

Reference position	Arc length (in)	Reference diameter (in)	Per cent of maximum stress	Stress (ksi)
1	0.73	0.348	37.52	13.05
2	0.70	0.340		
3	0.67	0.334		
4	0.64	0.326	45.64	15.87
5	0.60	0.317	49.64	17.26
6	0.57	0.310		
7	0.54	0.304		
8	0.52	0.300	58.57	20.37
9	0.48	0.293	62.86	21.86
10	0.45	0.288		
11	0.42	0.283		
12	0.38	0.277	74.40	25.88
13	0.35	0.274	76.87	26.74
14	0.32	0.270		
15	0.28	0.265		
16	0.25	0.263	86.93	30.23
17	0.22	0.260	89.97	31.29
18	0.19	0.258		
19	0.16	0.255		
20	0.13	0.254	96.50	33.56
21	0.10	0.253	97.64	33.96
22	0.07	0.252		
23	0.03	0.251		
24	0.00	0.251	100.00	34.78

B. Stress-strain Records

Fig. 46. Reproductions of the autographic load-strain records from axial cyclic tension and compression tests of normal uranium at room temperature (specimen diameter = 0.250 in) (Cycle No. 1 and Cycle No. 2)



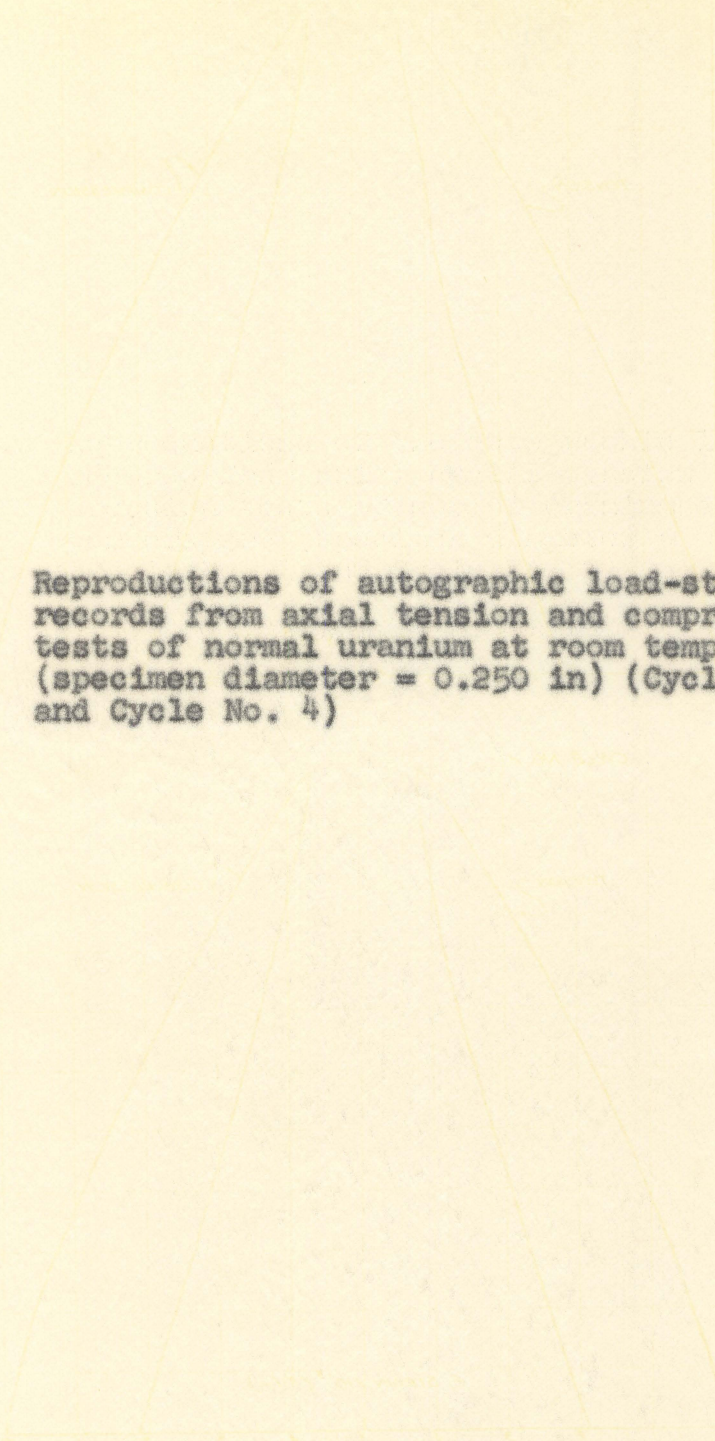


Fig. 47. Reproductions of autographic load-strain records from axial tension and compression tests of normal uranium at room temperature (specimen diameter = 0.250 in) (Cycle No. 3 and Cycle No. 4)

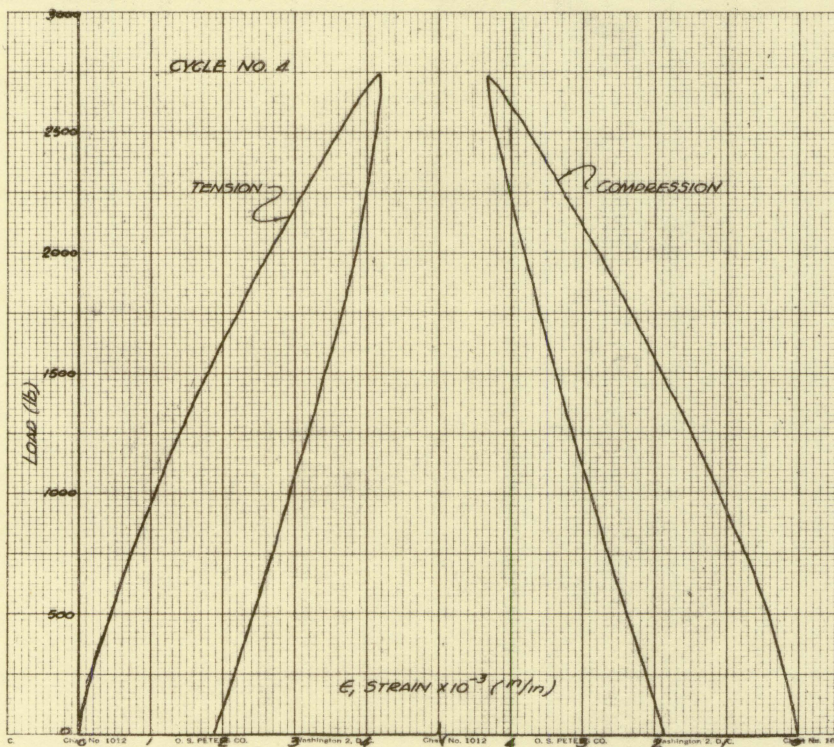
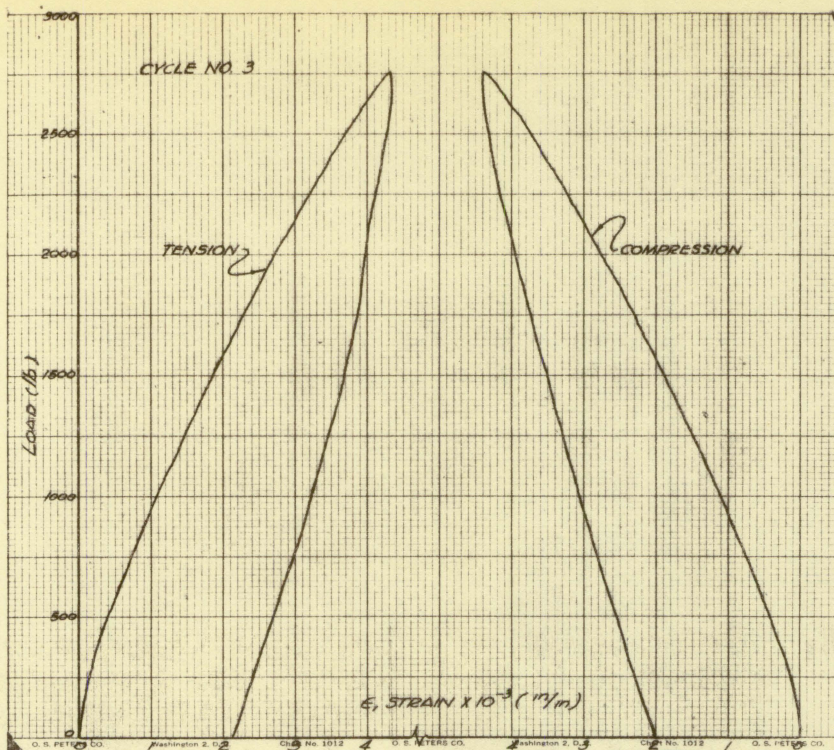


Fig. 48. Reproductions of the autographic load-strain records from axial tension and compression tests of chromium-uranium alloy at room temperature (specimen diameter = 0.253 in) (Cycle No. 1 and Cycle No. 2)

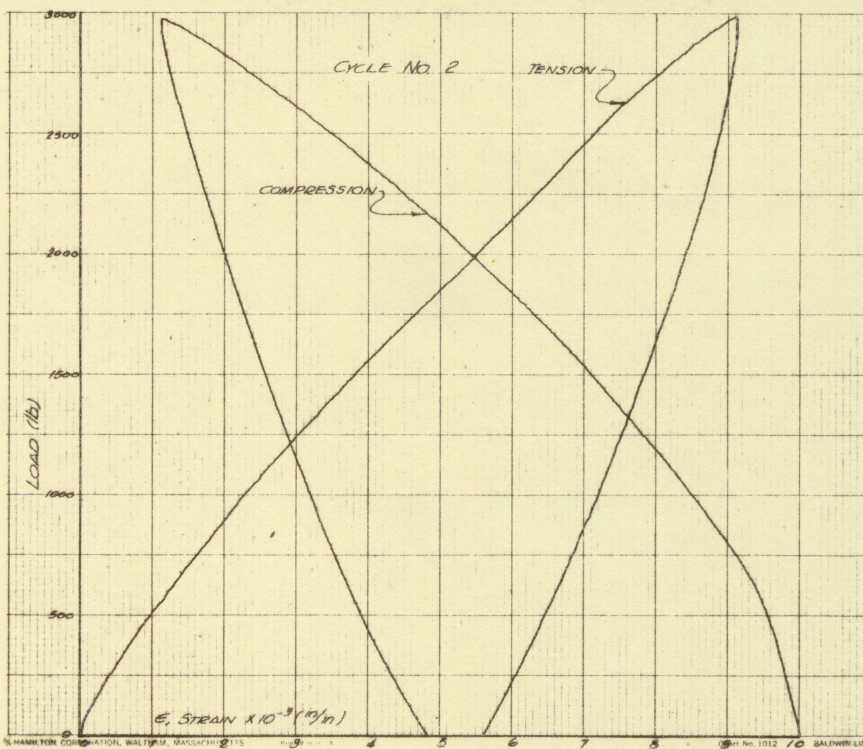
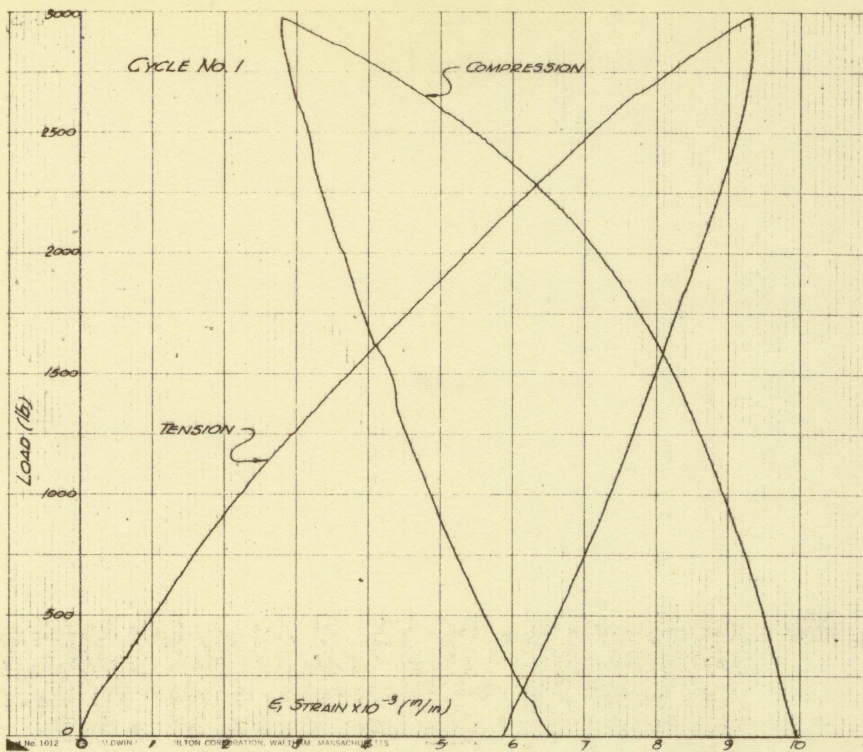


Fig. 49. Reproductions of the autographic load-strain records from axial tension and compression tests of chromium-uranium alloy at room temperature (specimen diameter = 0.253 in) (Cycle No. 3 and Cycle No. 4)

